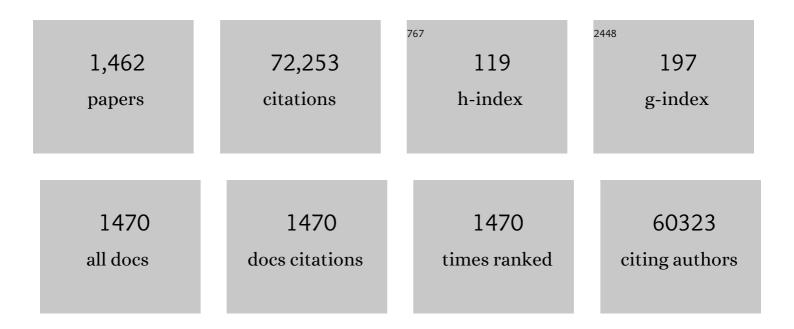
List of Publications by Year in descending order

Source: https://exaly.com/author-pdf/10909229/publications.pdf Version: 2024-02-01



Рани К Сни

#	Article	IF	CITATIONS
1	A new technique to optimize the properties of photonic crystal fibers supporting transmission of multiple orbital angular momentum modes. Journal of Optics (India), 2023, 52, 307-316.	1.7	7
2	Selective inhibition effects on cancer cells and bacteria of Ni–Ti–O nanoporous layers grown on biomedical NiTi alloy by anodization. Rare Metals, 2022, 41, 78-85.	7.1	21
3	Hard and tough CrN coatings strengthened by high-density distorted coherent grain boundaries. Journal of Alloys and Compounds, 2022, 894, 162139.	5.5	8
4	In situ preparation of Mn-doped perovskite nanocrystalline films and application to white light emitting devices. Journal of Colloid and Interface Science, 2022, 606, 1163-1169.	9.4	16
5	A multifunctional antibacterial coating on bone implants for osteosarcoma therapy and enhanced osteointegration. Chemical Engineering Journal, 2022, 428, 131155.	12.7	23
6	Highly active cobalt-doped nickel sulfide porous nanocones for high-performance quasi-solid-state zinc-ion batteries. Journal of Energy Chemistry, 2022, 66, 237-249.	12.9	15
7	Magnesium cationic cue enriched interfacial tissue microenvironment nurtures the osseointegration of gamma-irradiated allograft bone. Bioactive Materials, 2022, 10, 32-47.	15.6	10
8	Highly Sensitive Dual-core Photonic Crystal Fiber Based on a Surface Plasmon Resonance Sensor with Gold Film. Plasmonics, 2022, 17, 543-550.	3.4	8
9	Photonic fibre crystal sensor with a D-shape based on surface plasma resonance containing microfluidic channels for detection of a wide range of refractive indexes. Journal of Modern Optics, 2022, 69, 1-11.	1.3	2
10	Recent advances in structural engineering of 2D hexagonal boron nitride electrocatalysts. Nano Energy, 2022, 91, 106661.	16.0	49
11	Short-brush NiFeOxHy films and the Pt derivative as high-performance electrode materials for efficient electrocatalytic water splitting. Applied Surface Science, 2022, 574, 151636.	6.1	7
12	Hydrogen permeation behavior and mechanism of multi-layered graphene coatings and mitigation of hydrogen embrittlement of pipe steel. Applied Surface Science, 2022, 573, 151529.	6.1	27
13	Porous Mo2C-Mo3N2 heterostructure/rGO with synergistic functions as polysulfides regulator for high-performance lithium sulfur batteries. Chemical Engineering Journal, 2022, 433, 133629.	12.7	10
14	Recent progress and perspective of cobalt-based catalysts for water splitting: design and nanoarchitectonics. Materials Today Energy, 2022, 23, 100911.	4.7	28
15	Stable static zinc-iodine redox battery constructed with graphene quantum dots coated graphite felt. Journal of Power Sources, 2022, 520, 230861.	7.8	6
16	A novel photonic quasi-crystal fiber for transmission of orbital angular momentum modes. Optik, 2022, 251, 168446.	2.9	5
17	A square-lattice D-shaped photonic crystal fiber sensor based on SPR to detect analytes with large refractive indexes. Physica E: Low-Dimensional Systems and Nanostructures, 2022, 138, 115106.	2.7	35
18	Size-dependent flame retardancy of black phosphorus nanosheets. Nanoscale, 2022, 14, 2599-2604.	5.6	16

#	Article	IF	CITATIONS
19	Commercialization of Electric Vehicles in Hong Kong. Energies, 2022, 15, 942.	3.1	11
20	Improved corrosion and wear resistance of micro-arc oxidation coatings on the 2024 aluminum alloy by incorporation of quasi-two-dimensional sericite microplates. Applied Surface Science, 2022, 585, 152693.	6.1	29
21	A programmed surface on polyetheretherketone for sequentially dictating osteoimmunomodulation and bone regeneration to achieve ameliorative osseointegration under osteoporotic conditions. Bioactive Materials, 2022, 14, 364-376.	15.6	39
22	A zinc-doped coating prepared on the magnesium alloy by plasma electrolytic oxidation for corrosion protection. Surface and Coatings Technology, 2022, 433, 128148.	4.8	19
23	Fan-shape Mn-doped CoO/C microspheres for high lithium-ion storage capacity. Journal of Alloys and Compounds, 2022, 903, 163980.	5.5	8
24	Enhanced ion conductivity and electrode–electrolyte interphase stability of porous Si anodes enabled by silicon nitride nanocoating for high-performance Li-ion batteries. Journal of Energy Chemistry, 2022, 69, 616-625.	12.9	35
25	Origin of superior pseudocapacitive mechanism of transition metal nitrides. Journal of Energy Chemistry, 2022, 69, 561-568.	12.9	11
26	Fabrication and cutting performance of CrAlN/CrAl multilayer coatings deposited by continuous high-power magnetron sputtering. Ceramics International, 2022, 48, 14528-14536.	4.8	3
27	Balancing the biocompatibility and bacterial resistance of polypyrrole by optimized silver incorporation. Materials Science and Engineering C, 2022, 134, 112701.	7.3	9
28	Finite phosphorene derived partial reduction of metal organic framework nanofoams for enhanced lithium storage capability. Journal of Power Sources, 2022, 525, 231025.	7.8	1
29	Plasma Engineering of Basal Sulfur Sites on MoS ₂ @Ni ₃ S ₂ Nanorods for the Alkaline Hydrogen Evolution Reaction. Advanced Science, 2022, 9, e2104774.	11.2	26
30	Plasma modified and tailored defective electrocatalysts for water electrolysis and hydrogen fuel cells. EcoMat, 2022, 4, .	11.9	22
31	Versatile Phenolâ€Incorporated Nanoframes for In Situ Antibacterial Activity Based on Oxidative and Physical Damages. Advanced Functional Materials, 2022, 32, .	14.9	17
32	Surface and interface control of black phosphorus. CheM, 2022, 8, 632-662.	11.7	28
33	Dynamic active sites on plasma engraved Ni hydroxide for enhanced electro-catalytic urea oxidation. Journal of Energy Chemistry, 2022, 71, 150-158.	12.9	23
34	Diamond-like carbon coating and surface grafting of osteoprotegerin and alendronate on polyetheretherketone to ameliorate the mechanical performance and osseointegration simultaneously. Composites Part B: Engineering, 2022, 236, 109815.	12.0	14
35	Fabrication and hydrogen permeation resistance of dense CrN coatings. Surface and Coatings Technology, 2022, 437, 128326.	4.8	10
36	Sodium alginate coating on biodegradable high-purity magnesium with a hydroxide/silane transition layer for corrosion retardation. Colloids and Surfaces A: Physicochemical and Engineering Aspects, 2022, 642, 128647.	4.7	10

#	Article	IF	CITATIONS
37	Effects of acid treatment and plasma micromachining on the surface properties of carbon fibers. Applied Surface Science, 2022, 592, 153261.	6.1	9
38	Se-NiSe2 hybrid nanosheet arrays with self-regulated elemental Se for efficient alkaline water splitting. Journal of Materials Science and Technology, 2022, 118, 136-143.	10.7	46
39	Hofmeister Effect and Electrostatic Interaction Enhanced Ionic Conductive Organohydrogels for Electronic Applications. Advanced Functional Materials, 2022, 32, .	14.9	41
40	Degradation of gemfibrozil in aqueous solutions by gas–liquid dielectric barrier discharge plasma combined with CNTs/γFe ₂ O ₃ . Plasma Processes and Polymers, 2022, 19, .	3.0	3
41	A highly sensitive D-type photonic crystal fiber infrared sensor with indium tin oxide based on surface plasmon resonance. Modern Physics Letters B, 2022, 36, .	1.9	14
42	Near-infrared photonic artificial synapses based on organic heterojunction phototransistors. Applied Physics Letters, 2022, 120, .	3.3	8
43	A silicate-loaded MgAl LDH self-healing coating on biomedical Mg alloys for corrosion retardation and cytocompatibility enhancement. Surface and Coatings Technology, 2022, 439, 128442.	4.8	16
44	Detection of kerosene adulteration in automobile fuel by a low-loss surface plasmon resonance (SPR) chemical sensor. Analytical Methods, 2022, 14, 2153-2160.	2.7	3
45	Inâ€Plane Mott–Schottky Effects Enabling Efficient Hydrogen Evolution from Mo ₅ N ₆ â€MoS ₂ Heterojunction Nanosheets in Universalâ€pH Electrolytes. Small, 2022, 18, e2201137.	10.0	37
46	Exosomes derived from magnesium ion—stimulated macrophages inhibit angiogenesis. Biomedical Materials (Bristol), 2022, 17, 045008.	3.3	2
47	In-Situ and controllable construction of Mo2N embedded Mo2C nanobelts as robust electrocatalyst for superior pH-universal hydrogen evolution reaction. Journal of Alloys and Compounds, 2022, 918, 165611.	5.5	11
48	Subnanometer MoP clusters confined in mesoporous carbon (CMK-3) as superior electrocatalytic sulfur hosts for high-performance lithium-sulfur batteries. Chemical Engineering Journal, 2022, 446, 137050.	12.7	9
49	High-precision modeling of dynamic etching in high-power magnetron sputtering. Journal Physics D: Applied Physics, 2022, 55, 325203.	2.8	1
50	Numerical Analysis of Multifunctional Biosensor with Dual-Channel Photonic Crystal Fibers Based on Localized Surface Plasmon Resonance. Coatings, 2022, 12, 742.	2.6	3
51	Ti ₃ C ₂ T <i>_X</i> MXene Modified with ZnTCPP with Bacteria Capturing Capability and Enhanced Visible Light Photocatalytic Antibacterial Activity. Small, 2022, 18, .	10.0	49
52	Interface Polarization Strengthened Microwave Catalysis of MoS ₂ /FeS/Rhein for the Therapy of Bacteriaâ€Infected Osteomyelitis. Advanced Functional Materials, 2022, 32, .	14.9	26
53	In situ synthesis of 3D metal oxides/Ni3C on the macroporous electrically conductive network for enhanced electron field emission. Materials Letters, 2022, 323, 132524.	2.6	1
54	Plasmon-enhanced hydrogen evolution on Pt-anchored titanium nitride nanowire arrays. Applied Surface Science, 2022, 598, 153745.	6.1	14

#	Article	IF	CITATIONS
55	General synthesis of nanostructured Mo2C electrocatalysts using a carbon template for electrocatalytic applications. Carbon, 2022, 197, 238-245.	10.3	14
56	Construction of α-MnO2 on Carbon Fibers Modified with Carbon Nanotubes for Ultrafast Flexible Supercapacitors in Ionic Liquid Electrolytes with Wide Voltage Windows. Nanomaterials, 2022, 12, 2020.	4.1	9
57	Highly Durable and Efficient Ni-FeO <i>_x</i> /FeNi ₃ Electrocatalysts Synthesized by a Facile <i>In Situ</i> Combustion-Based Method for Overall Water Splitting with Large Current Densities. ACS Applied Materials & Interfaces, 2022, 14, 27842-27853.	8.0	34
58	HE1,1 mode-excited surface plasmon resonance for refractive index sensing by photonic crystal fibers with high sensitivity and long detection distance. Optik, 2022, 265, 169471.	2.9	10
59	A photonic quasi-crystal fibre supporting stable transmission of 150 OAM modes with high mode quality and flat dispersion. Journal of Modern Optics, 2022, 69, 887-896.	1.3	3
60	A static three-chamber zinc-polyiodide redox battery for decoupling of active anions and cations. Journal of Energy Storage, 2022, 54, 105258.	8.1	1
61	Utilization of coal fly ash in China: a mini-review on challenges and future directions. Environmental Science and Pollution Research, 2021, 28, 18727-18740.	5.3	76
62	Electrochemical stability, corrosion behavior, and biological properties of Ni–Ti–O nanoporous layers anodically on NiTi alloy. Corrosion Science, 2021, 179, 109104.	6.6	21
63	Investigation of the microstructure on the nanoporous carbon based capacitive performance. Microporous and Mesoporous Materials, 2021, 310, 110629.	4.4	6
64	Synergistic antibacterial activity of physical-chemical multi-mechanism by TiO2 nanorod arrays for safe biofilm eradication on implant. Bioactive Materials, 2021, 6, 12-25.	15.6	111
65	Enhanced corrosion resistance, antibacterial properties, and biocompatibility by hierarchical hydroxyapatite/ciprofloxacin-calcium phosphate coating on nitrided NiTi alloy. Materials Science and Engineering C, 2021, 118, 111524.	7.3	25
66	Stepwise 3D-spatio-temporal magnesium cationic niche: Nanocomposite scaffold mediated microenvironment for modulating intramembranous ossification. Bioactive Materials, 2021, 6, 503-519.	15.6	27
67	Silicon monophosphides with controlled size and crystallinity for enhanced lithium anodic performance. Nanoscale, 2021, 13, 51-58.	5.6	9
68	Complete ablation of resistant tumors with photosensitive black phosphorus quantum dots-based lipid nanocapsules. Chemical Engineering Journal, 2021, 421, 127879.	12.7	5
69	Large-scale and low-cost synthesis of in situ generated SiC/C nano-composites from rice husks for advanced electromagnetic wave absorption applications. Surface and Coatings Technology, 2021, 406, 126641.	4.8	23
70	Effects of the target-to-substrate distance on the microstructure and properties of TiN coatings fabricated by pulse-enhanced vacuum arc evaporation. Journal of Adhesion Science and Technology, 2021, 35, 1125-1137.	2.6	4
71	Uniform cobalt nanoparticles-decorated biscuit-like VN nanosheets by in situ segregation for Li-ion batteries and oxygen evolution reaction. Applied Surface Science, 2021, 536, 147982.	6.1	23
72	Ultra-short and dual-core photonic crystal fiber polarization splitter composed of metal and gallium arsenide. Optik, 2021, 226, 165779.	2.9	25

#	Article	IF	CITATIONS
73	A Biomimetic Nanoâ€Engineered Platform for Functional Tissue Engineering of Cartilage Superficial Zone. Advanced Healthcare Materials, 2021, 10, e2001018.	7.6	14
74	Graphene-encapsulated blackberry-like porous silicon nanospheres prepared by modest magnesiothermic reduction for high-performance lithium-ion battery anode. Rare Metals, 2021, 40, 383-392.	7.1	65
75	Black phosphorus: Versatile twoâ€dimensional materials in cancer therapies. View, 2021, 2, 2020043.	5.3	16
76	Artificial synapses with a sponge-like double-layer porous oxide memristor. NPG Asia Materials, 2021, 13, .	7.9	31
77	Overview of refractive index sensors comprising photonic crystal fibers based on the surface plasmon resonance effect [Invited]. Chinese Optics Letters, 2021, 19, 102202.	2.9	65
78	Field emission from geometrically modulated tungsten-nickel sulfide / graphitic carbon nanobelts on Si microchannel plates. Ceramics International, 2021, 47, 4034-4042.	4.8	5
79	High-performance multi-dimensional nitrogen-doped N+MnO2@TiC/C electrodes for supercapacitors. Electrochimica Acta, 2021, 370, 137716.	5.2	24
80	3D urchin-like NiCo2O4 coated with carbon nanospheres prepared on flexible graphite felt for efficient bifunctional electrocatalytic water splitting. Journal of Materials Science, 2021, 56, 9961-9973.	3.7	12
81	Near-infrared light II - assisted rapid biofilm elimination platform for bone implants at mild temperature. Biomaterials, 2021, 269, 120634.	11.4	90
82	Surface plasmon resonance sensor based on U-shaped photonic quasi-crystal fiber. Applied Optics, 2021, 60, 1761.	1.8	27
83	A cationic alternating copolymer composed of ornithine and glycine with an ordered sequence for enhanced bacterial activity. Polymer Engineering and Science, 2021, 61, 1405-1414.	3.1	4
84	Wear and corrosion resistant coatings prepared on LY12 aluminum alloy by plasma electrolytic oxidation. Surface and Coatings Technology, 2021, 409, 126885.	4.8	23
85	Carbon-encapsulated nanosphere-assembled MoS2 nanosheets with large interlayer distance for flexible lithium-ion batteries. Journal of Solid State Electrochemistry, 2021, 25, 1657-1665.	2.5	8
86	Titania-zinc phosphate/nanocrystalline zinc composite coatings for corrosion protection of biomedical WE43 magnesium alloy. Surface and Coatings Technology, 2021, 410, 126940.	4.8	18
87	Improving exposure of anodically ordered Ni–Ti–O and corrosion resistance and biological properties of NiTi alloys by substrate electropolishing. Rare Metals, 2021, 40, 3575-3587.	7.1	17
88	Multi-functional gallium arsenide photonic crystal polarization splitter with a gold core. Modern Physics Letters B, 2021, 35, 2150229.	1.9	3
89	Effects of hydrogen etching on MnO2 electrode materials for supercapacitors. Surface and Coatings Technology, 2021, 410, 126951.	4.8	5
90	Effects of the tantalum intermediate layer on the nanomechanical properties and biocompatibility of nanostructured tantalum/tantalum nitride bilayer coating deposited by magnetron sputtering on the nickel titanium alloy. Applied Nanoscience (Switzerland), 2021, 11, 1867-1880.	3.1	5

#	Article	IF	CITATIONS
91	A composite coating with physical interlocking and chemical bonding on WE43 magnesium alloy for corrosion protection and cytocompatibility enhancement. Surface and Coatings Technology, 2021, 412, 127078.	4.8	22
92	A photonic quasi-crystal fiber composed of circular air holes with high birefringence and low confinement loss. Optik, 2021, 231, 166497.	2.9	3
93	Cost-effective liquid-junction solar devices with plasma-implanted Ni/TiN/CNF hierarchically structured nanofibers. Journal of Electroanalytical Chemistry, 2021, 887, 115167.	3.8	10
94	Corrosion Behavior and Biocompatibility of Diamond-like Carbon-Coated Zinc: An In Vitro Study. ACS Omega, 2021, 6, 9843-9851.	3.5	25
95	Substitution of quartz and clay with fly ash in the production of architectural ceramics: A mechanistic study. Ceramics International, 2021, 47, 12514-12525.	4.8	13
96	Enhanced Hydrogen Evolution Activity of Phosphorusâ€Rich Tungsten Phosphide by Cobalt Doping: A Comprehensive Study of the Active Sites and Electronic Structure. ChemElectroChem, 2021, 8, 1658-1664.	3.4	7
97	Investigation of a high-sensitivity surface plasmon resonance sensor based on the eccentric core quasi D-shape photonic quasi-crystal fiber. Journal of Modern Optics, 2021, 68, 555-563.	1.3	4
98	Optoelectronic Artificial Synapses Based on Two-Dimensional Transitional-Metal Trichalcogenide. ACS Applied Materials & Interfaces, 2021, 13, 30797-30805.	8.0	41
99	Characteristics of continuous high power magnetron sputtering (C-HPMS) in reactive O2/Ar atmospheres. Journal of Applied Physics, 2021, 129, .	2.5	3
100	Strategies to improve cobalt-based electrocatalysts for electrochemical water splitting. Journal of Catalysis, 2021, 398, 54-66.	6.2	58
101	Enhanced corrosion resistance and reduced cytotoxicity of the <scp>AZ91</scp> Mg alloy by plasma nitriding and a hierarchical structure composed of ciprofloxacinâ€loaded polymeric multilayers and calcium phosphate coating. Journal of Biomedical Materials Research - Part A, 2021, 109, 2657-2672.	4.0	6
102	Macroscale Superlubricity on Engineering Steel in the Presence of Black Phosphorus. Nano Letters, 2021, 21, 5308-5315.	9.1	42
103	Plasma-activated interfaces for biomedical engineering. Bioactive Materials, 2021, 6, 2134-2143.	15.6	17
104	Graphene-mediated ferromagnetic coupling in the nickel nano-islands/graphene hybrid. Science Advances, 2021, 7, .	10.3	12
105	Ni ₃ S ₂ Nanocomposite Structures Doped with Zn and Co as Long-Lifetime, High-Energy-Density, and Binder-Free Cathodes in Flexible Aqueous Nickel-Zinc Batteries. ACS Applied Materials & Interfaces, 2021, 13, 34292-34300.	8.0	29
106	Graphitic carbon nitride-based materials for photocatalytic antibacterial application. Materials Science and Engineering Reports, 2021, 145, 100610.	31.8	145
107	Optimization and cuttingâ€edge design of fuelâ€cell hybrid electric vehicles. International Journal of Energy Research, 2021, 45, 18392-18423.	4.5	44
108	Circular anti-resonance fibre supporting orbital angular momentum modes with flat dispersion, high purity and low confinement loss. Journal of Modern Optics, 2021, 68, 784-791.	1.3	17

#	Article	IF	CITATIONS
109	In situ construction of γ-MoC/VN heterostructured electrocatalysts with strong electron coupling for highly efficient hydrogen evolution reaction. Chemical Engineering Journal, 2021, 416, 129130.	12.7	31
110	Simultaneous application of diamond-like carbon coating and surface amination on polyether ether ketone: Towards superior mechanical performance and osseointegration. Smart Materials in Medicine, 2021, 2, 219-228.	6.7	28
111	Experimental and theoretical investigation of the control and balance of active sites on oxygen plasma-functionalized MoSe2 nanosheets for efficient hydrogen evolution reaction. Applied Catalysis B: Environmental, 2021, 288, 119983.	20.2	40
112	Programmed surface on poly(aryl-ether-ether-ketone) initiating immune mediation and fulfilling bone regeneration sequentially. Innovation(China), 2021, 2, 100148.	9.1	21
113	Engineering CsPbBr3 quantum dots with efficient luminescence and stability by damage-free encapsulation with a-SiCx:H. Journal of Luminescence, 2021, 236, 118086.	3.1	3
114	Facile synthesis of ZnO doped with Au nanoparticles for sensitive and reliable photoelectrochemical detection of glucose. Ionics, 2021, 27, 4449-4459.	2.4	3
115	GaO <i>_x</i> @GaN Nanowire Arrays on Flexible Graphite Paper with Tunable Persistent Photoconductivity. ACS Applied Materials & Interfaces, 2021, 13, 41916-41925.	8.0	4
116	TiO2 film supported by vertically aligned gold nanorod superlattice array for enhanced photocatalytic hydrogen evolution. Chemical Engineering Journal, 2021, 417, 127900.	12.7	23
117	Cationic Alternating Polypeptide Fixed on Polyurethane at Multiple Sites for Excellent Antibacterial and Antifouling Properties. Langmuir, 2021, 37, 10657-10667.	3.5	10
118	Three-dimensional nano/micro-structured porous MoP/CNTs microspheres as high-capacity anode for lithium-ion batteries. Journal of Alloys and Compounds, 2021, 872, 159608.	5.5	7
119	High efficient co-doping in plasma electrolytic oxidation to obtain long-term self-lubrication on Ti6Al4V. Tribology International, 2021, 160, 107018.	5.9	9
120	Regulation of extracellular bioactive cations in bone tissue microenvironment induces favorable osteoimmune conditions to accelerate in situ bone regeneration. Bioactive Materials, 2021, 6, 2315-2330.	15.6	69
121	Subsurface intercalation activating basal plane of black phosphorus for nitrogen reduction. Journal of Energy Chemistry, 2021, 60, 293-299.	12.9	8
122	Morphological modulation of cobalt selenide on carbon cloth by Ni doping for high-performance electrodes in supercapacitors. Colloids and Surfaces A: Physicochemical and Engineering Aspects, 2021, 624, 126818.	4.7	27
123	Fabrication of Bimetallic Oxides (MCo2O4: M=Cu, Mn) on Ordered Microchannel Electro-Conductive Plate for High-Performance Hybrid Supercapacitors. Sustainability, 2021, 13, 9896.	3.2	11
124	Porous manganese dioxide nanosheets on modified graphite felt for cathodes in high-capacity flexible Zinc-MnO2 batteries. Vacuum, 2021, 191, 110353.	3.5	10
125	Enhancement of unidirectional forward scattering and suppression of backward scattering in hollow silicon nanoblocks. Applied Optics, 2021, 60, 8737.	1.8	1
126	Degradation of tetracycline in water by gas–liquid plasma in conjunction with rGO-TiO ₂ nanocomposite. Plasma Science and Technology, 2021, 23, 115503.	1.5	5

#	Article	IF	CITATIONS
127	High-sensitivity methane sensor composed of photonic quasi-crystal fiber based on surface plasmon resonance. Journal of the Optical Society of America A: Optics and Image Science, and Vision, 2021, 38, 1438.	1.5	11
128	Plasma-activated thermosensitive biogel as an exogenous ROS carrier for post-surgical treatment of cancer. Biomaterials, 2021, 276, 121057.	11.4	37
129	Insights into enhancement of photocatalytic properties of g-C3N4 by local electric field induced by polarization of MgO(111). Journal of Environmental Chemical Engineering, 2021, 9, 105922.	6.7	13
130	In vitro and in vivo antibacterial performance of Zr & O PIII magnesium alloys with high concentration of oxygen vacancies. Bioactive Materials, 2021, 6, 3049-3061.	15.6	12
131	Waste-glass-derived silicon/CNTs composite with strong Si-C covalent bonding for advanced anode materials in lithium-ion batteries. Applied Surface Science, 2021, 563, 150280.	6.1	25
132	Development and application of fuel cells in the automobile industry. Journal of Energy Storage, 2021, 42, 103124.	8.1	91
133	Experimental and theoretical investigation of reconstruction and active phases on honeycombed Ni3N-Co3N/C in water splitting. Applied Catalysis B: Environmental, 2021, 297, 120461.	20.2	62
134	A high-performance electrocatalyst composed of nickel clusters encapsulated with a carbon network on TiN nanaowire arrays for the oxygen evolution reaction. Applied Surface Science, 2021, 567, 150779.	6.1	25
135	Hybrid photovoltaic-triboelectric nanogenerators for simultaneously harvesting solar and mechanical energies. Nano Energy, 2021, 89, 106376.	16.0	31
136	Co-doped Ni3S2 porous nanocones as high-performance bifunctional electrocatalysts in water splitting. Chemical Engineering Journal, 2021, 425, 130455.	12.7	42
137	A water-soluble membrane for SARS-CoV-2 viral nucleic acid sampling and detection. Nanoscale, 2021, 13, 18084-18088.	5.6	1
138	MXene Coatings: Novel Hydrogen Permeation Barriers for Pipe Steels. Nanomaterials, 2021, 11, 2737.	4.1	9
139	Activating Carbon Nitride by BP@Ni for the Enhanced Photocatalytic Hydrogen Evolution and Selective Benzyl Alcohol Oxidation. ACS Applied Materials & amp; Interfaces, 2021, 13, 50988-50995.	8.0	14
140	ZnL ₂ -BPs Integrated Bone Scaffold under Sequential Photothermal Mediation: A Win–Win Strategy Delivering Antibacterial Therapy and Fostering Osteogenesis Thereafter. ACS Nano, 2021, 15, 17854-17869.	14.6	85
141	Efficient photonic crystal fiber polarization splitters composed of gallium arsenide and nematic liquid crystals. Modern Physics Letters B, 2021, 35, 2150077.	1.9	2
142	Surface plasmon resonance chemical sensor composed of a microstructured optical fiber for the detection of an ultra-wide refractive index range and gas-liquid pollutants. Optics Express, 2021, 29, 40734.	3.4	68
143	Efficient coupling of MnO ₂ /TiN on carbon cloth positive electrode and Fe ₂ O ₃ /TiN on carbon cloth negative electrode for flexible ultra-fast hybrid supercapacitors. RSC Advances, 2021, 11, 35726-35736.	3.6	8
144	Graphene for Energy Storage and Conversion: Synthesis and Interdisciplinary Applications. Electrochemical Energy Reviews, 2020, 3, 395-430.	25.5	59

#	Article	IF	CITATIONS
145	Synthesis of tetragonal prismatic Î ³ -In2Se3 nanostructures with predominantly {110} facets and photocatalytic degradation of tetracycline. Applied Catalysis B: Environmental, 2020, 260, 118218.	20.2	65
146	Corrosion behavior of functionally graded and self-healing nanostructured TiO2–Al2O3 - Benzotriazole coatings deposited on AA 2024-T3 by the sol-gel method. Materials Chemistry and Physics, 2020, 240, 122233.	4.0	23
147	Fundamentals and applications of surface-enhanced Raman spectroscopy–based biosensors. Current Opinion in Biomedical Engineering, 2020, 13, 51-59.	3.4	82
148	Reconstructed chitosan with alkylamine for enhanced gene delivery by promoting endosomal escape. Carbohydrate Polymers, 2020, 227, 115339.	10.2	31
149	A bifunctional hydrogel incorporated with CuS@MoS2 microspheres for disinfection and improved wound healing. Chemical Engineering Journal, 2020, 382, 122849.	12.7	124
150	Modulation of the mechanosensing of mesenchymal stem cells by laser-induced patterning for the acceleration of tissue reconstruction through the Wnt/β-catenin signaling pathway activation. Acta Biomaterialia, 2020, 101, 152-167.	8.3	51
151	EIS and noise study of zirconia-alumina- benzotriazole nano-composite coating applied on Al2024 by the sol-gel method. Journal of Alloys and Compounds, 2020, 816, 152662.	5.5	11
152	Selfâ€Regulated Superâ€Hydrophobic Cu/CuO Electrode Film Deposited by One‣tep Highâ€Power Sputtering. Advanced Electronic Materials, 2020, 6, 1900891.	5.1	10
153	Ultrathin carbon layer-encapsulated TiN nanotubes array with enhanced capacitance and electrochemical stability for supercapacitors. Applied Surface Science, 2020, 503, 144293.	6.1	19
154	Nonleaching Antibacterial Concept Demonstrated by In Situ Construction of 2D Nanoflakes on Magnesium. Advanced Science, 2020, 7, 1902089.	11.2	39
155	Graphite felt incorporated with MoS2/rGO for electrochemical detoxification of high-arsenic fly ash. Chemical Engineering Journal, 2020, 382, 122763.	12.7	20
156	Modeling and plasma characteristics of high-power direct current discharge. Plasma Sources Science and Technology, 2020, 29, 025016.	3.1	13
157	Dual light-induced <i>in situ</i> antibacterial activities of biocompatibleTiO ₂ /MoS ₂ /PDA/RGD nanorod arrays on titanium. Biomaterials Science, 2020, 8, 391-404.	5.4	44
158	Rapid and scalable production of high-quality phosphorene by plasma–liquid technology. Chemical Communications, 2020, 56, 221-224.	4.1	24
159	A hybrid Co NPs@CNT nanocomposite as highly efficient electrocatalyst for oxygen evolution reaction. Applied Surface Science, 2020, 507, 145155.	6.1	34
160	Atomic-Scale Intercalation of Graphene Layers into MoSe ₂ Nanoflower Sheets as a Highly Efficient Catalyst for Hydrogen Evolution Reaction. ACS Applied Materials & Interfaces, 2020, 12, 2460-2468.	8.0	47
161	In situ formation of N-doped carbon-coated porous MoP nanowires: a highly efficient electrocatalyst for hydrogen evolution reaction in a wide pH range. Applied Catalysis B: Environmental, 2020, 263, 118358.	20.2	112
162	Tuning the surface immunomodulatory functions of polyetheretherketone for enhanced osseointegration. Biomaterials, 2020, 230, 119642.	11.4	100

#	Article	IF	CITATIONS
163	Analysis of defect states in optical microcavities based on the photonic quantum well structure. Optics Communications, 2020, 458, 124880.	2.1	1
164	Numerical analysis of a high-birefringent photonic quasi-crystal fiber with circular air holes. Optik, 2020, 207, 163850.	2.9	2
165	Recent advances of two-dimensional transition metal nitrides for energy storage and conversion applications. FlatChem, 2020, 19, 100149.	5.6	54
166	Hollow Spheres Consisting of SnS Nanosheets Conformally Coated with Sâ€Doped Carbon for Advanced Lithium…Sodiumâ€Ion Battery Anodes. ChemElectroChem, 2020, 7, 914-921.	3.4	20
167	Dimensional-dependent antibacterial behavior on bioactive micro/nano polyetheretherketone (PEEK) arrays. Chemical Engineering Journal, 2020, 392, 123736.	12.7	64
168	Freestanding, Hierarchical, and Porous Bilayered Na _{<i>x</i>} V ₂ O ₅ · <i>n</i> H ₂ O/rGO/CNT Composites as High-Performance Cathode Materials for Nonaqueous K-Ion Batteries and Aqueous Zinc-Ion Batteries. ACS Applied Materials & amp; Interfaces, 2020, 12, 706-716.	8.0	82
169	2D black phosphorus dotted with silver nanoparticles: An excellent lubricant additive for tribological applications. Chemical Engineering Journal, 2020, 392, 123631.	12.7	115
170	Biodegradable Bi ₂ O ₂ Se Quantum Dots for Photoacoustic Imagingâ€Guided Cancer Photothermal Therapy. Small, 2020, 16, e1905208.	10.0	56
171	Hierarchical micro-flowers self-assembled from SnS monolayers and nitrogen-doped graphene lamellar nanosheets as advanced anode for lithium-ion battery. Electrochimica Acta, 2020, 331, 135292.	5.2	24
172	Recent Progress in Electrode Materials for Nonaqueous Lithium-Ion Capacitors. Journal of Nanoscience and Nanotechnology, 2020, 20, 2652-2667.	0.9	14
173	Wrinkledâ€Surfaceâ€Induced Memristive Behavior of MoS 2 Wrapped GaN Nanowires. Advanced Electronic Materials, 2020, 6, 2000571.	5.1	4
174	Study of TiAlN coatings deposited by continuous high power magnetron sputtering (C-HPMS). Surface and Coatings Technology, 2020, 402, 126315.	4.8	13
175	From Octahedron Crystals to 2D Silicon Nanosheets: Facetâ€Selective Cleavage and Biophotonic Applications. Small, 2020, 16, e2003594.	10.0	11
176	Calcium phosphate coating on biomedical WE43 magnesium alloy pretreated with a magnesium phosphate layer for corrosion protection. Surface and Coatings Technology, 2020, 401, 126248.	4.8	26
177	Gate-tunable two-dimensional superconductivity revealed in flexible wafer-scale hybrid structures. Journal of Materials Chemistry C, 2020, 8, 14605-14610.	5.5	4
178	Robust and durable surperhydrophobic F-DLC coating for anti-icing in aircrafts engineering. Surface and Coatings Technology, 2020, 404, 126468.	4.8	23
179	Surface plasmon resonance sensor based on coupling effects of dual photonic crystal fibers for low refractive indexes detection. Results in Physics, 2020, 18, 103240.	4.1	60
180	Pd/ZnO/Ni photoelectrochemical ethanol sensor. Journal of Photochemistry and Photobiology A: Chemistry, 2020, 401, 112785.	3.9	5

#	Article	IF	CITATIONS
181	Mediated Drug Release from Nanovehicles by Black Phosphorus Quantum Dots for Efficient Therapy of Chronic Obstructive Pulmonary Disease. Angewandte Chemie - International Edition, 2020, 59, 20568-20576.	13.8	56
182	Calcium Phosphate Mineralized Black Phosphorous with Enhanced Functionality and Anticancer Bioactivity. Advanced Functional Materials, 2020, 30, 2003069.	14.9	42
183	Flexible Surface-Enhanced Raman Scattering Chip: A Universal Platform for Real-Time Interfacial Molecular Analysis with Femtomolar Sensitivity. ACS Applied Materials & Interfaces, 2020, 12, 54174-54180.	8.0	27
184	A hollow dual-core PCF-SPR sensor with gold layers on the inner and outer surfaces of the thin cladding. Results in Optics, 2020, 1, 100004.	2.0	31
185	Needle-like CoO nanowire composites with NiO nanosheets on carbon cloth for hybrid flexible supercapacitors and overall water splitting electrodes. RSC Advances, 2020, 10, 37489-37499.	3.6	23
186	Insight into the overpotentials of electrocatalytic hydrogen evolution on black phosphorus decorated with metal clusters. Electrochimica Acta, 2020, 358, 136902.	5.2	9
187	Nitrogen-doped carbon coated TiC nanofiber arrays deposited on Ti-6Al-4V for selective and sensitive electrochemical detection of dopamine. Surface and Coatings Technology, 2020, 402, 126266.	4.8	3
188	Intercalator-assisted plasma-liquid technology: an efficient exfoliation method for few-layer two-dimensional materials. Science China Materials, 2020, 63, 2079-2085.	6.3	5
189	Zirconium-based nanostructured coating on the Mg-4Y-3RE alloy for corrosion retardation. Chemical Physics Letters, 2020, 756, 137824.	2.6	10
190	Formation of self-layered hydrothermal coating on magnesium aided by titanium ion implantation: Synergistic control of corrosion resistance and cytocompatibility. Surface and Coatings Technology, 2020, 401, 126251.	4.8	21
191	Hierarchical binder-free MnO2/TiO2 composite nanostructure on flexible seed graphite felt for high-performance supercapacitors. Vacuum, 2020, 181, 109648.	3.5	22
192	In-Situ Synthesis of Heterostructured Carbon-Coated Co/MnO Nanowire Arrays for High-Performance Anodes in Asymmetric Supercapacitors. Molecules, 2020, 25, 3218.	3.8	9
193	Mediated Drug Release from Nanovehicles by Black Phosphorus Quantum Dots for Efficient Therapy of Chronic Obstructive Pulmonary Disease. Angewandte Chemie, 2020, 132, 20749-20757.	2.0	8
194	Forward and Backward Unidirectional Scattering by the Core-Shell Nanocube Dimer with Balanced Gain and Loss. Nanomaterials, 2020, 10, 1440.	4.1	3
195	Tuning surface topographies on biomaterials to control bacterial infection. Biomaterials Science, 2020, 8, 6840-6857.	5.4	44
196	Recent advance and prospectives of electrocatalysts based on transition metal selenides for efficient water splitting. Nano Energy, 2020, 78, 105234.	16.0	250
197	Influence of Acetylene on Ti Target Poisoning During Pulse-Enhanced Vacuum Arc Evaporation. IEEE Transactions on Plasma Science, 2020, 48, 2799-2809.	1.3	0
198	A tailored positively-charged hydrophobic surface reduces the risk of implant associated infections. Acta Biomaterialia, 2020, 114, 421-430.	8.3	22

#	Article	IF	CITATIONS
199	Composite plates utilizing dealkalized red mud, acid leaching slag and dealkalized red mud-fly ash: Preparation and performance comparison. Construction and Building Materials, 2020, 261, 120495.	7.2	16
200	Phaseâ€Changing Microcapsules Incorporated with Black Phosphorus for Efficient Solar Energy Storage. Advanced Science, 2020, 7, 2000602.	11.2	95
201	Enhanced discharge and surface properties of TiSiCN coatings deposited by pulse-enhanced vacuum arc evaporation. Surface and Coatings Technology, 2020, 403, 126413.	4.8	13
202	Biofunctional Elements Incorporated Nano/Microstructured Coatings on Titanium Implants with Enhanced Osteogenic and Antibacterial Performance. Advanced Healthcare Materials, 2020, 9, e2000681.	7.6	42
203	A Quantitative Bacteria Monitoring and Killing Platform Based on Electron Transfer from Bacteria to a Semiconductor. Advanced Materials, 2020, 32, e2003616.	21.0	31
204	Corrosion Behavior and Mechanism of Carbon Ion-Implanted Magnesium Alloy. Coatings, 2020, 10, 734.	2.6	7
205	Ambipolar Plasmonâ€Enhanced Photodetector Built on Germanium Nanodots Array/Graphene Hybrid. Advanced Materials Interfaces, 2020, 7, 2001122.	3.7	10
206	Enhanced Osteogenic Differentiation of Human Mesenchymal Stem Cells on Amine-Functionalized Titanium Using Humidified Ammonia Supplied Nonthermal Atmospheric Pressure Plasma. International Journal of Molecular Sciences, 2020, 21, 6085.	4.1	10
207	NiFe-Layered Double Hydroxide Synchronously Activated by Heterojunctions and Vacancies for the Oxygen Evolution Reaction. ACS Applied Materials & amp; Interfaces, 2020, 12, 42850-42858.	8.0	105
208	Design of bimetal-coated photonic crystal fiber filter based on surface plasmon resonance. Results in Optics, 2020, 1, 100027.	2.0	9
209	Hierarchical 0Dâ^'2D Co/Mo Selenides as Superior Bifunctional Electrocatalysts for Overall Water Splitting. Frontiers in Chemistry, 2020, 8, 382.	3.6	36
210	High-Potential surface on zirconia ceramics for bacteriostasis and biocompatibility. Colloids and Surfaces B: Biointerfaces, 2020, 193, 111074.	5.0	9
211	Photochemical Activity of Black Phosphorus for Nearâ€Infrared Light Controlled In Situ Biomineralization. Advanced Science, 2020, 7, 2000439.	11.2	51
212	Design and synthesis of dendritic Co3O4@Co2(CO3)(OH)2 nanoarrays on carbon cloth for high-performance supercapacitors. Journal of Materials Science, 2020, 55, 12091-12102.	3.7	33
213	Effects of Ion Energy and Density on the Plasma Etchingâ€Induced Surface Area, Edge Electrical Field, and Multivacancies in MoSe ₂ Nanosheets for Enhancement of the Hydrogen Evolution Reaction. Small, 2020, 16, e2001470.	10.0	38
214	Strain-enhanced power conversion efficiency of a BP/SnSe van der Waals heterostructure. Physical Chemistry Chemical Physics, 2020, 22, 14787-14795.	2.8	21
215	Crystalline Red Phosphorus Nanoribbons: Large‣cale Synthesis and Electrochemical Nitrogen Fixation. Angewandte Chemie, 2020, 132, 14489-14493.	2.0	9
216	Sensitive and selective ctDNA detection based on functionalized black phosphorus nanosheets. Biosensors and Bioelectronics, 2020, 165, 112384.	10.1	32

#	Article	IF	CITATIONS
217	Wafer-scale growth of single-crystal graphene on vicinal Ge(001) substrate. Nano Today, 2020, 34, 100908.	11.9	23
218	Crystalline Red Phosphorus Nanoribbons: Large‣cale Synthesis and Electrochemical Nitrogen Fixation. Angewandte Chemie - International Edition, 2020, 59, 14383-14387.	13.8	58
219	Biomimetic osteogenic peptide with mussel adhesion and osteoimmunomodulatory functions to ameliorate interfacial osseointegration under chronic inflammation. Biomaterials, 2020, 255, 120197.	11.4	103
220	Nanopatterned silk-coated AZ31 magnesium alloy with enhanced antibacterial and corrosion properties. Materials Science and Engineering C, 2020, 116, 111173.	7.3	23
221	Interface Engineering-Assisted 3D-Graphene/Germanium Heterojunction for High-Performance Photodetectors. ACS Applied Materials & Interfaces, 2020, 12, 15606-15614.	8.0	33
222	Twoâ€Dimensional Transition Metal Chalcogenides for Alkali Metal Ions Storage. ChemSusChem, 2020, 13, 1114-1154.	6.8	69
223	Surface plasmon resonance sensor based on photonic crystal fiber with indium tin oxide film. Optical Materials, 2020, 102, 109800.	3.6	70
224	Vertical kinetically oriented MoS ₂ –Mo ₂ N heterostructures on carbon cloth: a highly efficient hydrogen evolution electrocatalyst. Sustainable Energy and Fuels, 2020, 4, 2201-2207.	4.9	28
225	Photoluminescence Properties of GaN Nanowires Grown in a Gradient-Plasma Environment. Journal of Physical Chemistry C, 2020, 124, 16002-16008.	3.1	2
226	Dynamic changes of hydrophobic behavior during icing. Surface and Coatings Technology, 2020, 397, 126043.	4.8	10
227	Structural engineering of hierarchically hetestructured Mo2C/Co conformally embedded in carbon for efficient water splitting. International Journal of Hydrogen Energy, 2020, 45, 22629-22637.	7.1	21
228	Toroidal dipole and magnetic multipole excitations from the same nanostructure with different direction of electric dipole emitters. Applied Physics A: Materials Science and Processing, 2020, 126, 1.	2.3	1
229	A zipped-up tunable metal coordinated cationic polymer for nanomedicine. Journal of Materials Chemistry B, 2020, 8, 1350-1358.	5.8	4
230	Surface plasmon resonance (SPR) infrared sensor based on D-shape photonic crystal fibers with ITO coatings. Optics Communications, 2020, 464, 125496.	2.1	157
231	Enhanced Peltier Effect in Wrinkled Graphene Constriction by Nanoâ€Bubble Engineering. Small, 2020, 16, e1907170.	10.0	19
232	Nano-second temporal particle behavior in high-power impulse magnetron sputtering discharge in a cylindrical cathode. Journal of Applied Physics, 2020, 127, 023301.	2.5	3
233	3D printing of hydrogels: Rational design strategies and emerging biomedical applications. Materials Science and Engineering Reports, 2020, 140, 100543.	31.8	494
234	Multiple flocculant prepared with dealkalized red mud and fly ash: Properties and characterization. Journal of Water Process Engineering, 2020, 34, 101173.	5.6	15

#	Article	IF	CITATIONS
235	Near-infrared surface plasmon resonance sensor based on photonic crystal fiber with big open rings. Optik, 2020, 207, 164466.	2.9	41
236	Edge-Rich Black Phosphorus for Photocatalytic Nitrogen Fixation. Journal of Physical Chemistry Letters, 2020, 11, 1052-1058.	4.6	57
237	Improving the performance of light-emitting diodes via plasmonic-based strategies. Journal of Applied Physics, 2020, 127, .	2.5	30
238	Corrosion-resistant plasma electrolytic oxidation coating modified by Zinc phosphate and self-healing mechanism in the salt-spray environment. Surface and Coatings Technology, 2020, 384, 125321.	4.8	24
239	Comparative study of TiAlN coatings deposited by different high-ionization physical vapor deposition techniques. Ceramics International, 2020, 46, 10814-10819.	4.8	19
240	Photoelectrochemical Synthesis of Ammonia with Black Phosphorus. Advanced Functional Materials, 2020, 30, 2002731.	14.9	69
241	Effects of Ti, Ni, and Dual Ti/Ni Plasma Immersion Ion Implantation on the Corrosion and Wear Properties of Magnesium Alloy. Coatings, 2020, 10, 313.	2.6	12
242	Ultrathin hybrid nanobelts of single-crystalline VO2 and Poly(3,4-ethylenedioxythiophene) as cathode materials for aqueous zinc ion batteries with large capacity and high-rate capability. Journal of Power Sources, 2020, 463, 228223.	7.8	65
243	Articular cartilage inspired bilayer coating on Ti6Al4V alloy with low friction and high load-bearing properties. Applied Surface Science, 2020, 515, 146065.	6.1	13
244	Electronic Modulation between Tungsten Nitride and Cobalt Dopants for Enhanced Hydrogen Evolution Reaction at a Wide Range of pH. ChemCatChem, 2020, 12, 2962-2966.	3.7	20
245	Self-assembled anodization of NiTi alloys for biomedical applications. Applied Surface Science, 2020, 517, 146118.	6.1	67
246	Bioactive phospho-therapy with black phosphorus for <i>in vivo</i> tumor suppression. Theranostics, 2020, 10, 4720-4736.	10.0	26
247	Ultrafine Co nanodots embedded in N-doped carbon nanotubes grafted on hexagonal VN for highly efficient overall water splitting. Nano Energy, 2020, 73, 104788.	16.0	71
248	A novel self-branching MnCo2O4/ nanographene hybrid composites on macroporous electrically conductive network as bifunctional electrodes for boosting miniature supercapacitors and sodium ion batteries. Journal of Alloys and Compounds, 2020, 846, 155720.	5.5	24
249	High-sensitivity SPR sensor based on the eightfold eccentric core PQF with locally coated indium tin oxide. Applied Optics, 2020, 59, 6484.	1.8	10
250	Ag as Cocatalyst and Electron-Hole Medium in CeO2 QDs/Ag/Ag2Se Z-scheme Heterojunction Enhanced the Photo-Electrocatalytic Properties of the Photoelectrode. Nanomaterials, 2020, 10, 253.	4.1	17
251	Single-polarization photonic crystal fiber filter composed of elliptical gold films. Optical Engineering, 2020, 59, 1.	1.0	4
252	Ultra-sensitive hexagonal PCF-SPR sensor with a broad detection range. Journal of Modern Optics, 2020, 67, 1545-1554.	1.3	9

#	Article	IF	CITATIONS
253	Black Phosphorus: Bioactive Nanomaterials with Inherent and Selective Chemotherapeutic Effects. Angewandte Chemie, 2019, 131, 779-784.	2.0	34
254	Enhanced mechanical and electrochemical properties of TiNx thin films prepared by magnetron sputtering with an anode layer ion source. Surface and Coatings Technology, 2019, 365, 253-260.	4.8	6
255	Biaxially strained germanium micro-dot array by hydrogen ion implantation. Surface and Coatings Technology, 2019, 365, 248-252.	4.8	1
256	High-performance anode materials based on 3D orderly and vertically macroporous graphene-Si framework for Li-ion batteries. Ionics, 2019, 25, 467-473.	2.4	4
257	In situ formation of porous TiO2 nanotube array with MgTiO3 nanoparticles for enhanced photocatalytic activity. Surface and Coatings Technology, 2019, 365, 222-226.	4.8	10
258	Effects of ion flux density and energy on the composition of TiNx thin films prepared by magnetron sputtering with an anode layer ion source. Surface and Coatings Technology, 2019, 365, 58-64.	4.8	8
259	Orthopedic Implants. , 2019, , 425-439.		47
260	Antibacterial and Cytocompatible Nanoengineered Silk-Based Materials for Orthopedic Implants and Tissue Engineering. ACS Applied Materials & Interfaces, 2019, 11, 31605-31614.	8.0	27
261	Electrostatic Self-Assembly of Ti ₃ C ₂ T _{<i>x</i>} MXene and Gold Nanorods as an Efficient Surface-Enhanced Raman Scattering Platform for Reliable and High-Sensitivity Determination of Organic Pollutants. ACS Sensors, 2019, 4, 2303-2310.	7.8	106
262	Ex-centric core photonic crystal fiber sensor with gold nanowires based on surface plasmon resonance. Optik, 2019, 196, 163173.	2.9	34
263	NiFeP nanoflakes composite with CoP on carbon cloth as flexible and durable electrocatalyst for efficient overall water splitting. Nanotechnology, 2019, 30, 485402.	2.6	9
264	Nano-mechanical properties of zirconia-alumina-benzotriazole nano-composite coating deposited on Al2024 by the sol-gel method. Thin Solid Films, 2019, 689, 137417.	1.8	10
265	The single-polarization filter composed of gold-coated photonic crystal fiber. Physics Letters, Section A: General, Atomic and Solid State Physics, 2019, 383, 3200-3206.	2.1	32
266	Rapid synthesis, microstructure, and thermoelectric properties of skutterudites. Journal of Alloys and Compounds, 2019, 806, 537-542.	5.5	10
267	A functionalized TiO2/Mg2TiO4 nano-layer on biodegradable magnesium implant enables superior bone-implant integration and bacterial disinfection. Biomaterials, 2019, 219, 119372.	11.4	84
268	Transfer matrix method for simulation of the fiber Bragg grating in polarization maintaining fiber. Optics Communications, 2019, 452, 185-188.	2.1	11
269	Interconnected nanoporous carbon structure delivering enhanced mass transport and conductivity toward exceptional performance in supercapacitor. Journal of Power Sources, 2019, 435, 226811.	7.8	24
270	Al2O3 coating for densification of SiC ceramics and sintering kinetics. Surface and Coatings Technology, 2019, 374, 603-609.	4.8	10

#	Article	lF	CITATIONS
271	Corrosion behavior of ZnO-reinforced coating on aluminum alloy prepared by plasma electrolytic oxidation. Surface and Coatings Technology, 2019, 374, 1015-1023.	4.8	20
272	Effect of Ti interlayer on corrosion behavior of nanostructured Ti/TiN multilayer coating deposited on TiAl ₆ V ₄ . Materials and Corrosion - Werkstoffe Und Korrosion, 2019, 70, 2113-2127.	1.5	6
273	Unique Role of Arginine in Positivelyâ€Charged Surface for Promotion of Antibacterial and Osteogenetic Capabilities. Advanced Materials Interfaces, 2019, 6, 1901414.	3.7	4
274	Rapid Activation of Platinum with Black Phosphorus for Efficient Hydrogen Evolution. Angewandte Chemie - International Edition, 2019, 58, 19060-19066.	13.8	79
275	Tungstenâ€Ðoped CoP Nanoneedle Arrays Grown on Carbon Cloth as Efficient Bifunctional Electrocatalysts for Overall Water Splitting. ChemElectroChem, 2019, 6, 5229-5236.	3.4	36
276	Influence of plasma excitation power on mechanical property and biocompatibility of titania/alumina composite thin films for medical implant prepared by magnetron sputtering. Materials Research Express, 2019, 6, 116418.	1.6	0
277	Facile mass production of self-supported two-dimensional transition metal oxides for catalytic applications. Chemical Communications, 2019, 55, 11406-11409.	4.1	10
278	Localized Surface Plasmon Resonance Properties of Concentric Dual-Ring Nanodisk. Nano, 2019, 14, 1950071.	1.0	0
279	3D-printed nanocomposite scaffolds with tunable magnesium ionic microenvironment induce in situ bone tissue regeneration. Applied Materials Today, 2019, 16, 493-507.	4.3	43
280	Enhanced oxygen-induced properties of bulk oxygenated amorphous carbon films deposited with an an anode layer ion source. Vacuum, 2019, 169, 108915.	3.5	9
281	A surface-engineered multifunctional TiO2 based nano-layer simultaneously elevates the corrosion resistance, osteoconductivity and antimicrobial property of a magnesium alloy. Acta Biomaterialia, 2019, 99, 495-513.	8.3	38
282	Modulation of Phosphorene for Optimal Hydrogen Evolution Reaction. ACS Applied Materials & Interfaces, 2019, 11, 37787-37795.	8.0	38
283	Effects of Benzotriazole on nano-mechanical properties of zirconia–alumina–Benzotriazole nanocomposite coating deposited on Al 2024 by the sol–gel method. Applied Physics A: Materials Science and Processing, 2019, 125, 1.	2.3	13
284	Synthesis of high-quality black phosphorus sponges for all-solid-state supercapacitors. Materials Horizons, 2019, 6, 176-181.	12.2	53
285	Recent progress of transition metal nitrides for efficient electrocatalytic water splitting. Sustainable Energy and Fuels, 2019, 3, 366-381.	4.9	305
286	Discharge and Deposition Characteristics of High-Power Impulse Magnetron Sputtering Using Various Target Materials. IEEE Transactions on Plasma Science, 2019, 47, 193-198.	1.3	12
287	Synergistic Antibacterial Activity of Black Phosphorus Nanosheets Modified with Titanium Aminobenzenesulfanato Complexes. ACS Applied Nano Materials, 2019, 2, 1202-1209.	5.0	36
288	Achieving an acid resistant surface on magnesium alloy via bio-inspired design. Applied Surface Science, 2019, 478, 150-161.	6.1	60

#	Article	IF	CITATIONS
289	Modulation of resistive switching in Pt/LiCoO2/SiO2/Si stacks. Journal of Materials Science: Materials in Electronics, 2019, 30, 4753-4759.	2.2	2
290	Asymmetrical photonic crystal fiber based on the surface plasmon resonance sensor and analysis by the lower-birefringence peak method. Optik, 2019, 189, 121-129.	2.9	3
291	Inherent Chemotherapeutic Antiâ€Cancer Effects of Lowâ€Dimensional Nanomaterials. Chemistry - A European Journal, 2019, 25, 10995-11006.	3.3	17
292	A quasi-2D material CePO4 and the self-lubrication in micro-arc oxidized coatings on Al alloy. Tribology International, 2019, 138, 157-165.	5.9	12
293	InSe Nanosheets for Efficient NIR-II-Responsive Drug Release. ACS Applied Materials & Interfaces, 2019, 11, 27521-27528.	8.0	30
294	Stability and Repeatability of a Karst-like Hierarchical Porous Silicon Oxide-Based Memristor. ACS Applied Materials & Interfaces, 2019, 11, 21734-21740.	8.0	24
295	Ultrafast Synthesis of Te-Doped CoSb ₃ with Excellent Thermoelectric Properties. ACS Applied Energy Materials, 2019, 2, 4477-4485.	5.1	25
296	Multifunctional nitrogen-doped nanoporous carbons derived from metal–organic frameworks for efficient CO ₂ storage and high-performance lithium-ion batteries. New Journal of Chemistry, 2019, 43, 10405-10412.	2.8	12
297	Optical and Optoelectronic Properties of Black Phosphorus and Recent Photonic and Optoelectronic Applications. Small Methods, 2019, 3, 1900165.	8.6	68
298	General synthesis of NiCo alloy nanochain arrays with thin oxide coating: a highly efficient bifunctional electrocatalyst for overall water splitting. Journal of Alloys and Compounds, 2019, 797, 1216-1223.	5.5	56
299	Dual-band unidirectional forward scattering of Au–Si sliced nanorod in the visible region. Applied Physics A: Materials Science and Processing, 2019, 125, 1.	2.3	4
300	Hybrid ZnO–graphene electrode with palladium nanoparticles on Ni foam and application to self-powered nonenzymatic glucose sensing. RSC Advances, 2019, 9, 12134-12145.	3.6	16
301	Biochar/struvite composite as a novel potential material for slow release of N and P. Environmental Science and Pollution Research, 2019, 26, 17152-17162.	5.3	20
302	Formation of ultra-small Mn3O4 nanoparticles trapped in nanochannels of hollow carbon spheres by nanoconfinement with excellent supercapacitor performance. International Journal of Hydrogen Energy, 2019, 44, 13675-13683.	7.1	17
303	Bioactive inorganic-ion-doped titania nanotube coatings on bone implants with enhanced osteogenic activity and antibacterial properties. , 2019, , 401-427.		2
304	Simultaneous texturing and conductivity tailoring of mesoporous NaTi2(PO4)3 nanocrystals by gadolinium doping for enhanced Na storage. Electrochimica Acta, 2019, 309, 177-186.	5.2	19
305	Optical diode composed of subwavelength slit-groove arrays with ultrahigh transmission contrast based on surface plasmon polariton. Optik, 2019, 186, 266-274.	2.9	3
306	N-doped TiO ₂ nanotube arrays with uniformly embedded Co _x P nanoparticles for high-efficiency hydrogen evolution reaction. RSC Advances, 2019, 9, 11676-11682.	3.6	9

#	Article	IF	CITATIONS
307	Investigation of corrosion mechanism of NiTi modified by carbon plasma immersion ion implantation (C-PIII) by electrochemical impedance spectroscopy. Journal of Alloys and Compounds, 2019, 790, 1067-1075.	5.5	14
308	Template growth of Au/Ag nanocomposites on phosphorene for sensitive SERS detection of pesticides. Nanotechnology, 2019, 30, 275604.	2.6	15
309	Octahedral SnO ₂ /Graphene Composites with Enhanced Gas-Sensing Performance at Room Temperature. ACS Applied Materials & Interfaces, 2019, 11, 12958-12967.	8.0	54
310	Vanadium Dioxide Nanocoating Induces Tumor Cell Death through Mitochondrial Electron Transport Chain Interruption. Global Challenges, 2019, 3, 1800058.	3.6	33
311	A high-birefringent photonic quasi-crystal fiber with two elliptical air holes. Optik, 2019, 184, 10-15.	2.9	10
312	A Novel Hybrid‣ayered Organic Phototransistor Enables Efficient Intermolecular Charge Transfer and Carrier Transport for Ultrasensitive Photodetection. Advanced Materials, 2019, 31, e1900763.	21.0	89
313	Lithium ion trapping mechanism of SiO2 in LiCoO2 based memristors. Scientific Reports, 2019, 9, 5081.	3.3	14
314	Inconel 718 treated with two-stage solution and aging processes: microstructure evolution and enhanced properties. Materials Research Express, 2019, 6, 075803.	1.6	8
315	Modification of Layered Graphitic Carbon Nitride by Nitrogen Plasma for Improved Electrocatalytic Hydrogen Evolution. Nanomaterials, 2019, 9, 568.	4.1	14
316	Direct Synthesis of Metalâ€Doped Phosphorene with Enhanced Electrocatalytic Hydrogen Evolution. Small Methods, 2019, 3, 1900083.	8.6	56
317	A surface-engineered polyetheretherketone biomaterial implant with direct and immunoregulatory antibacterial activity against methicillin-resistant Staphylococcus aureus. Biomaterials, 2019, 208, 8-20.	11.4	122
318	Controlled fiberization of dipeptide in merging phases leads to collagen-level strength and opto/electric mechanofunctionalities. Biomaterials, 2019, 208, 1-7.	11.4	4
319	Ecofriendly and Biodegradable Soybean Protein Isolate Films Incorporated with ZnO Nanoparticles for Food Packaging. ACS Applied Bio Materials, 2019, 2, 2202-2207.	4.6	42
320	Scalable synthesis of ant-nest-like bulk porous silicon for high-performance lithium-ion battery anodes. Nature Communications, 2019, 10, 1447.	12.8	494
321	Mo2C/VC heterojunction embedded in graphitic carbon network: An advanced electrocatalyst for hydrogen evolution. Nano Energy, 2019, 60, 520-526.	16.0	124
322	Three-dimensional carbon-coating silicon nanoparticles welded on carbon nanotubes composites for high-stability lithium-ion battery anodes. Applied Surface Science, 2019, 479, 896-902.	6.1	47
323	Hollow cathode effect modified time-dependent global model and high-power impulse magnetron sputtering discharge and transport in cylindrical cathode. Journal of Applied Physics, 2019, 125, .	2.5	12
324	Tailored Plum Puddingâ€Like Co ₂ P/Sn Encapsulated with Carbon Nanobox Shell as Superior Anode Materials for Highâ€Performance Sodiumâ€Ion Capacitors. Advanced Energy Materials, 2019, 9, 1900091.	19.5	70

#	Article	IF	CITATIONS
325	Co3O4 and Co(OH)2 loaded graphene on Ni foam for high-performance supercapacitor electrode. Ionics, 2019, 25, 1783-1792.	2.4	13
326	Temperature-responsive tungsten doped vanadium dioxide thin film starves bacteria to death. Materials Today, 2019, 22, 35-49.	14.2	44
327	Spatially controlled synthesis of superlattice-like SnS/nitrogen-doped graphene hybrid nanobelts as high-rate and durable anode materials for sodium-ion batteries. Journal of Materials Chemistry A, 2019, 7, 27475-27483.	10.3	29
328	Theoretical assessment of a highly sensitive photonic crystal fibre based on surface plasmon resonance sensor operating in the near-infrared wavelength. Journal of Modern Optics, 2019, 66, 1-6.	1.3	74
329	Recent progress in nanostructured transition metal nitrides for advanced electrochemical energy storage. Journal of Materials Chemistry A, 2019, 7, 14-37.	10.3	181
330	Evolution of microstructures and properties of the GH4169 superalloy during short-term and high-temperature processing. Materials Science & Engineering A: Structural Materials: Properties, Microstructure and Processing, 2019, 744, 255-266.	5.6	41
331	Self-supported electrodes composed of silicon nanocrystals in 3D hierarchical carbon network for reversible sodium storage. Journal of Materials Science: Materials in Electronics, 2019, 30, 2732-2742.	2.2	3
332	A Low ost Metalâ€Free Photocatalyst Based on Black Phosphorus. Advanced Science, 2019, 6, 1801321.	11.2	79
333	Black Phosphorus: Bioactive Nanomaterials with Inherent and Selective Chemotherapeutic Effects. Angewandte Chemie - International Edition, 2019, 58, 769-774.	13.8	113
334	Preferential production of reactive species and bactericidal efficacy of gas-liquid plasma discharge. Chemical Engineering Journal, 2019, 362, 402-412.	12.7	102
335	Conductive Mesoporous Niobium Nitride Microspheres/Nitrogen-Doped Graphene Hybrid with Efficient Polysulfide Anchoring and Catalytic Conversion for High-Performance Lithium–Sulfur Batteries. ACS Applied Materials & Interfaces, 2019, 11, 2961-2969.	8.0	63
336	An eco-friendly and cleaner process for preparing architectural ceramics from coal fly ash: Pre-activation of coal fly ash by a mechanochemical method. Journal of Cleaner Production, 2019, 214, 419-428.	9.3	48
337	Selective and high-sensitive label-free detection of ascorbic acid by carbon nitride quantum dots with intense fluorescence from lone pair states. Talanta, 2019, 196, 530-536.	5.5	23
338	Air-stable n-doped black phosphorus transistor by thermal deposition of metal adatoms. Nanotechnology, 2019, 30, 135201.	2.6	16
339	Activation of graphitic carbon nitride by surface discharge plasma treatment for enhanced photocatalysis. Vacuum, 2019, 159, 235-238.	3.5	9
340	High-efficiency hydrogen evolution from seawater using hetero-structured T/Td phase ReS2 nanosheets with cationic vacancies. Nano Energy, 2019, 55, 42-48.	16.0	102
341	Molybdenum diselenide – black phosphorus heterostructures for electrocatalytic hydrogen evolution. Applied Surface Science, 2019, 467-468, 328-334.	6.1	47
342	Near-infrared light control of bone regeneration with biodegradable photothermal osteoimplant. Biomaterials, 2019, 193, 1-11.	11.4	181

#	Article	IF	CITATIONS
343	Hierarchical MoS ₂ @Nâ€Doped Carbon Hollow Spheres with Enhanced Performance in Sodium Dualâ€lon Batteries. ChemElectroChem, 2019, 6, 661-667.	3.4	24
344	Biomass-derived robust three-dimensional porous carbon for high volumetric performance supercapacitors. Journal of Power Sources, 2019, 412, 1-9.	7.8	150
345	Corrosion protection and enhanced biocompatibility of biomedical Mg-Y-RE alloy coated with tin dioxide. Surface and Coatings Technology, 2019, 357, 78-82.	4.8	19
346	High-ion-energy and low-temperature deposition of diamond-like carbon (DLC) coatings with pulsed kV bias. Surface and Coatings Technology, 2019, 365, 152-157.	4.8	21
347	Abrasion and erosion behavior of DLC-coated oil-well tubings in a heavy oil/sand environment. Surface and Coatings Technology, 2019, 357, 379-383.	4.8	13
348	Enhancement of mechanical properties and corrosion resistance of NiTi alloy by carbon plasma immersion ion implantation. Surface and Coatings Technology, 2019, 365, 52-57.	4.8	22
349	Tunable single-polarization bimetal-coated and liquid-filled photonic crystal fiber filter based on surface plasmon resonance. Applied Optics, 2019, 58, 6308.	1.8	22
350	Surface plasmon resonance sensor based onÂeccentric core photonic quasi-crystal fiberÂwith indium tin oxide. Applied Optics, 2019, 58, 6848.	1.8	22
351	Photonic spin Hall effect: a new window in D-shaped fiber by weak measurements. Optics Express, 2019, 27, 14064.	3.4	3
352	Black Phosphorus: An Effective Feedstock for the Synthesis of Phosphorus-Based Chemicals. CCS Chemistry, 2019, 1, 166-172.	7.8	8
353	Tuning Superhydrophobic Materials with Negative Surface Energy Domains. Research, 2019, 2019, 1391804.	5.7	15
354	Dual-band directional scattering with all-dielectric trimer in the near-infrared region. Applied Optics, 2019, 58, 5082.	1.8	3
355	Fano resonances in symmetric plasmonic split-ring/ring dimer nanostructures. Applied Optics, 2019, 58, 8069.	1.8	0
356	Biodegradable near-infrared-photoresponsive shape memory implants based on black phosphorus nanofillers. Biomaterials, 2018, 164, 11-21.	11.4	94
357	Blackâ€Phosphorusâ€Incorporated Hydrogel as a Sprayable and Biodegradable Photothermal Platform for Postsurgical Treatment of Cancer. Advanced Science, 2018, 5, 1700848.	11.2	289
358	Stable black phosphorus/Bi2O3 heterostructures for synergistic cancer radiotherapy. Biomaterials, 2018, 171, 12-22.	11.4	94
359	Electrochemical surface engineering of titanium-based alloys for biomedical application. Electrochimica Acta, 2018, 271, 699-718.	5.2	168
360	Hierarchical TiN nanoparticles-assembled nanopillars for flexible supercapacitors with high volumetric capacitance. Nanoscale, 2018, 10, 8728-8734.	5.6	67

#	Article	IF	CITATIONS
361	Tunable magnetic coupling in Mn-doped monolayer MoS ₂ under lattice strain. Journal of Physics Condensed Matter, 2018, 30, 215801.	1.8	8
362	Investigation of Corrosion Behavior of Ti/TiN Multilayers on Al7075 Deposited by High-Vacuum Magnetron Sputtering in 3.5% NaCl Solution. Journal of Materials Engineering and Performance, 2018, 27, 2216-2225.	2.5	3
363	Few-Layer Antimonene: Anisotropic Expansion and Reversible Crystalline-Phase Evolution Enable Large-Capacity and Long-Life Na-Ion Batteries. ACS Nano, 2018, 12, 1887-1893.	14.6	175
364	Barrier Reduction of Lithium Ion Tunneling through Graphene with Hybrid Defects: Firstâ€Principles Calculations. Advanced Theory and Simulations, 2018, 1, 1700009.	2.8	11
365	VO ₂ /TiN Plasmonic Thermochromic Smart Coatings for Roomâ€Temperature Applications. Advanced Materials, 2018, 30, 1705421.	21.0	179
366	<i>In situ</i> growth of all-inorganic perovskite nanocrystals on black phosphorus nanosheets. Chemical Communications, 2018, 54, 2365-2368.	4.1	36
367	Copolymer P(BS-co-LA) Enhanced Compatibility of PBS/PLA Composite. Journal of Polymers and the Environment, 2018, 26, 3060-3068.	5.0	19
368	In vitro antimicrobial effects and mechanisms of direct current air-liquid discharge plasma on planktonic Staphylococcus aureus and Escherichia coli in liquids. Bioelectrochemistry, 2018, 121, 125-134.	4.6	63
369	Recent advances in cell-mediated nanomaterial delivery systems for photothermal therapy. Journal of Materials Chemistry B, 2018, 6, 1296-1311.	5.8	22
370	Inâ€Plane Black Phosphorus/Dicobalt Phosphide Heterostructure for Efficient Electrocatalysis. Angewandte Chemie, 2018, 130, 2630-2634.	2.0	55
371	Molecular Dynamics Simulation of Nanocrack Propagation in Single-Layer MoS2Nanosheets. Journal of Physical Chemistry C, 2018, 122, 1351-1360.	3.1	44
372	Effects of silica and Ag on the electrochemical behavior of titania-based nanocomposite coatings deposited on 2024 aluminum alloy by the sol-gel method. Journal of Alloys and Compounds, 2018, 739, 92-100.	5.5	8
373	Valence State Manipulation of Cerium Oxide Nanoparticles on a Titanium Surface for Modulating Cell Fate and Bone Formation. Advanced Science, 2018, 5, 1700678.	11.2	114
374	Inâ€Plane Black Phosphorus/Dicobalt Phosphide Heterostructure for Efficient Electrocatalysis. Angewandte Chemie - International Edition, 2018, 57, 2600-2604.	13.8	209
375	Electrocatalytic hydrogen evolution of palladium nanoparticles electrodeposited on nanographene coated macroporous electrically conductive network. International Journal of Hydrogen Energy, 2018, 43, 2171-2183.	7.1	12
376	Dealkalization of Red Mud by Carbide Slag and Flue Gas. Clean - Soil, Air, Water, 2018, 46, 1700634.	1.1	12
377	Cellular response to nano-structured Zr and ZrO2 alloyed layers on Ti-6Al-4V. Materials Science and Engineering C, 2018, 90, 523-530.	7.3	20
378	Discharge and Plasma Characteristics of Pulse-Enhanced Vacuum Arc Evaporation (PEVAE) for Titanium Cathode. IEEE Transactions on Plasma Science, 2018, 46, 2619-2625.	1.3	7

#	Article	IF	CITATIONS
379	Control of multidrug-resistant planktonic <i>Acinetobacter baumannii</i> : biocidal efficacy study by atmospheric-pressure air plasma. Plasma Science and Technology, 2018, 20, 065513.	1.5	10
380	Highly efficient field emission from indium-doped ZnO nanostructure on nanographene/macroporous electric conductive network. Materials Letters, 2018, 222, 25-28.	2.6	13
381	Enhancement of toughness and wear resistance by CrN/CrCN multilayered coatings for wood processing. Surface and Coatings Technology, 2018, 344, 204-213.	4.8	62
382	In situ Synthesis of V ₂ O ₃ â€Intercalated Nâ€doped Graphene Nanobelts from VO _{<i>x</i>} â€Amine Hybrid as Highâ€Performance Anode Material for Alkaliâ€Ion Batteries. ChemElectroChem, 2018, 5, 1387-1393.	3.4	26
383	Hierarchical porous carbon materials from nanosized metal-organic complex for high-performance symmetrical supercapacitor. Electrochimica Acta, 2018, 269, 580-589.	5.2	47
384	Heterogeneous phosphorus-doped WO _{3â^'x} /nitrogen-doped carbon nanowires with high rate and long life for advanced lithium-ion capacitors. Journal of Materials Chemistry A, 2018, 6, 6916-6921.	10.3	49
385	Oriented MoS ₂ Nanoflakes on Nâ€Doped Carbon Nanosheets Derived from Dodecylamineâ€Intercalated MoO ₃ for Highâ€Performance Lithiumâ€Ion Battery Anodes. ChemElectroChem, 2018, 5, 1350-1356.	3.4	21
386	Analysis of a Surface Plasmon Resonance Probe Based on Photonic Crystal Fibers for Low Refractive Index Detection. Plasmonics, 2018, 13, 779-784.	3.4	137
387	Preparation and effectiveness of slowâ€release silicon fertilizer by sintering with iron ore tailings. Environmental Progress and Sustainable Energy, 2018, 37, 1011-1019.	2.3	16
388	Effects of dopant separation on electronic states and magnetism in monolayer MoS2. Applied Surface Science, 2018, 428, 226-232.	6.1	16
389	High-performance asymmetrical supercapacitor composed of rGO-enveloped nickel phosphite hollow spheres and N/S co-doped rGO aerogel. Nano Research, 2018, 11, 1651-1663.	10.4	58
390	Nano Ag/ZnO-Incorporated Hydroxyapatite Composite Coatings: Highly Effective Infection Prevention and Excellent Osteointegration. ACS Applied Materials & amp; Interfaces, 2018, 10, 1266-1277.	8.0	127
391	2D Material-Based Nanofibrous Membrane for Photothermal Cancer Therapy. ACS Applied Materials & Interfaces, 2018, 10, 1155-1163.	8.0	32
392	Excellent adhered thick diamond-like carbon coatings by optimizing hetero-interfaces with sequential highly energetic Cr and C ion treatment. Journal of Alloys and Compounds, 2018, 735, 155-162.	5.5	27
393	Surface functionalization of biomaterials by plasma and ion beam. Surface and Coatings Technology, 2018, 336, 2-8.	4.8	22
394	Effects of copper nanoparticles in porous TiO2 coatings on bacterial resistance and cytocompatibility of osteoblasts and endothelial cells. Materials Science and Engineering C, 2018, 82, 110-120.	7.3	96
395	Rapid Sterilization and Accelerated Wound Healing Using Zn ²⁺ and Graphene Oxide Modified g ₃ N ₄ under Dual Light Irradiation. Advanced Functional Materials, 2018, 28, 1800299.	14.9	246
396	In Silico Screening and Design of Coating Materials for PEMFC Bipolar Plates. Coatings, 2018, 8, 386.	2.6	4

#	Article	IF	CITATIONS
397	Tunable band offsets in the BP/P ₄ O ₁₀ van der Waals heterostructure: first-principles calculations. Physical Chemistry Chemical Physics, 2018, 20, 29931-29938.	2.8	7
398	Sequentially Triggered Delivery System of Black Phosphorus Quantum Dots with Surface Charge-Switching Ability for Precise Tumor Radiosensitization. ACS Nano, 2018, 12, 12401-12415.	14.6	100
399	Degradable and Photocatalytic Antibacterial Au-TiO2/Sodium Alginate Nanocomposite Films for Active Food Packaging. Nanomaterials, 2018, 8, 930.	4.1	57
400	Improving of tribology properties of TiAl6V4 with nanostructured Ti/TiN-multilayered coating deposited by high-vacuum magnetron sputtering. Applied Physics A: Materials Science and Processing, 2018, 124, 1.	2.3	5
401	A CRISPR–Cas9-triggered strand displacement amplification method for ultrasensitive DNA detection. Nature Communications, 2018, 9, 5012.	12.8	244
402	Seamless lateral graphene p–n junctions formed by selective in situ doping for high-performance photodetectors. Nature Communications, 2018, 9, 5168.	12.8	71
403	Highly Fluorescent and Stable Black Phosphorus Quantum Dots in Water. Small, 2018, 14, e1803132.	10.0	58
404	Highly Luminescent and Stable Siâ€Based CsPbBr 3 Quantum Dot Thin Films Prepared by Glow Discharge Plasma with Realâ€Time and In Situ Diagnosis. Advanced Functional Materials, 2018, 28, 1805214.	14.9	14
405	Sn-C bonding riveted SnSe nanoplates vertically grown on nitrogen-doped carbon nanobelts for high-performance sodium-ion battery anodes. Nano Energy, 2018, 54, 322-330.	16.0	152
406	Highly Stretchable Conductive Glue for Highâ€Performance Silicon Anodes in Advanced Lithiumâ€Ion Batteries. Advanced Functional Materials, 2018, 28, 1704858.	14.9	113
407	Black Phosphorus/Platinum Heterostructure: A Highly Efficient Photocatalyst for Solarâ€Driven Chemical Reactions. Advanced Materials, 2018, 30, e1803641.	21.0	105
408	Noninvasive rapid bacteria-killing and acceleration of wound healing through photothermal/photodynamic/copper ion synergistic action of a hybrid hydrogel. Biomaterials Science, 2018, 6, 2110-2121.	5.4	168
409	Synthesis of lipid–black phosphorus quantum dot bilayer vesicles for near-infrared-controlled drug release. Chemical Communications, 2018, 54, 6060-6063.	4.1	53
410	Flexible Nb ₄ N ₅ /rGO Electrode for High-Performance Solid State Supercapacitors. Journal of Nanoscience and Nanotechnology, 2018, 18, 30-38.	0.9	20
411	Neuromorphic Computing with Memristor Crossbar. Physica Status Solidi (A) Applications and Materials Science, 2018, 215, 1700875.	1.8	60
412	The effect of copper pretreatment on graphene synthesis by ion implantation into Ni/Cu substrate. Semiconductor Science and Technology, 2018, 33, 074001.	2.0	0
413	An antibacterial platform based on capacitive carbon-doped TiO2 nanotubes after direct or alternating currentÂcharging. Nature Communications, 2018, 9, 2055.	12.8	153
414	Ag/AgBr-loaded mesoporous silica for rapid sterilization and promotion of wound healing. Biomaterials Science, 2018, 6, 1735-1744.	5.4	65

#	Article	IF	CITATIONS
415	A promising orthopedic implant material with enhanced osteogenic and antibacterial activity: Al2O3-coated aluminum alloy. Applied Surface Science, 2018, 457, 1025-1034.	6.1	34
416	Ultrafast hetero-assembly of monolithic interwoven V2O5 nanobelts/carbon nanotubes architectures for high-energy alkali-ion batteries. Journal of Power Sources, 2018, 395, 295-304.	7.8	37
417	Core-shell CoMoO4@Ni(OH)2 on ordered macro-porous electrode plate for high-performance supercapacitor. Electrochimica Acta, 2018, 283, 538-547.	5.2	29
418	Hard and adherent a-C:H gradient coatings by stress engineering. Journal of Alloys and Compounds, 2018, 765, 921-926.	5.5	14
419	Near-infrared light-triggered drug delivery system based on black phosphorus for inÂvivo bone regeneration. Biomaterials, 2018, 179, 164-174.	11.4	115
420	Lanthanide oordinated Black Phosphorus. Small, 2018, 14, e1801405.	10.0	65
421	Tantalum nitride films for corrosion protection of biomedical Mg-Y-RE alloy. Journal of Alloys and Compounds, 2018, 764, 947-958.	5.5	19
422	Symmetrical dual D-shape photonic crystal fibers for surface plasmon resonance sensing. Optics Express, 2018, 26, 9039.	3.4	213
423	Birefringent PCF-Based SPR Sensor for a Broad Range of Low Refractive Index Detection. IEEE Photonics Technology Letters, 2018, 30, 1471-1474.	2.5	50
424	Oxygen Vacancy Enhanced Gas-Sensing Performance of CeO ₂ /Graphene Heterostructure at Room Temperature. Analytical Chemistry, 2018, 90, 9821-9829.	6.5	77
425	Construction of perfluorohexane/IR780@liposome coating on Ti for rapid bacteria killing under permeable near infrared light. Biomaterials Science, 2018, 6, 2460-2471.	5.4	28
426	Roles of membrane protein damage and intracellular protein damage in death of bacteria induced by atmospheric-pressure air discharge plasmas. RSC Advances, 2018, 8, 21139-21149.	3.6	20
427	Black Phosphorus: Lanthanide-Coordinated Black Phosphorus (Small 29/2018). Small, 2018, 14, 1870134.	10.0	3
428	Controlled-temperature photothermal and oxidative bacteria killing and acceleration of wound healing by polydopamine-assisted Au-hydroxyapatite nanorods. Acta Biomaterialia, 2018, 77, 352-364.	8.3	180
429	Precisely controlled delivery of magnesium ions thru sponge-like monodisperse PLCA/nano-MgO-alginate core-shell microsphere device to enable in-situ bone regeneration. Biomaterials, 2018, 174, 1-16.	11.4	140
430	In Situ Synthesis of MoP Nanoflakes Intercalated Nâ€Doped Graphene Nanobelts from MoO ₃ –Amine Hybrid for Highâ€Efficient Hydrogen Evolution Reaction. Small, 2018, 14, e1800667.	10.0	85
431	Magnetron-sputtered fluorocarbon polymeric film on magnesium for corrosion protection. Surface and Coatings Technology, 2018, 352, 437-444.	4.8	22
432	Ni-doped amorphous iron phosphide nanoparticles on TiN nanowire arrays: An advanced alkaline hydrogen evolution electrocatalyst. Nano Energy, 2018, 53, 66-73.	16.0	115

#	Article	IF	CITATIONS
433	Ni/Co-based nanosheet arrays for efficient oxygen evolution reaction. Nano Energy, 2018, 52, 360-368.	16.0	135
434	Zincâ€Modified Sulfonated Polyetheretherketone Surface with Immunomodulatory Function for Guiding Cell Fate and Bone Regeneration. Advanced Science, 2018, 5, 1800749.	11.2	184
435	Morphological control of gold nanorods via thermally driven bi-surfactant growth and application for detection of heavy metal ions. Nanotechnology, 2018, 29, 334001.	2.6	6
436	Tuning the Bandgap of Photo-Sensitive Polydopamine/Ag ₃ PO ₄ /Graphene Oxide Coating for Rapid, Noninvasive Disinfection of Implants. ACS Central Science, 2018, 4, 724-738.	11.3	227
437	Highly sensitive PCF-SPR biosensor for hyperthermia temperature monitoring. Journal of Optics (India), 2018, 47, 288-294.	1.7	14
438	Spatially confined synthesis of vanadium nitride nanodots intercalated carbon nanosheets with ultrahigh volumetric capacitance and long life for flexible supercapacitors. Nano Energy, 2018, 51, 128-136.	16.0	87
439	Multiple unidirectional forward scattering of hybrid metal-dielectric nanoantenna in the near-infrared region. Optical Materials Express, 2018, 8, 3410.	3.0	1
440	Recent advances in anti-infection surfaces fabricated on biomedical implants by plasma-based technology. Surface and Coatings Technology, 2017, 312, 2-6.	4.8	14
441	Bactericidal Effects of Plasma Induced Reactive Species in Dielectric Barrier Gas–Liquid Discharge. Plasma Chemistry and Plasma Processing, 2017, 37, 415-431.	2.4	69
442	Cold atmospheric-pressure air plasma treatment of C6 glioma cells: effects of reactive oxygen species in the medium produced by the plasma on cell death. Plasma Science and Technology, 2017, 19, 025503.	1.5	8
443	Zinc Electrodeposition on Polycrystalline Copper: Electrochemical Study of Early-Stage Growth Mechanism. Journal of Physical Chemistry C, 2017, 121, 3938-3946.	3.1	17
444	Tin repellence on wave-soldering stainless steel holders coated with Ti/TiC/DLC. Surface and Coatings Technology, 2017, 320, 614-618.	4.8	4
445	TiL ₄ oordinated Black Phosphorus Quantum Dots as an Efficient Contrast Agent for In Vivo Photoacoustic Imaging of Cancer. Small, 2017, 13, 1602896.	10.0	251
446	Hierarchical Porous Carbon Materials Derived from Self-Template Bamboo Leaves for Lithium–Sulfur Batteries. Electrochimica Acta, 2017, 229, 352-360.	5.2	55
447	Facile design of ultra-thin anodic aluminum oxide membranes for the fabrication of plasmonic nanoarrays. Nanotechnology, 2017, 28, 105301.	2.6	60
448	Fabrication of irregular-layer-free and diameter-tunable Ni–Ti–O nanopores by anodization of NiTi alloy. Electrochemistry Communications, 2017, 76, 10-14.	4.7	23
449	Osteogenesis Catalyzed by Titanium-Supported Silver Nanoparticles. ACS Applied Materials & Interfaces, 2017, 9, 5149-5157.	8.0	57
450	Tensile loading induced phase transition and rippling in single-layer MoS 2. Applied Surface Science, 2017, 404, 180-187.	6.1	20

#	Article	IF	CITATIONS
451	Ge@CNFs Anchored on 3D Graphene Foam for Binderâ€Free and Highâ€Efficiency Anodes in Li–Ion Batteries. ChemElectroChem, 2017, 4, 1002-1006.	3.4	6
452	Different-sized black phosphorus nanosheets with good cytocompatibility and high photothermal performance. RSC Advances, 2017, 7, 14618-14624.	3.6	58
453	Direct anodic exfoliation of graphite onto high-density aligned graphene for large capacity supercapacitors. Nano Energy, 2017, 34, 515-523.	16.0	56
454	Antibacterial effects of titanium embedded with silver nanoparticles based on electron-transfer-induced reactive oxygen species. Biomaterials, 2017, 124, 25-34.	11.4	219
455	Efficient Enrichment and Self-Assembly of Hybrid Nanoparticles into Removable and Magnetic SERS Substrates for Sensitive Detection of Environmental Pollutants. ACS Applied Materials & Interfaces, 2017, 9, 7472-7480.	8.0	84
456	Vertically-oriented few-layer graphene supported by silicon microchannel plates as a counter electrode in dye-sensitized solar cells. Organic Electronics, 2017, 45, 74-80.	2.6	9
457	<i>In vitro</i> antimicrobial effects and mechanism of atmospheric-pressure He/O ₂ plasma jet on <i>Staphylococcus aureus</i> biofilm. Journal Physics D: Applied Physics, 2017, 50, 105201.	2.8	41
458	Imaging and motion of cathode group spots during pulse-enhanced vacuum arc evaporation. Vacuum, 2017, 139, 37-43.	3.5	12
459	Functionalized Polymeric Membrane with Enhanced Mechanical and Biological Properties to Control the Degradation of Magnesium Alloy. Advanced Healthcare Materials, 2017, 6, 1601269.	7.6	46
460	In situ segregation of cobalt nanoparticles on VN nanosheets via nitriding of Co 2 V 2 O 7 nanosheets as efficient oxygen evolution reaction electrocatalysts. Nano Energy, 2017, 34, 1-7.	16.0	119
461	In situ fabrication of Ni nanoparticles on N-doped TiO ₂ nanowire arrays by nitridation of NiTiO ₃ for highly sensitive and enzyme-free glucose sensing. Journal of Materials Chemistry B, 2017, 5, 1779-1786.	5.8	19
462	Effects of high concentration of Benzotriazole on corrosion behavior of nanostructured titania-alumina composite coating deposited on Al 2024 by sol-gel method. Surface and Coatings Technology, 2017, 321, 36-44.	4.8	30
463	Cell-borne 2D nanomaterials for efficient cancer targeting and photothermal therapy. Biomaterials, 2017, 133, 37-48.	11.4	63
464	Designing Core–Shell Gold and Selenium Nanocomposites for Cancer Radiochemotherapy. ACS Nano, 2017, 11, 4848-4858.	14.6	150
465	Long-term antibacterial characteristics and cytocompatibility of titania nanotubes loaded with Au nanoparticles without photocatalytic effects. Applied Surface Science, 2017, 414, 230-237.	6.1	25
466	Fabrication of Ni-Ti-O nanoporous film on NiTi alloy in ethylene glycol containing NaCl. Surface and Coatings Technology, 2017, 321, 136-145.	4.8	15
467	Ultrahigh quantum efficiency photodetector and ultrafast reversible surface wettability transition of square In2O3 nanowires. Nano Research, 2017, 10, 2772-2781.	10.4	27
468	Effects of one-step hydrothermal treatment on the surface morphology and corrosion resistance of ZK60 magnesium alloy. Surface and Coatings Technology, 2017, 309, 490-496.	4.8	31

#	Article	IF	CITATIONS
469	Facet-engineered CeO ₂ /graphene composites for enhanced NO ₂ gas-sensing. Journal of Materials Chemistry C, 2017, 5, 6973-6981.	5.5	29
470	Nickel plasma modification of graphene for high-performance non-enzymatic glucose sensing. Sensors and Actuators B: Chemical, 2017, 251, 842-850.	7.8	31
471	Relationship between Ni release and cytocompatibility of Ni-Ti-O nanotubes prepared on biomedical NiTi alloy. Corrosion Science, 2017, 123, 209-216.	6.6	45
472	Germanium-Assisted Direct Growth of Graphene on Arbitrary Dielectric Substrates for Heating Devices. Small, 2017, 13, 1700929.	10.0	33
473	Dual carbon layer hybridized mesoporous tin hollow spheres for fast-rechargeable and highly-stable lithium-ion battery anodes. Journal of Materials Chemistry A, 2017, 5, 14422-14429.	10.3	39
474	The controlled drug release by pH-sensitive molecularly imprinted nanospheres for enhanced antibacterial activity. Materials Science and Engineering C, 2017, 77, 84-91.	7.3	45
475	Antibacterial, osteogenic, and angiogenic activities of SrTiO 3 nanotubes embedded with Ag 2 O nanoparticles. Materials Science and Engineering C, 2017, 75, 1049-1058.	7.3	45
476	Excellent corrosion resistance of P and Fe modified micro-arc oxidation coating on Al alloy. Journal of Alloys and Compounds, 2017, 710, 452-459.	5.5	53
477	Targeting ETS1 with RNAi-based supramolecular nanoassemblies for multidrug-resistant breast cancer therapy. Journal of Controlled Release, 2017, 253, 110-121.	9.9	43
478	Lanthanide-integrated supramolecular polymeric nanoassembly with multiple regulation characteristics for multidrug-resistant cancer therapy. Biomaterials, 2017, 129, 83-97.	11.4	37
479	Three-dimensional graphene nanosheets supported by NiO/Si-MCP as electrode materials for high-performance supercapacitors. Ionics, 2017, 23, 2185-2191.	2.4	0
480	Fully degradable PLA-based composite reinforced with 2D-braided Mg wires for orthopedic implants. Composites Science and Technology, 2017, 142, 180-188.	7.8	34
481	Three-dimensional tetsubo-like Co(OH)2 nanorods on a macroporous electrically conductive network as an efficient electroactive framework for the hydrogen evolution reaction. Journal of Materials Chemistry A, 2017, 5, 2629-2639.	10.3	34
482	Biofunctionalization of carbon nanotubes/chitosan hybrids on Ti implants by atom layer deposited ZnO nanostructures. Applied Surface Science, 2017, 400, 14-23.	6.1	96
483	Microstructure and mechanical properties of (AlTi)xN1-x films by magnetic-field-enhanced high power impulse magnetron sputtering. Journal of Vacuum Science and Technology A: Vacuum, Surfaces and Films, 2017, 35, .	2.1	7
484	Freestanding hollow double-shell Se@CNx nanobelts as large-capacity and high-rate cathodes for Li-Se batteries. Nano Energy, 2017, 32, 1-9.	16.0	108
485	Enhancement of Ferromagnetism in Nonmagnetic Metal Oxide Nanoparticles by Facet Engineering. Small, 2017, 13, 1602951.	10.0	12
486	Protein-assisted assembly of mesoporous nanocrystals and carbon nanotubes for self-supporting high-performance sodium electrodes. Journal of Materials Chemistry A, 2017, 5, 2749-2758.	10.3	24

#	Article	IF	CITATIONS
487	A Highly Sensitive Dual-Core Photonic Crystal Fiber Based on a Surface Plasmon Resonance Biosensor with Silver-Graphene Layer. Plasmonics, 2017, 12, 1847-1853.	3.4	70
488	Identification of Lattice Oxygen in Few-Layer Black Phosphorous Exfoliated in Ultrahigh Vacuum and Largely Improved Ambipolar Field-Effect Mobilities by Hydrogenation and Phosphorization. ACS Applied Materials & Interfaces, 2017, 9, 39804-39811.	8.0	10
489	Three-dimensional CoMoO 4 nanorods/nanographene composites on a Ni coated macroporous electrically conductive network with excellent electrochemical performance. Materials Science and Engineering B: Solid-State Materials for Advanced Technology, 2017, 226, 177-187.	3.5	7
490	Monolithic Hierarchical Carbon Assemblies Embedded with Mesoporous NaTi2(PO4)3 Nanocrystals for Flexible High-Performance Sodium Anodes. Electrochimica Acta, 2017, 254, 328-336.	5.2	20
491	Reduction in Chemical Oxygen Demand of TNT Red Water Using Layered Double Hydroxide Prepared from Red Mud and Brucite. Environmental Engineering Science, 2017, 34, 721-730.	1.6	7
492	Controlled Patterning of Plasmonic Dimers by Using an Ultrathin Nanoporous Alumina Membrane as a Shadow Mask. ACS Applied Materials & Interfaces, 2017, 9, 36199-36205.	8.0	50
493	Metalâ€ionâ€Modified Black Phosphorus with Enhanced Stability and Transistor Performance. Advanced Materials, 2017, 29, 1703811.	21.0	431
494	Balancing Bacteria–Osteoblast Competition through Selective Physical Puncture and Biofunctionalization of ZnO/Polydopamine/Arginine-Glycine-Aspartic Acid-Cysteine Nanorods. ACS Nano, 2017, 11, 11250-11263.	14.6	230
495	Improved interfacial adhesion between TiAlN/DLC multi-layered coatings by controlling the morphology via bias. Surface and Coatings Technology, 2017, 331, 15-20.	4.8	10
496	Tannic Acid/Fe ³⁺ /Ag Nanofilm Exhibiting Superior Photodynamic and Physical Antibacterial Activity. ACS Applied Materials & Interfaces, 2017, 9, 39657-39671.	8.0	76
497	Photo-Inspired Antibacterial Activity and Wound Healing Acceleration by Hydrogel Embedded with Ag/Ag@AgCl/ZnO Nanostructures. ACS Nano, 2017, 11, 9010-9021.	14.6	591
498	Self-assembled bundled TiO2nanowire arrays encapsulated with indium tin oxide for broadband absorption in plasmonic photocatalysis. Physical Chemistry Chemical Physics, 2017, 19, 27059-27064.	2.8	5
499	Elucidating the Intercalation Pseudocapacitance Mechanism of MoS ₂ –Carbon Monolayer Interoverlapped Superstructure: Toward High-Performance Sodium-Ion-Based Hybrid Supercapacitor. ACS Applied Materials & Interfaces, 2017, 9, 32745-32755.	8.0	156
500	Freestanding carbon encapsulated mesoporous vanadium nitride nanowires enable highly stable sulfur cathodes for lithium-sulfur batteries. Nano Energy, 2017, 40, 655-662.	16.0	159
501	Self-assembly and enhanced visible-light-driven photocatalytic activity of reduced graphene oxide-Bi2WO6 photocatalysts. Nanotechnology Reviews, 2017, 6, 505-516.	5.8	11
502	Two-dimensional black phosphorus: Synthesis, modification, properties, and applications. Materials Science and Engineering Reports, 2017, 120, 1-33.	31.8	130
503	Hierarchical CoMoO ₄ @Co ₃ O ₄ nanocomposites on an ordered macro-porous electrode plate as a multi-dimensional electrode in high-performance supercapacitors. Journal of Materials Chemistry A, 2017, 5, 17312-17324.	10.3	76
504	Nano mechanical and wear properties of multi-layer Ti/TiN coatings deposited on Al 7075 by high-vacuum magnetron sputtering. Thin Solid Films, 2017, 638, 96-104.	1.8	33

#	Article	IF	CITATIONS
505	Corrosion behavior of reactive sputtered Ti/TiN nanostructured coating and effects of intermediate titanium layer on self-healing properties. Surface and Coatings Technology, 2017, 326, 156-164.	4.8	28
506	Intertwined Nitrogenâ€Doped Carbon Nanotubes for Highâ€Rate and Longâ€Life Sodiumâ€Ion Battery Anodes. ChemElectroChem, 2017, 4, 2542-2546.	3.4	24
507	Synergistic Bacteria Killing through Photodynamic and Physical Actions of Graphene Oxide/Ag/Collagen Coating. ACS Applied Materials & Interfaces, 2017, 9, 26417-26428.	8.0	223
508	Freestanding Nanoengineered [001] Preferentially Oriented TiO ₂ Nanosheetsâ^'Graphene Planarly Aligned Nanohybrids with Enhanced Liâ€Storage Properties. ChemElectroChem, 2017, 4, 2819-2825.	3.4	9
509	Stable and Multifunctional Dye-Modified Black Phosphorus Nanosheets for Near-Infrared Imaging-Guided Photothermal Therapy. Chemistry of Materials, 2017, 29, 7131-7139.	6.7	158
510	Influence of dynamic compressive loading on the in vitro degradation behavior of pure PLA and Mg/PLA composite. Acta Biomaterialia, 2017, 64, 269-278.	8.3	23
511	Highly efficient field emission from ZnO nanorods and nanographene hybrids on a macroporous electric conductive network. Journal of Materials Chemistry C, 2017, 5, 9296-9305.	5.5	13
512	Linker-free covalent immobilization of heparin, SDF- $1\hat{l}\pm$, and CD47 on PTFE surface for antithrombogenicity, endothelialization and anti-inflammation. Biomaterials, 2017, 140, 201-211.	11.4	80
513	Black phosphorus: a two-dimensional reductant for in situ nanofabrication. Npj 2D Materials and Applications, 2017, 1, .	7.9	63
514	In vitro degradation kinetics of pure PLA and Mg/PLA composite: Effects of immersion temperature and compression stress. Acta Biomaterialia, 2017, 48, 468-478.	8.3	57
515	Preparation of layered double hydroxides using boron mud and red mud industrial wastes and adsorption mechanism to phosphate. Water and Environment Journal, 2017, 31, 145-157.	2.2	31
516	Free-standing electrodes composed of carbon-coated Li 4 Ti 5 O 12 nanosheets and reduced graphene oxide for advanced sodium ion batteries. Journal of Power Sources, 2017, 337, 180-188.	7.8	61
517	Corrosion resistance and cytocompatibility of tantalum-surface-functionalized biomedical ZK60 Mg alloy. Corrosion Science, 2017, 114, 45-56.	6.6	106
518	Numerical analysis of a photonic crystal fiber based on a surface plasmon resonance sensor with an annular analyte channel. Optics Communications, 2017, 382, 162-166.	2.1	91
519	EFFECT OF INHIBITOR AGENTS ADDITION ON CORROSION RESISTANCE PERFORMANCE OF TITANIA SOL–GEL COATINGS APPLIED ON 304 STAINLESS STEEL. Surface Review and Letters, 2017, 24, 1750055.	1.1	8
520	Investigation of nano-structured Zirconium oxide film on Ti6Al4V substrate to improve tribological properties prepared by PIII&D. Applied Surface Science, 2017, 394, 586-597.	6.1	24
521	Effects of diamond-like carbon film on the corrosion behavior of NdFeB permanent magnet. Surface and Coatings Technology, 2017, 312, 66-74.	4.8	13
522	Decorated ultrathin bismuth selenide nanosheets as targeted theranostic agents for in vivo imaging guided cancer radiation therapy. NPG Asia Materials, 2017, 9, e439-e439.	7.9	70

#	Article	IF	CITATIONS
523	Manganese molybdate nanoflakes on silicon microchannel plates as novel nano energetic material. Royal Society Open Science, 2017, 4, 171229.	2.4	5
524	Mid-infrared surface plasmon resonance sensor based on photonic crystal fibers. Optics Express, 2017, 25, 14227.	3.4	222
525	<i>In situ</i> plasma fabrication of ceramicâ€like structure on polymeric implant with enhanced surface hardness, cytocompatibility and antibacterial capability. Journal of Biomedical Materials Research - Part A, 2016, 104, 1102-1112.	4.0	4
526	Metabolizable Ultrathin Bi ₂ Se ₃ Nanosheets in Imagingâ€Guided Photothermal Therapy. Small, 2016, 12, 4136-4145.	10.0	203
527	Energy dissipation in mechanical loading of nano-grained graphene sheets. RSC Advances, 2016, 6, 60856-60861.	3.6	2
528	Modification of Biomaterials and Biomedical Devices by Plasma Immersion Ion Implantation & Deposition and Related Techniques. , 2016, , .		2
529	Metabolizable Small Gold Nanorods: Size-dependent Cytotoxicity, Cell Uptake and <i>In Vivo</i> Biodistribution. ACS Biomaterials Science and Engineering, 2016, 2, 789-797.	5.2	51
530	Mesoporous nitrogen-doped carbon hollow spheres as high-performance anodes for lithium-ion batteries. Journal of Power Sources, 2016, 324, 233-238.	7.8	108
531	Plasma and ion-beam modification of metallic biomaterials for improved anti-bacterial properties. Surface and Coatings Technology, 2016, 306, 140-146.	4.8	18
532	Synergistic WO ₃ ·2H ₂ O Nanoplates/WS ₂ Hybrid Catalysts for High-Efficiency Hydrogen Evolution. ACS Applied Materials & Interfaces, 2016, 8, 13966-13972.	8.0	120
533	Electrochemical analysis of interface adsorption phenomena on three-dimensional nano-nickel electrode deposited on silicon microchannel plate. Electrochimica Acta, 2016, 194, 253-262.	5.2	6
534	Hafnium-implanted WE43 magnesium alloy for enhanced corrosion protection and biocompatibility. Surface and Coatings Technology, 2016, 306, 11-15.	4.8	18
535	Substitutional doping of Ag into epitaxial graphene on 6H-SiC substrates during thermal decomposition. Carbon, 2016, 104, 233-240.	10.3	16
536	Systematic Study of Inherent Antibacterial Properties of Magnesium-based Biomaterials. ACS Applied Materials & Interfaces, 2016, 8, 9662-9673.	8.0	79
537	In situ synthesis of Ni(OH)2/TiO2 composite film on NiTi alloy for non-enzymatic glucose sensing. Sensors and Actuators B: Chemical, 2016, 232, 150-157.	7.8	80
538	Crumpled N-doped carbon nanotubes encapsulated with peapod-like Ge nanoparticles for high-rate and long-life Li-ion battery anodes. Journal of Materials Chemistry A, 2016, 4, 7585-7590.	10.3	44
539	Size-dependent elastic modulus of single-layer MoS2 nano-sheets. Journal of Materials Science, 2016, 51, 6850-6859.	3.7	13
540	Antibacterial Surface Design of Titanium-Based Biomaterials for Enhanced Bacteria-Killing and Cell-Assisting Functions Against Periprosthetic Joint Infection. ACS Applied Materials & Interfaces, 2016, 8, 11162-11178.	8.0	95

#	Article	IF	CITATIONS
541	Synthesis of mesoporous niobium nitride nanobelt arrays and their capacitive properties. Applied Surface Science, 2016, 383, 57-63.	6.1	58
542	Corrosion resistance of Ti-Si-N coatings in blood and cytocompatibility with vascular endothelial cells. Vacuum, 2016, 128, 45-55.	3.5	7
543	How Graphene Islands Are Unidirectionally Aligned on the Ge(110) Surface. Nano Letters, 2016, 16, 3160-3165.	9.1	92
544	Surface functionalization of biomaterials by radical polymerization. Progress in Materials Science, 2016, 83, 191-235.	32.8	120
545	Polyimide composites composed of covalently bonded BaTiO ₃ @GO hybrids with high dielectric constant and low dielectric loss. RSC Advances, 2016, 6, 86817-86823.	3.6	23
546	Enhanced cytocompatibility and reduced genotoxicity of polydimethylsiloxane modified by plasma immersion ion implantation. Colloids and Surfaces B: Biointerfaces, 2016, 148, 139-146.	5.0	14
547	Design of magnesium alloys with controllable degradation for biomedical implants: From bulk to surface. Acta Biomaterialia, 2016, 45, 2-30.	8.3	306
548	Electrochemical characteristics of nano-graphene on a macroporous electrically conductive network prepared by hydrothermal carbonization. Electrochimica Acta, 2016, 215, 515-524.	5.2	5
549	Effects of external stress on biodegradable orthopedic materials: A review. Bioactive Materials, 2016, 1, 77-84.	15.6	25
550	Dynamic transition in the discharge current between gas-dominant discharge and self-sputtering in high-power impulse magnetron sputtering. Surface and Coatings Technology, 2016, 306, 319-322.	4.8	5
551	Communication between nitric oxide synthase and positively-charged surface and bone formation promotion. Colloids and Surfaces B: Biointerfaces, 2016, 148, 354-362.	5.0	11
552	Tribological and Corrosion Properties of Nickel/TiC Bilayered Coatings Produced by Electroless Deposition and PACVD. Journal of Materials Engineering and Performance, 2016, 25, 4796-4804.	2.5	2
553	The modulation of stem cell behaviors by functionalized nanoceramic coatings on Ti-based implants. Bioactive Materials, 2016, 1, 65-76.	15.6	25
554	Dominant Factors Governing the Electron Transfer Kinetics and Electrochemical Biosensing Properties of Carbon Nanofiber Arrays. ACS Applied Materials & Interfaces, 2016, 8, 28872-28879.	8.0	19
555	Electrochemical degradation and extraction capability of magnesium wastes in sewage treatment. Materials and Design, 2016, 111, 537-540.	7.0	4
556	Lithiation Kinetics in High-Performance Porous Vanadium Nitride Nanosheet Anode. Electrochimica Acta, 2016, 214, 201-207.	5.2	41
557	Anomalous but massive removal of two organic dye pollutants simultaneously. Journal of Hazardous Materials, 2016, 318, 54-60.	12.4	31
558	Biomedical Applications of Functionalized ZnO Nanomaterials: from Biosensors to Bioimaging. Advanced Materials Interfaces, 2016, 3, 1500494.	3.7	138

#	Article	lF	CITATIONS
559	Mesoporous TiO ₂ Nanocrystals/Graphene as an Efficient Sulfur Host Material for High-Performance Lithium–Sulfur Batteries. ACS Applied Materials & Interfaces, 2016, 8, 23784-23792.	8.0	89
560	Flexible Nb2O5 nanowires/graphene film electrode for high-performance hybrid Li-ion supercapacitors. Journal of Power Sources, 2016, 328, 599-606.	7.8	95
561	Three-dimensional flexible carbon electrode for symmetrical supercapacitors. Materials Letters, 2016, 185, 193-196.	2.6	11
562	High-energy lithium-ion hybrid supercapacitors composed of hierarchical urchin-like WO ₃ /C anodes and MOF-derived polyhedral hollow carbon cathodes. Nanoscale, 2016, 8, 16761-16768.	5.6	85
563	Extracellular Electron Transfer from Aerobic Bacteria to Au-Loaded TiO ₂ Semiconductor without Light: A New Bacteria-Killing Mechanism Other than Localized Surface Plasmon Resonance or Microbial Fuel Cells. ACS Applied Materials & Interfaces, 2016, 8, 24509-24516.	8.0	62
564	Black Phosphorus Based Photocathodes in Wideband Bifacial Dye‣ensitized Solar Cells. Advanced Materials, 2016, 28, 8937-8944.	21.0	116
565	Anodic growth of ultra-long Ni-Ti-O nanopores. Electrochemistry Communications, 2016, 71, 28-32.	4.7	22
566	Effects of annealing ambient on oxygen vacancies and phase transition temperature of VO ₂ thin films. RSC Advances, 2016, 6, 79383-79388.	3.6	56
567	Effects of Atmospheric-Pressure Nonthermal Nitrogen and Air Plasma on Bacteria Inactivation. IEEE Transactions on Plasma Science, 2016, 44, 2699-2707.	1.3	27
568	Fabrication and enhanced supercapacitance of hollow nanostructured MoS2 prepared by a CATB-assisted hydrothermal process. Materials Letters, 2016, 184, 96-99.	2.6	16
569	Peapod-like V2O3 nanorods encapsulated into carbon as binder-free and flexible electrodes in lithium-ion batteries. Journal of Power Sources, 2016, 331, 58-66.	7.8	86
570	General fabrication of mesoporous Nb ₂ O ₅ nanobelts for lithium ion battery anodes. RSC Advances, 2016, 6, 90489-90493.	3.6	34
571	Nitrogen-doped multilayered nanographene derived from Ni ₃ C with efficient electron field emission. Journal of Materials Chemistry C, 2016, 4, 9251-9260.	5.5	9
572	Selfâ€Supporting and Binderâ€Free Anode Film Composed of Beaded Streamâ€Like Li ₄ Ti ₅ O ₁₂ Nanoparticles for Highâ€Performance Lithiumâ€lon Batteries. ChemElectroChem, 2016, 3, 1301-1305.	3.4	21
573	Study on the strain in a silicon microchannel plate by micro-Raman analysis. Semiconductor Science and Technology, 2016, 31, 055010.	2.0	0
574	Optical Identification of Topological Defect Types in Monolayer Arsenene by First-Principles Calculation. Journal of Physical Chemistry C, 2016, 120, 24917-24924.	3.1	24
575	A sandwich-type electrochemical immunosensor based on the biotin- streptavidin-biotin structure for detection of human immunoglobulin G. Scientific Reports, 2016, 6, 22694.	3.3	18
576	Biodegradable black phosphorus-based nanospheres for in vivo photothermal cancer therapy. Nature Communications, 2016, 7, 12967.	12.8	835

#	Article	IF	CITATIONS
577	Biodegradable Mg-Cu alloys with enhanced osteogenesis, angiogenesis, and long-lasting antibacterial effects. Scientific Reports, 2016, 6, 27374.	3.3	144
578	Large-Scale Synthesis and Mechanism of Î ² -SiC Nanoparticles from Rice Husks by Low-Temperature Magnesiothermic Reduction. ACS Sustainable Chemistry and Engineering, 2016, 4, 6600-6607.	6.7	62
579	Evaporative Selfâ€Assembly of Gold Nanorods into Macroscopic 3D Plasmonic Superlattice Arrays. Advanced Materials, 2016, 28, 2511-2517.	21.0	160
580	Drawing-fabrication of multifarious nanoplasmonic platform on PLLA paper for optimized SERS performance. Journal of Raman Spectroscopy, 2016, 47, 687-691.	2.5	8
581	MoS ₂ â€Quantumâ€Dotâ€Interspersed Li ₄ Ti ₅ O ₁₂ Nanoshee with Enhanced Performance for Li―and Naâ€ion Batteries. Advanced Functional Materials, 2016, 26, 3349-3358.	ts 14.9	128
582	Three-dimensional homo-nanostructured MnO ₂ /nanographene membranes on a macroporous electrically conductive network for high performance supercapacitors. Journal of Materials Chemistry A, 2016, 4, 11317-11329.	10.3	24
583	Vanadium carbide nanoparticles encapsulated in graphitic carbon network nanosheets: A high-efficiency electrocatalyst for hydrogen evolution reaction. Nano Energy, 2016, 26, 603-609.	16.0	120
584	Theoretical Assessment of Localized Surface Plasmon Resonance Properties of Au-Interlayer-Ag Multilayered Nanoshells. Plasmonics, 2016, 11, 1589-1595.	3.4	10
585	Reutilization of industrial ultrafine carbon ash (<scp>PM</scp> 2.5) as rubber reinforcement filler. Environmental Progress and Sustainable Energy, 2016, 35, 1132-1138.	2.3	2
586	Lowâ€Temperature Synthesis of Mesoporous SiC Hollow Spheres by Magnesiothermic Reduction. Journal of the American Ceramic Society, 2016, 99, 1859-1861.	3.8	19
587	Antibacterial Activity of Silver Doped Titanate Nanowires on Ti Implants. ACS Applied Materials & Interfaces, 2016, 8, 16584-16594.	8.0	102
588	Hydrogenated V ₂ O ₅ Nanosheets for Superior Lithium Storage Properties. Advanced Functional Materials, 2016, 26, 784-791.	14.9	149
589	Surface Coordination of Black Phosphorus for Robust Air and Water Stability. Angewandte Chemie, 2016, 128, 5087-5091.	2.0	116
590	Surface Coordination of Black Phosphorus for Robust Air and Water Stability. Angewandte Chemie - International Edition, 2016, 55, 5003-5007.	13.8	479
591	Influence of sulfur content on bone formation and antibacterial ability of sulfonated PEEK. Biomaterials, 2016, 83, 115-126.	11.4	189
592	Effects of cerium ion implantation on the corrosion behavior of magnesium in different biological media. Surface and Coatings Technology, 2016, 306, 6-10.	4.8	28
593	Enhanced corrosion resistance and biocompatibilty of PMMA-coated ZK60 magnesium alloy. Materials Letters, 2016, 173, 178-181.	2.6	19
594	Simultaneous arsenate and alkali removal from alkaline wastewater by in-situ formation of Zn–Al layered double hydroxide. Microporous and Mesoporous Materials, 2016, 227, 137-143.	4.4	11

#	Article	IF	CITATIONS
595	Au Nanoparticles Decorated TiO ₂ Nanotube Arrays as a Recyclable Sensor for Photoenhanced Electrochemical Detection of Bisphenol A. Environmental Science & Technology, 2016, 50, 4430-4438.	10.0	124
596	Large and porous carbon sheets derived from water hyacinth for high-performance supercapacitors. RSC Advances, 2016, 6, 29996-30003.	3.6	43
597	Size-dependent corrosion behavior and cytocompatibility of Ni–Ti–O nanotubes prepared by anodization of biomedical NiTi alloy. Corrosion Science, 2016, 103, 173-180.	6.6	47
598	Development of novel implants with self-antibacterial performance through in-situ growth of 1D ZnO nanowire. Colloids and Surfaces B: Biointerfaces, 2016, 141, 623-633.	5.0	23
599	Unusual anti-bacterial behavior and corrosion resistance of magnesium alloy coated with diamond-like carbon. RSC Advances, 2016, 6, 14756-14762.	3.6	13
600	Lactose-Functionalized Gold Nanorods for Sensitive and Rapid Serological Diagnosis of Cancer. ACS Applied Materials & Interfaces, 2016, 8, 5813-5820.	8.0	28
601	Preparation of multi-layer graphene on nickel-coated silicon microchannel plates by a hydrothermal carbonization procedure and its improved field emission properties. Journal of Materials Chemistry C, 2016, 4, 2079-2087.	5.5	23
602	Plasma Surface Functionalized Polyetheretherketone for Enhanced Osseo-Integration at Bone-Implant Interface. ACS Applied Materials & Interfaces, 2016, 8, 3901-3911.	8.0	64
603	Effects of pulse voltage and deposition time on the adhesion strength of graded metal/carbon films deposited on bendable stainless steel foils by hybrid cathodic arc – glow discharge plasma assisted chemical vapor deposition. Applied Surface Science, 2016, 366, 535-544.	6.1	4
604	Self-passivating carbon film as bipolar plate protective coating in polymer electrolyte membrane fuel cell. International Journal of Hydrogen Energy, 2016, 41, 5783-5792.	7.1	28
605	Hybrid Co(OH)2/nano-graphene/Ni nano-composites on silicon microchannel plates for miniature supercapacitors. Materials Letters, 2016, 172, 40-43.	2.6	15
606	Gypsum blocks produced from TiO ₂ production by-products. Environmental Technology (United Kingdom), 2016, 37, 1094-1100.	2.2	28
607	Smart polymeric particle encapsulated gadolinium oxide and europium: theranostic probes for magnetic resonance/optical imaging and antitumor drug delivery. Journal of Materials Chemistry B, 2016, 4, 1100-1107.	5.8	16
608	Praseodymium-surface-modified magnesium alloy: Retardation of corrosion in artificial hand sweat. Materials Letters, 2016, 163, 85-89.	2.6	11
609	A highly temperature-sensitive photonic crystal fiber based on surface plasmon resonance. Optics Communications, 2016, 359, 378-382.	2.1	59
610	Gold-nanorods-siRNA nanoplex for improved photothermal therapy by gene silencing. Biomaterials, 2016, 78, 27-39.	11.4	192
611	Self-assembly of mesoporous ZnCo ₂ O ₄ nanomaterials: density functional theory calculation and flexible all-solid-state energy storage. Journal of Materials Chemistry A, 2016, 4, 568-577.	10.3	73
612	Corrosion resistance of dicalcium phosphate dihydrate/poly(lactic-co-glycolic acid) hybrid coating on AZ31 magnesium alloy. Corrosion Science, 2016, 102, 209-221.	6.6	86

#	Article	IF	CITATIONS
613	Small gold nanorods laden macrophages for enhanced tumor coverage in photothermal therapy. Biomaterials, 2016, 74, 144-154.	11.4	247
614	Utilization of recycled chemical residues from sodium hydrosulfite production in solid lubricant for drilling fluids. Desalination and Water Treatment, 2016, 57, 1804-1813.	1.0	6
615	Cylindric high power impulse magnetron sputtering source and its discharge characteristics. Wuli Xuebao/Acta Physica Sinica, 2016, 65, 185202.	0.5	5
616	Plasma Surface Modification of Magnesium-Based and Related Materials. , 2016, , 329-330.		0
617	Aluminum plasmonic photocatalysis. Scientific Reports, 2015, 5, 15288.	3.3	59
618	Mitigation of Corrosion on Magnesium Alloy by Predesigned Surface Corrosion. Scientific Reports, 2015, 5, 17399.	3.3	59
619	Discharge current modes of high power impulse magnetron sputtering. AIP Advances, 2015, 5, .	1.3	12
620	Ultrasmall Black Phosphorus Quantum Dots: Synthesis and Use as Photothermal Agents. Angewandte Chemie - International Edition, 2015, 54, 11526-11530.	13.8	906
621	Synthesis of Layerâ€Tunable Graphene: A Combined Kinetic Implantation and Thermal Ejection Approach. Advanced Functional Materials, 2015, 25, 3666-3675.	14.9	43
622	Nitrogenâ€Doped Carbon Encapsulated Mesoporous Vanadium Nitride Nanowires as Selfâ€Supported Electrodes for Flexible Allâ€Solidâ€State Supercapacitors. Advanced Materials Interfaces, 2015, 2, 1500211.	3.7	104
623	From Black Phosphorus to Phosphorene: Basic Solvent Exfoliation, Evolution of Raman Scattering, and Applications to Ultrafast Photonics. Advanced Functional Materials, 2015, 25, 6996-7002.	14.9	862
624	Demagnification and Magnification Effects in One-Step Noncontact Pattern Transfer by Direct-Current Plasma Immersion Ion Implantation. IEEE Transactions on Plasma Science, 2015, 43, 552-556.	1.3	1
625	High-current anodization: A novel strategy to functionalize titanium-based biomaterials. Electrochimica Acta, 2015, 173, 345-353.	5.2	52
626	Anionic Group Self-Doping as a Promising Strategy: Band-Gap Engineering and Multi-Functional Applications of High-Performance CO ₃ ^{2–} -Doped Bi ₂ O ₂ CO ₃ . ACS Catalysis, 2015, 5, 4094-4103.	11.2	690
627	Interfacial reactions and zigzag groove strengthening of C/C composite and Rene N5 single crystal brazed joint. Ceramics International, 2015, 41, 11605-11610.	4.8	40
628	Effects and Mechanism of Atmospheric-Pressure Dielectric Barrier Discharge Cold Plasmaon Lactate Dehydrogenase (LDH) Enzyme. Scientific Reports, 2015, 5, 10031.	3.3	119
629	Multilayered paper-like electrodes composed of alternating stacked mesoporous Mo ₂ N nanobelts and reduced graphene oxide for flexible all-solid-state supercapacitors. Journal of Materials Chemistry A, 2015, 3, 14617-14624.	10.3	75
630	Bamboo leaf derived ultrafine Si nanoparticles and Si/C nanocomposites for high-performance Li-ion battery anodes. Nanoscale, 2015, 7, 13840-13847.	5.6	105

#	Article	IF	CITATIONS
631	Manipulation of strain state in silicon nanoribbons by top-down approach. Applied Physics Letters, 2015, 106, .	3.3	7
632	Characterization of carbon ion implantation induced graded microstructure and phase transformation in stainless steel. Materials Characterization, 2015, 106, 11-19.	4.4	21
633	Lattice shearing in nano-grained graphene sheets: a molecular dynamics simulation. RSC Advances, 2015, 5, 105194-105199.	3.6	4
634	Robust Electrodes Based on Coaxial TiC/C-MnO ₂ Core/Shell Nanofiber Arrays with Excellent Cycling Stability for High-Performance Supercapacitors. Small, 2015, 11, 1847-1856.	10.0	15
635	Characteristics of DC Gas-Liquid Phase Atmospheric-Pressure Plasma and Bacteria Inactivation Mechanism. Plasma Processes and Polymers, 2015, 12, 252-259.	3.0	68
636	Biodegradable poly-lactic acid based-composite reinforced unidirectionally with high-strength magnesium alloy wires. Biomaterials, 2015, 49, 135-144.	11.4	86
637	Highly porous honeycomb manganese oxide@carbon fibers core–shell nanocables for flexible supercapacitors. Nano Energy, 2015, 13, 47-57.	16.0	65
638	Emission from Trions in Carbon Quantum Dots. Journal of Physical Chemistry C, 2015, 119, 2956-2962.	3.1	53
639	Fluorinated Graphene in Interface Engineering of Geâ€Based Nanoelectronics. Advanced Functional Materials, 2015, 25, 1805-1813.	14.9	40
640	Engineering and functionalization of biomaterials via surface modification. Journal of Materials Chemistry B, 2015, 3, 2024-2042.	5.8	138
641	Recyclable Nonâ€Enzymatic Glucose Sensor Based on Ni/NiTiO ₃ /TiO ₂ Nanotube Arrays. ChemPlusChem, 2015, 80, 576-582.	2.8	34
642	Highly-crystalline ultrathin Li4Ti5O12 nanosheets decorated with silver nanocrystals as a high-performance anode material for lithium ion batteries. Journal of Power Sources, 2015, 276, 247-254.	7.8	99
643	Folate-bovine serum albumin functionalized polymeric micelles loaded with superparamagnetic iron oxide nanoparticles for tumor targeting and magnetic resonance imaging. Acta Biomaterialia, 2015, 15, 117-126.	8.3	77
644	Bio-tribological properties and cytocompatibility of Ti–Si–N coatings. Vacuum, 2015, 115, 50-57.	3.5	10
645	Highly ordered Ni–Ti–O nanotubes for non-enzymatic glucose detection. Materials Science and Engineering C, 2015, 51, 37-42.	7.3	31
646	Supercapacitor Electrodes Based on Hierarchical Mesoporous MnO <i>_x</i> /Nitrided TiO ₂ Nanorod Arrays on Carbon Fiber Paper. Advanced Materials Interfaces, 2015, 2, 1400446.	3.7	22
647	Enhanced osteointegration on tantalum-implanted polyetheretherketone surface with bone-like elastic modulus. Biomaterials, 2015, 51, 173-183.	11.4	206
648	Quantum confinement effects across two-dimensional planes in MoS2 quantum dots. Applied Physics Letters, 2015, 106, .	3.3	180

#	Article	IF	CITATIONS
649	Balancing the Osteogenic and Antibacterial Properties of Titanium by Codoping of Mg and Ag: An in Vitro and in Vivo Study. ACS Applied Materials & Interfaces, 2015, 7, 17826-17836.	8.0	70
650	Effects of Al and N plasma immersion ion implantation on surface microhardness, oxidation resistance and antibacterial characteristics of Cu. Transactions of Nonferrous Metals Society of China, 2015, 25, 1944-1949.	4.2	7
651	Facet-controlled synthesis and facet-dependent photocatalytic properties of SnO2 micropolyhedrons. Applied Surface Science, 2015, 349, 798-804.	6.1	32
652	Structure, molecular simulation, and release of a spirin from intercalated Zn–Al-layered double hydroxides. Colloids and Surfaces B: Biointerfaces, 2015, 135, 339-345.	5.0	33
653	Evaluation of corrosion resistance and cytocompatibility of graded metal carbon film on Ti and NiTi prepared by hybrid cathodic arc/glow discharge plasma-assisted chemical vapor deposition. Corrosion Science, 2015, 97, 126-138.	6.6	38
654	Zn/Ag micro-galvanic couples formed on titanium and osseointegration effects in the presence of S.Aaureus. Biomaterials, 2015, 65, 22-31.	11.4	89
655	Hybrid MnO ₂ /C nano-composites on a macroporous electrically conductive network for supercapacitor electrodes. Journal of Materials Chemistry A, 2015, 3, 16695-16707.	10.3	41
656	Effects of plasma-generated nitrogen functionalities on the upregulation of osteogenesis of bone marrow-derived mesenchymal stem cells. Journal of Materials Chemistry B, 2015, 3, 1856-1863.	5.8	7
657	Achieving significantly enhanced visible-light photocatalytic efficiency using a polyelectrolyte: the composites of exfoliated titania nanosheets, graphene, and poly(diallyl-dimethyl-ammonium chloride). Nanoscale, 2015, 7, 14002-14009.	5.6	27
658	Effects of N ₂ /O ₂ flow rate on the surface properties and biocompatibility of nano-structured TiO _{<i>x</i>} N _{<i>y</i>} thin films prepared by high vacuum magnetron sputtering. Chinese Physics B, 2015, 24, 075202.	1.4	7
659	Nanostructured titanium–silver coatings with good antibacterial activity and cytocompatibility fabricated by one-step magnetron sputtering. Applied Surface Science, 2015, 355, 32-44.	6.1	56
660	Temperature and strain-rate effects on the deformation behaviors of nano-crystalline graphene sheets. European Physical Journal B, 2015, 88, 1.	1.5	24
661	Enhanced cytocompatibility of silver-containing biointerface by constructing nitrogen functionalities. Applied Surface Science, 2015, 349, 327-332.	6.1	10
662	Size-dependent deformation behavior of nanocrystalline graphene sheets. Materials Science and Engineering B: Solid-State Materials for Advanced Technology, 2015, 198, 95-101.	3.5	17
663	Reduced graphene oxide encapsulated selenium nanoparticles for high-power lithium–selenium battery cathode. Journal of Power Sources, 2015, 288, 214-220.	7.8	88
664	Corrosion resistance of praseodymium-ion-implanted TiN coatings in blood and cytocompatibility with vascular endothelial cells. Vacuum, 2015, 117, 73-80.	3.5	17
665	Microstructure and mechanical properties of C/C composite/TC4 joint with inactive AgCu filler metal. Ceramics International, 2015, 41, 7021-7027.	4.8	51
666	Inactivation Effects of Nonâ€Thermal Atmosphericâ€Pressure Helium Plasma Jet on <i>Staphylococcus aureus</i> Biofilms. Plasma Processes and Polymers, 2015, 12, 827-835.	3.0	63

#	Article	IF	CITATIONS
667	Improvement of corrosion resistance and biocompatibility of rare-earth WE43 magnesium alloy by neodymium self-ion implantation. Corrosion Science, 2015, 94, 142-155.	6.6	161
668	Electronic structure and magnetism in <i>g</i> -C4N3 controlled by strain engineering. Applied Physics Letters, 2015, 106, .	3.3	23
669	Hierarchical 3-dimensional CoMoO ₄ nanoflakes on a macroporous electrically conductive network with superior electrochemical performance. Journal of Materials Chemistry A, 2015, 3, 13776-13785.	10.3	61
670	Upregulation of BMSCs Osteogenesis by Positively-Charged Tertiary Amines on Polymeric Implants via Charge/iNOS Signaling Pathway. Scientific Reports, 2015, 5, 9369.	3.3	36
671	Magnetic, fluorescent, and thermo-responsive poly(MMA-NIPAM-Tb(AA) ₃ Phen)/Fe ₃ O ₄ multifunctional nanospheres prepared by emulsifier-free emulsion polymerization. Journal of Biomaterials Applications. 2015. 30. 201-211.	2.4	12
672	Removal of organic pollutants from red water by magnetic-activated coke. Desalination and Water Treatment, 2015, 54, 2710-2722.	1.0	17
673	Engineering Nanoparticle-Coated Bacteria as Oral DNA Vaccines for Cancer Immunotherapy. Nano Letters, 2015, 15, 2732-2739.	9.1	213
674	Amorphous nickel/cobalt tungsten sulfide electrocatalysts for high-efficiency hydrogen evolution reaction. Applied Surface Science, 2015, 341, 149-156.	6.1	76
675	Design and theoretical analysis of a photonic crystal fiber based on surface plasmon resonance sensing. Journal of Nanophotonics, 2015, 9, 093050.	1.0	33
676	A General and Facile Approach to Heterostructured Core/Shell BiVO ₄ /BiOI <i>p–n</i> Junction: Room-Temperature <i>in Situ</i> Assembly and Highly Boosted Visible-Light Photocatalysis. ACS Sustainable Chemistry and Engineering, 2015, 3, 3262-3273.	6.7	285
677	Trifunctional Polymeric Nanocomposites Incorporated with Fe ₃ O ₄ /lodine-Containing Rare Earth Complex for Computed X-ray Tomography, Magnetic Resonance, and Optical Imaging. ACS Applied Materials & Interfaces, 2015, 7, 24523-24532.	8.0	19
678	Selective growth of Pb islands on graphene/SiC buffer layers. Journal of Applied Physics, 2015, 117, 065304.	2.5	11
679	Genetic effects of an air discharge plasma on <i>Staphylococcus aureus</i> at the gene transcription level. Applied Physics Letters, 2015, 106, .	3.3	30
680	Tunable photoluminescence from sheet-like black phosphorus crystal by electrochemical oxidation. Applied Physics Letters, 2015, 107, 021901.	3.3	34
681	3C-SiC/ZnS heterostructured nanospheres with high photocatalytic activity and enhancement mechanism. AIP Advances, 2015, 5, .	1.3	6
682	Electrochemical investigation of the corrosion properties of three-dimensional nickel electrodes on silicon microchannel plates. Corrosion Science, 2015, 100, 113-120.	6.6	6
683	Paramagnetic, pH and temperature-sensitive polymeric particles for anticancer drug delivery and brain tumor magnetic resonance imaging. RSC Advances, 2015, 5, 87512-87520.	3.6	7
684	CVD Growth of Graphene on NiTi Alloy for Enhanced Biological Activity. ACS Applied Materials & Interfaces, 2015, 7, 19876-19881.	8.0	53

#	Article	IF	CITATIONS
685	Effects of silver plasma immersion ion implantation on the surface characteristics and cytocompatibility of titanium nitride films. Surface and Coatings Technology, 2015, 279, 166-170.	4.8	22
686	Supermolecular theranostic capsules for pH-sensitive magnetic resonance imaging and multi-responsive drug delivery. Journal of Materials Chemistry B, 2015, 3, 8499-8507.	5.8	10
687	Porous Dual‣ayered MoO _{<i>x</i>} Nanotube Arrays with Highly Conductive TiN Cores for Supercapacitors. ChemElectroChem, 2015, 2, 512-517.	3.4	30
688	Fabrication of Multiple Heterojunctions with Tunable Visible-Light-Active Photocatalytic Reactivity in BiOBr–BiOI Full-Range Composites Based on Microstructure Modulation and Band Structures. ACS Applied Materials & Interfaces, 2015, 7, 482-492.	8.0	671
689	Investigation of organic matter adsorption from TNT red water by modified bamboo charcoal. Desalination and Water Treatment, 2015, 56, 684-694.	1.0	5
690	Antibacterial and osteoinductive capability of orthopedic materials via cation–π interaction mediated positive charge. Journal of Materials Chemistry B, 2015, 3, 733-737.	5.8	28
691	Ordered-standing nickel hydroxide microchannel arrays: Synthesis and application for highly sensitive non-enzymatic glucose sensors. Microelectronic Engineering, 2015, 133, 11-15.	2.4	8
692	Graded metal carbon protein binding films prepared by hybrid cathodic arc — Glow discharge plasma assisted chemical vapor deposition. Surface and Coatings Technology, 2015, 265, 222-234.	4.8	10
693	Electrochemical corrosion behavior of biodegradable Mg–Y–RE and Mg–Zn–Zr alloys in Ringer's solution and simulated body fluid. Corrosion Science, 2015, 91, 160-184.	6.6	162
694	Strong phonon–plasmon coupling at the interface of 3C–SiC/metal oxide nanoparticles. Acta Materialia, 2015, 83, 113-119.	7.9	4
695	Fabrication of nanocomposite electrode based on Bi4Nd Ti3O12 perovskite supported by silicon microchannel plates for high performance electrochemical capacitors. Journal of Alloys and Compounds, 2015, 619, 748-753.	5.5	8
696	Synthesis, microstructure, and electronic band structure properties of nanocrystalline neodymium-doped bismuth titanate ferroelectric films fabricated by the sol–gel method. Materials Research Bulletin, 2015, 61, 238-244.	5.2	11
697	MnO2–TiO2/C nanocomposite arrays for high-performance supercapacitor electrodes. Thin Solid Films, 2015, 584, 61-65.	1.8	32
698	Enhanced Bioactivity of Biomedical NiTi Through Surface Plasma Polymerization. Nanoscience and Nanotechnology Letters, 2015, 7, 220-225.	0.4	6
699	Three-dimensional nanoscale Co3O4 electrode on ordered Ni/Si microchannel plates for electrochemical supercapacitors. Materials Letters, 2014, 132, 405-408.	2.6	12
700	Improved ion implant fluence uniformity in hydrogen enhanced glow discharge plasma immersion ion implantation into silicon. Review of Scientific Instruments, 2014, 85, 063506.	1.3	2
701	Cubic In ₂ O ₃ Microparticles for Efficient Photoelectrochemical Oxygen Evolution. Journal of Physical Chemistry Letters, 2014, 5, 4298-4304.	4.6	49
702	Improved corrosion resistance of Mg-Y-RE alloy coated with niobium nitride. Thin Solid Films, 2014, 572, 85-90.	1.8	17

#	Article	IF	CITATIONS
703	3C-SiC nanocrystals/TiO2 nanotube heterostructures with enhanced photocatalytic performance. Applied Physics Letters, 2014, 104, .	3.3	11
704	Engineered polycaprolactone–magnesium hybrid biodegradable porous scaffold for bone tissue engineering. Progress in Natural Science: Materials International, 2014, 24, 561-567.	4.4	58
705	Enhanced Photodegradation of Methyl Orange Synergistically by Microcrystal Facet Cutting and Flexible Electrically-Conducting Channels. Journal of Physical Chemistry C, 2014, 118, 28063-28068.	3.1	23
706	Enhanced fluorescence from dye molecules by Au nanoparticles on asymmetric double-stranded DNA and mechanism. Applied Physics Letters, 2014, 104, .	3.3	5
707	General Properties of Bulk SiC. Engineering Materials and Processes, 2014, , 7-114.	0.4	11
708	Plasma-target surface interaction during non-equilibrium plasma irradiation at atmospheric pressure: Generation of dusty plasma. Laser and Particle Beams, 2014, 32, 69-78.	1.0	6
709	Antibacterial effects and biocompatibility of titanium surfaces with graded silver incorporation in titania nanotubes. Biomaterials, 2014, 35, 4255-4265.	11.4	319
710	The effects of titania nanotubes with embedded silver oxide nanoparticles on bacteria and osteoblasts. Biomaterials, 2014, 35, 4223-4235.	11.4	305
711	Enhanced corrosion resistance and hemocompatibility of biomedical NiTi alloy by atmospheric-pressure plasma polymerized fluorine-rich coating. Applied Surface Science, 2014, 297, 109-115.	6.1	31
712	Eelectrochemical properties and corrosion resistance of carbon-ion-implanted magnesium. Corrosion Science, 2014, 82, 173-179.	6.6	65
713	Vascular endothelial cell compatibility of superhard ternary Ti–Si–N coatings with different Si contents. Vacuum, 2014, 106, 53-63.	3.5	5
714	Optical microcavities with tubular geometry: properties and applications. Laser and Photonics Reviews, 2014, 8, 521-547.	8.7	91
715	Sensitive and Robust Colorimetric Sensing of Sulfide Anion by Plasmonic Nanosensors Based on Quick Crystal Growth. Plasmonics, 2014, 9, 11-16.	3.4	28
716	Heterostructured Ni(OH)2–Co(OH)2 composites on 3D ordered Ni–Co nanoparticles fabricated on microchannel plates for advanced miniature supercapacitor. Journal of Alloys and Compounds, 2014, 589, 364-371.	5.5	37
717	Facet Cutting and Hydrogenation of In ₂ O ₃ Nanowires for Enhanced Photoelectrochemical Water Splitting. ACS Applied Materials & Interfaces, 2014, 6, 4081-4088.	8.0	58
718	Characteristics of atmospheric-pressure non-thermal N ₂ and N ₂ /O ₂ gas mixture plasma jet. Journal of Applied Physics, 2014, 115, 033303.	2.5	67
719	Core–shell TiC/C nanofiber arrays decorated with copper nanoparticles for high performance non-enzymatic glucose sensing. Sensors and Actuators B: Chemical, 2014, 192, 474-479.	7.8	35
720	Effects of zirconium and oxygen plasma ion implantation on the corrosion behavior of ZK60 Mg alloy in simulated body fluids. Corrosion Science, 2014, 82, 7-26.	6.6	106

#	Article	IF	CITATIONS
721	Novel Method for the Fabrication of Flexible Film with Oriented Arrays of Graphene in Poly(vinylidene) Tj ETQq1 1 10567-10573.	0.784314 3.1	rgBT /Overle 89
722	Rose-bengal-conjugated gold nanorods for inÂvivo photodynamic and photothermal oral cancer therapies. Biomaterials, 2014, 35, 1954-1966.	11.4	276
723	Plasma modified Mg–Nd–Zn–Zr alloy with enhanced surface corrosion resistance. Corrosion Science, 2014, 78, 121-129.	6.6	73
724	Self-assembled magnetic fluorescent polymeric micelles for magnetic resonance and optical imaging. Biomaterials, 2014, 35, 344-355.	11.4	67
725	Paper-based plasmonic platform for sensitive, noninvasive, and rapid cancer screening. Biosensors and Bioelectronics, 2014, 54, 128-134.	10.1	62
726	Dopant-Induced Surface Magnetism in β-SiC Controlled by Dopant Depth. Journal of Physical Chemistry C, 2014, 118, 25429-25433.	3.1	7
727	Observation of inactivation ofBacillus sbtilisspores under exposures of oxygen added argon atmospheric pressure plasma jet. Japanese Journal of Applied Physics, 2014, 53, 110310.	1.5	19
728	Synthesis of hollow rare-earth compound nanoparticles by a universal sacrificial template method. CrystEngComm, 2014, 16, 6141-6148.	2.6	29
729	Hydrothermal synthesis of perovskite-type MTiO ₃ (M = Zn, Co,) Tj ETQq1 1 0.784314 rgBT /Overlock 2014, 16, 10280-10285.	2 10 Tf 50 4 2.6	427 Td (Ni)/1 25
730	Asymmetrical Supercapacitor Composed of Thin Co(OH)2 Nanoflakes on Three-Dimensional Ni/Si Microchannel Plates with Superior Electrochemical Performance. Electrochimica Acta, 2014, 149, 18-27.	5.2	25
731	Atmospheric pressure plasma jet utilizing Ar and Ar/H ₂ O mixtures and its applications to bacteria inactivation. Chinese Physics B, 2014, 23, 075204.	1.4	34
732	Fabrication, modification, and biomedical applications of anodized TiO ₂ nanotube arrays. RSC Advances, 2014, 4, 17300-17324.	3.6	124
733	Polymeric Nanoarchitectures on Ti-Based Implants for Antibacterial Applications. ACS Applied Materials & Interfaces, 2014, 6, 17323-17345.	8.0	84
734	High temperature oxidation of Cr–N coatings prepared by high power pulsed magnetron sputtering – Plasma immersion ion implantation & deposition. Vacuum, 2014, 108, 66-70.	3.5	8
735	Biological Applications. Engineering Materials and Processes, 2014, , 317-330.	0.4	0
736	Functionalized TiO ₂ Based Nanomaterials for Biomedical Applications. Advanced Functional Materials, 2014, 24, 5464-5481.	14.9	208
737	Restoration of chemosensitivity by multifunctional micelles mediated by P-gp siRNA to reverse MDR. Biomaterials, 2014, 35, 8621-8634.	11.4	69
738	InÂvitro and inÂvivo anti-biofilm effects of silver nanoparticles immobilized on titanium. Biomaterials, 2014, 35, 9114-9125.	11.4	205

#	Article	IF	CITATIONS
739	CdS:Mn–Polysulfido Complex Nanoclusters with H ₂ O ₂ -Dependent and Site-Specific Color Changes. Journal of Physical Chemistry C, 2014, 118, 11085-11092.	3.1	3
740	Silicon Carbide Nanostructures. Engineering Materials and Processes, 2014, , .	0.4	63
741	Synergistic effects of dual Zn/Ag ion implantation in osteogenic activity and antibacterial ability of titanium. Biomaterials, 2014, 35, 7699-7713.	11.4	340
742	Photothermal Contribution to Enhanced Photocatalytic Performance of Graphene-Based Nanocomposites. ACS Nano, 2014, 8, 9304-9310.	14.6	240
743	Multifunctional cationic polymer decorated and drug intercalated layered silicate (NLS) for early gastric cancer prevention. Biomaterials, 2014, 35, 3298-3308.	11.4	24
744	All-silicon solid films with highly efficient and tunable full-color photoluminescence. Scripta Materialia, 2014, 76, 17-20.	5.2	5
745	Impedance study of adsorption phenomena on three-dimensional nano-nickel electrode deposited on silicon microchannel plate. Electrochimica Acta, 2014, 132, 165-171.	5.2	7
746	Surface electromagnetic wave equations in a warm magnetized quantum plasma. Physics of Plasmas, 2014, 21, 072114.	1.9	20
747	Rare-earth-incorporated polymeric vector for enhanced gene delivery. Biomaterials, 2014, 35, 479-488.	11.4	11
748	Multifunctional gold coated rare-earth hydroxide fluoride nanotubes for simultaneous wastewater purification and quantitative pollutant determination. Materials Research Bulletin, 2014, 52, 122-127.	5.2	6
749	Multilevel surface engineering of nanostructured TiO2 on carbon-fiber-reinforced polyetheretherketone. Biomaterials, 2014, 35, 5731-5740.	11.4	81
750	Irradiation effects on multilayered W/ZrO 2 film under 4 MeV Au ions. Journal of Nuclear Materials, 2014, 455, 86-90.	2.7	14
751	Functionalization of biomedical materials using plasma and related technologies. Applied Surface Science, 2014, 310, 11-18.	6.1	21
752	Metal oxide coating on first mirror in fusion reactor with carbon wall. Surface and Coatings Technology, 2014, 240, 464-469.	4.8	1
753	Fabrication of highly ordered porous nickel oxide anode materials and their electrochemical characteristics in lithium storage. Journal of Alloys and Compounds, 2014, 594, 65-69.	5.5	15
754	Removal of organic pollutants from super heavy oil wastewater by lignite activated coke. Colloids and Surfaces A: Physicochemical and Engineering Aspects, 2014, 447, 120-130.	4.7	28
755	Electrodeposition of nanostructured MnO2 electrode on three-dimensional nickel/silicon microchannel plates for miniature supercapacitors. Materials Letters, 2014, 126, 116-118.	2.6	15
756	Surface changes in Fe–Cr–Ni alloy bombarded by relativistic pulsed electron beam and associated mechanism. Vacuum, 2014, 101, 136-141.	3.5	3

#	Article	IF	CITATIONS
757	Enhanced antimicrobial properties, cytocompatibility, and corrosion resistance of plasma-modified biodegradable magnesium alloys. Acta Biomaterialia, 2014, 10, 544-556.	8.3	194
758	Synergistic effect of chloride ion and albumin on the corrosion of pure magnesium. Frontiers of Materials Science, 2014, 8, 244-255.	2.2	16
759	Electron density measurements of atmospheric-pressure non-thermal N2 plasma jet by Stark broadening and irradiance intensity methods. Physics of Plasmas, 2014, 21, .	1.9	46
760	Cyclodextrin-Based Host–Guest Supramolecular Nanoparticles for Delivery: From Design to Applications. Accounts of Chemical Research, 2014, 47, 2017-2025.	15.6	418
761	Poly(ethylene glycol)/carbon quantum dot composite solid films exhibiting intense and tunable blue–red emission. Applied Surface Science, 2014, 311, 490-497.	6.1	71
762	Effects of zirconium and nitrogen plasma immersion ion implantation on the electrochemical corrosion behavior of Mg–Y–RE alloy in simulated body fluid and cell culture medium. Corrosion Science, 2014, 86, 239-251.	6.6	53
763	Competitive Reaction Pathway for Siteâ€Selective Conjugation of Raman Dyes to Hotspots on Gold Nanorods for Greatly Enhanced SERS Performance. Small, 2014, 10, 4012-4019.	10.0	21
764	Stimulation of bone growth following zinc incorporation into biomaterials. Biomaterials, 2014, 35, 6882-6897.	11.4	241
765	Microporous N-doped carbon film produced by cold atmospheric plasma jet and its cell compatibility. Vacuum, 2014, 108, 27-34.	3.5	7
766	Antibacterial and mechanical properties of honeycomb ceramic materials incorporated with silver and zinc. Materials & Design, 2014, 59, 461-465.	5.1	28
767	Plasmon-induced broadband fluorescence enhancement on Al-Ag bimetallic substrates. Scientific Reports, 2014, 4, 6014.	3.3	24
768	Fabrication of Ni-Ti-O nanotube arrays by anodization of NiTi alloy and their potential applications. Scientific Reports, 2014, 4, 7547.	3.3	52
769	Rice Husk-Derived Activated Carbon for Li Ion Battery Anode. Nanoscience and Nanotechnology Letters, 2014, 6, 68-71.	0.4	32
770	Enhanced discharge of high power pulsed magnetron sputtering coupling with high voltage. Wuli Xuebao/Acta Physica Sinica, 2014, 63, 185207.	0.5	5
771	Progress in direct-current plasma immersion ion implantation and recent applications of plasma immersion ion implantation and deposition. Surface and Coatings Technology, 2013, 229, 2-11.	4.8	25
772	Surface engineering and modification of biomaterials. Thin Solid Films, 2013, 528, 93-105.	1.8	39
773	Interface analysis of inorganic films on polyimide with atomic oxygen exposure. Surface and Coatings Technology, 2013, 216, 121-126.	4.8	24
774	Bimodal optical diagnostics of oral cancer based on Rose Bengal conjugated gold nanorod platform. Biomaterials, 2013, 34, 4274-4283.	11.4	74

#	Article	IF	CITATIONS
775	Electron storage mediated dark antibacterial action of bound silver nanoparticles: Smaller is not always better. Acta Biomaterialia, 2013, 9, 5100-5110.	8.3	116
776	Nanoparticles for improving cancer diagnosis. Materials Science and Engineering Reports, 2013, 74, 35-69.	31.8	94
777	Micrograph and structure of CrN films prepared by plasma immersion ion implantation and deposition using HPPMS plasma source. Surface and Coatings Technology, 2013, 229, 210-216.	4.8	14
778	Microelectrode arrays based on carbon nanomaterials: emerging electrochemical sensors for biological and environmental applications. RSC Advances, 2013, 3, 18698.	3.6	34
779	Anode properties and morphology evolution of three-dimensional lithium-ion battery electrodes comprising Ni-coated Si microchannel plates. Journal of Alloys and Compounds, 2013, 563, 186-191.	5.5	9
780	Bone integration capability of a series of strontiumâ€containing hydroxyapatite coatings formed by microâ€arc oxidation. Journal of Biomedical Materials Research - Part A, 2013, 101A, 2465-2480.	4.0	84
781	Improved surface corrosion resistance of WE43 magnesium alloy by dual titanium and oxygen ion implantation. Thin Solid Films, 2013, 529, 407-411.	1.8	58
782	Antimicrobial effects of oxygen plasma modified medical grade Ti–6Al–4V alloy. Vacuum, 2013, 89, 271-279.	3.5	12
783	Transformation of Enhanced Glow Discharge Dynamics in Nitrogen Plasma Immersion Ion Implantation. IEEE Transactions on Plasma Science, 2013, 41, 553-558.	1.3	2
784	Direct and diffuse reflection of electron waves at armchair edges of epitaxial graphene. RSC Advances, 2013, 3, 25735.	3.6	6
785	Cytocompatibility, osseointegration, and bioactivity of three-dimensional porous and nanostructured network on polyetheretherketone. Biomaterials, 2013, 34, 9264-9277.	11.4	302
786	Surface design of biodegradable magnesium alloys — A review. Surface and Coatings Technology, 2013, 233, 2-12.	4.8	309
787	Direct formation of amine functionality on DLC films and surface cyto-compatibility. Diamond and Related Materials, 2013, 38, 28-31.	3.9	5
788	Improved in vitro and in vivo biocompatibility of dual plasma modified titanium alloy. Surface and Coatings Technology, 2013, 229, 130-134.	4.8	13
789	Tunable fluorescence from patterned silver nano-island arrays for sensitive sub-cell imaging. Journal Physics D: Applied Physics, 2013, 46, 495302.	2.8	7
790	Direct Growth of Graphene Film on Germanium Substrate. Scientific Reports, 2013, 3, 2465.	3.3	181
791	Graded nanostructured interfacial layers fabricated by high power pulsed magnetron sputtering — plasma immersion ion implantation and deposition (HPPMS–PIII&D). Surface and Coatings Technology, 2013, 236, 320-325.	4.8	5
792	Magnetic, fluorescent, and thermo-responsive Fe3O4/rare earth incorporated poly(St-NIPAM) core–shell colloidal nanoparticles in multimodal optical/magnetic resonance imaging probes. Biomaterials, 2013, 34, 2296-2306.	11.4	85

#	Article	IF	CITATIONS
793	In situ probing of intracellular pH by fluorescence from inorganic nanoparticles. Biomaterials, 2013, 34, 9183-9189.	11.4	26
794	Effects of loading mode and orientation on deformation mechanism of graphene nano-ribbons. Applied Physics Letters, 2013, 103, 191906.	3.3	5
795	Structure and properties of TiC/Ti coatings fabricated on NiTi by plasma immersion ion implantation and deposition. Vacuum, 2013, 89, 238-243.	3.5	13
796	Mechanism of Photoluminescence from Chemically Derived Graphene Oxide: Role of Chemical Reduction. Advanced Optical Materials, 2013, 1, 926-932.	7.3	160
797	Electrochemical Characteristics of Discrete, Uniform, and Monodispersed Hollow Mesoporous Carbon Spheres in Double‣ayered Supercapacitors. Chemistry - an Asian Journal, 2013, 8, 2627-2633.	3.3	18
798	Electronic states in hybrid boron nitride and graphene structures. Journal of Applied Physics, 2013, 114, 063707.	2.5	13
799	Structure and corrosion resistance of Ti/TiC coatings fabricated by plasma immersion ion implantation and deposition on nickel–titanium. Surface and Coatings Technology, 2013, 229, 151-155.	4.8	31
800	Coaxial PANI/TiN/PANI nanotube arrays for high-performance supercapacitor electrodes. Chemical Communications, 2013, 49, 10172.	4.1	92
801	Surface Characterization of Biomaterials. , 2013, , 105-174.		32
802	Optical identification of oxygen vacancy types in SnO2 nanocrystals. Applied Physics Letters, 2013, 102, .	3.3	65
803	Enhanced Photoelectrochemical Oxygen Evolution Reaction based on Surface Autocatalytic Effect of Ultrathin 3C-SiC Nanocrystals. Journal of the Electrochemical Society, 2013, 160, H620-H623.	2.9	1
804	C/CrN multilayer coating for polymer electrolyte membrane fuel cell metallic bipolar plates. Journal of Power Sources, 2013, 222, 351-358.	7.8	54
805	Thermal oxidation of titanium: Evaluation of corrosion resistance as a function of cooling rate. Materials Chemistry and Physics, 2013, 138, 565-572.	4.0	83
806	Dual-emitting nanocomposites derived from rare-earth compound nanotubes for ratiometric fluorescence sensing applications. Nanoscale, 2013, 5, 1629.	5.6	29
807	Electrochemical analysis of nickel electrode deposited on silicon microchannel plate. Electrochimica Acta, 2013, 90, 344-349.	5.2	18
808	Fabrication and enhanced dielectric properties of graphene–polyvinylidene fluoride functional hybrid films with a polyaniline interlayer. Journal of Materials Chemistry A, 2013, 1, 884-890.	10.3	110
809	Effects of chromium ion implantation voltage on the corrosion resistance and cytocompatibility of dual chromium and oxygen plasma-ion-implanted biodegradable magnesium. Surface and Coatings Technology, 2013, 235, 875-880.	4.8	12
810	Non-enzymatic hydrogen peroxide photoelectrochemical sensor based on WO3 decorated core–shell TiC/C nanofibers electrode. Electrochimica Acta, 2013, 108, 491-496.	5.2	51

#	Article	IF	CITATIONS
811	Self-protection against corrosion of aged magnesium alloy in simulated physiological environment. Corrosion Science, 2013, 68, 279-285.	6.6	56
812	Surface and interference co-enhanced Raman scattering from indium tin oxide nanocap arrays. Applied Surface Science, 2013, 280, 343-348.	6.1	10
813	InÂvivo stimulation of bone formation by aluminum and oxygen plasma surface-modified magnesium implants. Biomaterials, 2013, 34, 9863-9876.	11.4	99
814	Effects of silicon plasma ion implantation on electrochemical corrosion behavior of biodegradable Mg–Y–RE Alloy. Corrosion Science, 2013, 69, 158-163.	6.6	65
815	Low-modulus Mg/PCL hybrid bone substitute for osteoporotic fracture fixation. Biomaterials, 2013, 34, 7016-7032.	11.4	112
816	Osteogenic activity and antibacterial effects on titanium surfaces modified with Zn-incorporated nanotube arrays. Biomaterials, 2013, 34, 3467-3478.	11.4	269
817	Effects of carbon dioxide plasma immersion ion implantation on the electrochemical properties of AZ31 magnesium alloy in physiological environment. Applied Surface Science, 2013, 286, 257-260.	6.1	18
818	N-doped SnO2 nanocrystals with green emission dependent upon mutual effects of nitrogen dopant and oxygen vacancy. Acta Materialia, 2013, 61, 7342-7347.	7.9	28
819	Properties of carbon film deposited on stainless steel by close field unbalanced magnetron sputter ion plating. Thin Solid Films, 2013, 531, 320-327.	1.8	12
820	Thermal degradation and flame retarding characteristics of polypropylene composites incorporated with boron mud. Composites Science and Technology, 2013, 85, 131-135.	7.8	20
821	Effect of high fluence Au ion irradiation on nanocrystalline tungsten film. Journal of Nuclear Materials, 2013, 442, 189-194.	2.7	14
822	Microstructure evolution and mechanical properties of vacuum-brazed C/C composite with AgCuTi foil. Materials Science & Engineering A: Structural Materials: Properties, Microstructure and Processing, 2013, 564, 192-198.	5.6	59
823	Surface-induced structural transformation in nanowires. Materials Science and Engineering Reports, 2013, 74, 173-209.	31.8	23
824	Atomic layer deposition of platinum thin films on anodic aluminium oxide templates as surface-enhanced Raman scattering substrates. Vacuum, 2013, 89, 257-260.	3.5	15
825	Concentrated ion beam emitted from an enlarged cylindrical-anode-layer Hall plasma accelerator and mechanism. Journal of Applied Physics, 2013, 113, 043302.	2.5	1
826	Resonant Raman scattering from CdS nanocrystals enhanced by interstitial Mn. Applied Physics Letters, 2013, 102, .	3.3	24
827	Self-sealing SiO2 pores on silicon formed by oxidation of microporous silicon. Microporous and Mesoporous Materials, 2013, 174, 10-13.	4.4	1
828	Plasmon-Matter Interactions in Optoelectronic Metamaterials with Negative Refractive Index. Plasmonics, 2013, 8, 1309-1315.	3.4	5

#	Article	IF	CITATIONS
829	Control of Surface Degradation on Biodegradable Magnesium Alloys by Plasma-Based Technology. IEEE Transactions on Plasma Science, 2013, 41, 725-730.	1.3	7
830	Fluorescent Magnetic Fe ₃ O ₄ /Rare Earth Colloidal Nanoparticles for Dualâ€Modality Imaging. Small, 2013, 9, 2991-3000.	10.0	42
831	Evidence of atomically resolved 6×6 buffer layer with long-range order and short-range disorder during formation of graphene on 6H-SiC by thermal decomposition. Applied Physics Letters, 2013, 102, .	3.3	19
832	Microstructure and surface properties of chromium-doped diamond-like carbon thin films fabricated by high power pulsed magnetron sputtering. Applied Surface Science, 2013, 276, 31-36.	6.1	25
833	Recent advances in multifunctional magnetic nanoparticles and applications to biomedical diagnosis and treatment. RSC Advances, 2013, 3, 10598.	3.6	87
834	Electrochemically deposited chitosan/Ag complex coatings on biomedical NiTi alloy for antibacterial application. Surface and Coatings Technology, 2013, 232, 370-375.	4.8	49
835	WO3 nanoparticles decorated core–shell TiC–C nanofiber arrays for high sensitive and non-enzymatic photoelectrochemical biosensing. Chemical Communications, 2013, 49, 7091.	4.1	20
836	Effect of surface mechanical attrition treatment of titanium using alumina balls: surface roughness, contact angle and apatite forming ability. Frontiers of Materials Science, 2013, 7, 285-294.	2.2	19
837	Titania Nanotube Coatings on Dental Implants with Enhanced Osteogenic Activity and Anti-Infection Properties. , 2013, , 337-357.		1
838	In Situ Thermal Imaging and Absolute Temperature Monitoring by Luminescent Diphenylalanine Nanotubes. Biomacromolecules, 2013, 14, 2112-2116.	5.4	34
839	Enhanced Photocatalytic Oxygen Evolution by Crystal Cutting. Advanced Materials, 2013, 25, 2035-2039.	21.0	49
840	Ni-coated Si microchannel plate electrodes in three-dimensional lithium-ion battery anodes. Electrochimica Acta, 2013, 87, 250-255.	5.2	39
841	Breathing oscillations in enlarged cylindrical-anode-layer Hall plasma accelerator. Journal of Applied Physics, 2013, 113, 203302.	2.5	0
842	Is There Real Upconversion Photoluminescence from Graphene Quantum Dots?. Advanced Optical Materials, 2013, 1, 554-558.	7.3	128
843	Direct imprint of nanostructures in metals using porous anodic alumina stamps. Nanotechnology, 2013, 24, 255303.	2.6	10
844	Surface nano-architectures and their effects on the mechanical properties and corrosion behavior of Ti-based orthopedic implants. Surface and Coatings Technology, 2013, 233, 13-26.	4.8	65
845	Electrochemically-deposited nanostructured Co(OH) ₂ flakes on three-dimensional ordered nickel/silicon microchannel plates for miniature supercapacitors. Journal of Materials Chemistry A, 2013, 1, 532-540.	10.3	74
846	The osteogenic activity of strontium loaded titania nanotube arrays on titanium substrates. Biomaterials, 2013, 34, 19-29.	11.4	212

#	Article	IF	CITATIONS
847	The role of integrin-linked kinase/β-catenin pathway in the enhanced MG63 differentiation by micro/nano-textured topography. Biomaterials, 2013, 34, 631-640.	11.4	99
848	Crystallization Effects of Nanocrystalline GaN Films on Field Emission. Journal of Physical Chemistry C, 2013, 117, 1518-1523.	3.1	13
849	Effects of Carbon and Nitrogen Plasma Immersion Ion Implantation on In vitro and In vivo Biocompatibility of Titanium Alloy. ACS Applied Materials & Interfaces, 2013, 5, 1510-1516.	8.0	81
850	Carbon-Doped TiO ₂ Nanotube Array Platform for Visible Photocatalysis. Nanoscience and Nanotechnology Letters, 2013, 5, 1251-1257.	0.4	12
851	Magnetorotational instability in plasmas with mobile dust grains. Physics of Plasmas, 2013, 20, 032102.	1.9	4
852	Effects of surface properties of red mud on interactions with Escherichia coli. Journal of Materials Research, 2013, 28, 2332-2338.	2.6	3
853	Investigation of activated oxygen molecules on the surface of Y2O3 nanocrystals by Raman scattering. Journal of Applied Physics, 2013, 114, .	2.5	25
854	Photoluminescence properties of ordered Bi4â^'xNdxTi3O12 matrix supported by 3-dimensional silicon microchannel plate. Journal Physics D: Applied Physics, 2013, 46, 315105.	2.8	4
855	Characterization of SnO ₂ /Ni/SiO ₂ -MCP anode in three-dimensional lithium-ion battery. Proceedings of SPIE, 2013, , .	0.8	0
856	Wear mechanism and tribological characteristics of porous NiTi shape memory alloy for bone scaffold. Journal of Biomedical Materials Research - Part A, 2013, 101A, 2586-2601.	4.0	22
857	Surface-enhanced Raman Scattering Substrates Prepared by Magnetron Sputtering Using Anodized Titanium Oxide Nanotube Ends as Template. , 2013, , .		0
858	A novel method for effective sodium ion implantation into silicon. Review of Scientific Instruments, 2012, 83, 075116.	1.3	0
859	Adsorption of polyvinyl alcohol from wastewater by sintered porous red mud. Water Science and Technology, 2012, 65, 2055-2060.	2.5	11
860	Low-frequency Raman scattering of bioinspired self-assembled diphenylalanine nanotubes/microtubes. Optics Express, 2012, 20, 5119.	3.4	17
861	Oxidation resistance of quintuple Ti-Al-Si-C-N coatings and associated mechanism. Journal of Vacuum Science and Technology A: Vacuum, Surfaces and Films, 2012, 30, .	2.1	5
862	Tribological behavior of Ti-Al-Si-C-N hard coatings deposited by hybrid arc-enhanced magnetron sputtering. Journal of Vacuum Science and Technology A: Vacuum, Surfaces and Films, 2012, 30, 021501.	2.1	4
863	Tunable electroluminescence from polymer-passivated 3C-SiC quantum dot thin films. Applied Physics Letters, 2012, 101, 123110.	3.3	20
864	Group velocity of extraordinary waves in superdense magnetized quantum plasma with spin-1/2 effects. Physics of Plasmas, 2012, 19, .	1.9	21

#	Article	IF	CITATIONS
865	Improved corrosion resistance of stainless steel 316L by Ti ion implantation. Materials Letters, 2012, 68, 450-452.	2.6	37
866	Effects of carbon ash on rheological properties of water-based drilling fluids. Journal of Petroleum Science and Engineering, 2012, 100, 1-8.	4.2	85
867	Are all atmospheric pressure cold plasma jets electrically driven?. Applied Physics Letters, 2012, 100, .	3.3	54
868	Nickel-Palladium Nanoparticles for Nonenzymatic Methanol Detection. Analytical Letters, 2012, 45, 1447-1453.	1.8	7
869	Vascular lumen simulation and highly-sensitive nitric oxide detection using three-dimensional gelatin chip coupled to TiC/C nanowire arrays microelectrode. Lab on A Chip, 2012, 12, 4249.	6.0	29
870	Anisotropic etching of microscale β-FeSi2 particles: Formation, mechanism, and quantum confinement of β-FeSi2 nanowhiskers. RSC Advances, 2012, 2, 3254.	3.6	3
871	Surface Treatment of Polyethylene Terephthalate Using Plasma Ion Implantation Based on Direct Coupling of RF and High-Voltage Pulse. IEEE Transactions on Plasma Science, 2012, 40, 487-491.	1.3	5
872	Origin of strong white electroluminescence from dense Si nanodots embedded in silicon nitride. Optics Letters, 2012, 37, 692.	3.3	33
873	Oxygen-vacancy and depth-dependent violet double-peak photoluminescence from ultrathin cuboid SnO2 nanocrystals. Applied Physics Letters, 2012, 100, 121903.	3.3	45
874	Biodegradable Poly(Butylene Succinate) Modified by Gas Plasmas and Their In vitro Functions as Bone Implants. ACS Applied Materials & Interfaces, 2012, 4, 4380-4386.	8.0	31
875	The effect of interlayer on corrosion resistance of ceramic coating/Mg alloy substrate in simulated physiological environment. Surface and Coatings Technology, 2012, 206, 4892-4898.	4.8	39
876	Plasma immersion ion implantation into cylindrical bore using internal inductively-coupled radio-frequency discharge. Surface and Coatings Technology, 2012, 206, 5042-5045.	4.8	5
877	Inactivation of a 25.5µm Enterococcus faecalis biofilm by a room-temperature, battery-operated, handheld air plasma jet. Journal Physics D: Applied Physics, 2012, 45, 165205.	2.8	138
878	Photoluminescence induced by twinning interface in CdS nanocrystals. Applied Physics Letters, 2012, 100, 171911.	3.3	12
879	Ion trajectories and shadow effects in mesh-assisted plasma immersion ion implantation of insulator. Applied Surface Science, 2012, 258, 2910-2913.	6.1	1
880	Optical properties and chemical structures of Kapton-H film after proton irradiation by immersion in a hydrogen plasma. Applied Surface Science, 2012, 258, 3829-3834.	6.1	17
881	Mechanical and optical characteristics of multilayer inorganic films on polyimide for anti-atomic-oxygen erosion. Applied Surface Science, 2012, 258, 5810-5814.	6.1	23
882	Retardation of surface corrosion of biodegradable magnesium-based materials by aluminum ion implantation. Applied Surface Science, 2012, 258, 7651-7657.	6.1	59

#	Article	IF	CITATIONS
883	Corrosion behavior of chromium and oxygen plasma-modified magnesium in sulfate solution and simulated body fluid. Applied Surface Science, 2012, 258, 8273-8278.	6.1	19
884	Fabrication of Si–Ag "wire-cap―nanostructures for metal-enhanced fluorescence. Journal of Luminescence, 2012, 132, 2586-2589.	3.1	1
885	Plasmonic nano-lasers. Nano Energy, 2012, 1, 25-41.	16.0	75
886	New easy way preparation of core/shell structured SnO2@carbon spheres and application for lithium-ion batteries. Journal of Power Sources, 2012, 216, 475-481.	7.8	38
887	Improved corrosion resistance and cytocompatibility of magnesium alloy by two-stage cooling in thermal treatment. Corrosion Science, 2012, 59, 360-365.	6.6	63
888	Strain effect on lattice vibration, heat capacity, and thermal conductivity of graphene. Applied Physics Letters, 2012, 101, 111904.	3.3	89
889	Three-dimensional numerical investigation of electron transport with rotating spoke in a cylindrical anode layer Hall plasma accelerator. Physics of Plasmas, 2012, 19, .	1.9	12
890	Water-Sensitive High-Frequency Molecular Vibrations in Self-Assembled Diphenylalanine Nanotubes. Journal of Physical Chemistry C, 2012, 116, 9793-9799.	3.1	29
891	Optofluidic detection for cellular phenotyping. Lab on A Chip, 2012, 12, 3552.	6.0	38
892	Sensitive and simultaneous detection of different disease markers using multiplexed gold nanorods. Analytica Chimica Acta, 2012, 755, 108-114.	5.4	20
893	Improved corrosion resistance on biodegradable magnesium by zinc and aluminum ion implantation. Applied Surface Science, 2012, 263, 608-612.	6.1	37
894	Functional replication of the tendon tissue microenvironment by a bioimprinted substrate and the support of tenocytic differentiation of mesenchymal stem cells. Biomaterials, 2012, 33, 7686-7698.	11.4	84
895	The role of the Wnt/β-catenin pathway in the effect of implant topography on MG63 differentiation. Biomaterials, 2012, 33, 7993-8002.	11.4	91
896	Novel anionic fluorine-containing amphiphilic self-assembly polymer micelles for potential application in protein drug carrier. Journal of Fluorine Chemistry, 2012, 141, 21-28.	1.7	17
897	Effect of plasma CVD operating temperature on nanomechanical properties of TiC nanostructured coating investigated by atomic force microscopy. Materials Research Bulletin, 2012, 47, 2200-2205.	5.2	21
898	Novel functional materials with active adsorption and antimicrobial properties. Materials Letters, 2012, 89, 19-21.	2.6	3
899	In vitro corrosion inhibition on biomedical shape memory alloy by plasma-polymerized allylamine film. Materials Letters, 2012, 89, 51-54.	2.6	13
900	Interference effects on indium tin oxide enhanced Raman scattering. Journal of Applied Physics, 2012, 111, .	2.5	9

#	Article	IF	CITATIONS
901	Ultrathin Amorphous Alumina Nanoparticles with Quantum-Confined Oxygen-Vacancy-Induced Blue Photoluminescence as Fluorescent Biological Labels. Journal of Physical Chemistry C, 2012, 116, 2356-2362.	3.1	28
902	Hydrothermal Growth Mechanism of Controllable Hydrophilic Titanate Nanostructures on Medical NiTi Shape Memory Alloy. Journal of Materials Engineering and Performance, 2012, 21, 2600-2606.	2.5	11
903	Superelastic Porous NiTi with Adjustable Porosities Synthesized by Powder Metallurgical Method. Journal of Materials Engineering and Performance, 2012, 21, 2553-2558.	2.5	8
904	Wear Properties of Porous NiTi Orthopedic Shape Memory Alloy. Journal of Materials Engineering and Performance, 2012, 21, 2622-2627.	2.5	10
905	Three-dimensional particle-in-cell simulation of discharge characteristics in cylindrical anode layer hall plasma accelerator. Physics of Plasmas, 2012, 19, .	1.9	8
906	Interface dipole engineering in metal gate/high-k stacks. Science Bulletin, 2012, 57, 2872-2878.	1.7	22
907	Preparation and electrochemistry of Pd–Ni/Si nanowire nanocomposite catalytic anode for direct ethanol fuel cell. Dalton Transactions, 2012, 41, 5055.	3.3	23
908	Concentration- and time-dependent response of human gingival fibroblasts to fibroblast growth factor 2 immobilized on titanium dental implants. International Journal of Nanomedicine, 2012, 7, 1965.	6.7	17
909	High-Efficiency Electrochemical Hydrogen Evolution Based on Surface Autocatalytic Effect of Ultrathin 3C-SiC Nanocrystals. Nano Letters, 2012, 12, 1545-1548.	9.1	107
910	Controlled Fabrication of Core–Shell TiO ₂ /C and TiC/C Nanofibers on Ti Foils and Their Field-Emission Properties. ACS Applied Materials & Interfaces, 2012, 4, 1037-1042.	8.0	23
911	Tailoring of Mesenchymal Stem Cells Behavior on Plasmaâ€Modified Polytetrafluoroethylene. Advanced Materials, 2012, 24, 3315-3324.	21.0	47
912	Facile preparation of cationic P (Stâ€BAâ€METAC) copolymer nanoparticles and the investigation of their interaction with bovine serum albumin. Journal of Applied Polymer Science, 2012, 125, 864-869.	2.6	3
913	Heterostructured TiO ₂ Nanoparticles/Nanotube Arrays: Inâ€Situ Formation from Amorphous TiO ₂ Nanotube Arrays in Water and Enhanced Photocatalytic Activity. ChemPlusChem, 2012, 77, 323-329.	2.8	59
914	Silver Nanovoid Arrays for Surface-Enhanced Raman Scattering. Langmuir, 2012, 28, 8799-8803.	3.5	25
915	Electronic states and photoluminescence of TiO2 nanotubes with adsorbed surface oxygen. Applied Physics Letters, 2012, 100, 121904.	3.3	17
916	Removal of organic materials from TNT red water by Bamboo Charcoal adsorption. Chemical Engineering Journal, 2012, 193-194, 39-49.	12.7	60
917	Preparation and characterization of a novel nickel–palladium electrode supported by silicon nanowires for direct glucose fuel cell. Electrochimica Acta, 2012, 65, 149-152.	5.2	31
918	Intracellular pathways and nuclear localization signal peptide-mediated gene transfection by cationic polymeric nanovectors. Biomaterials, 2012, 33, 1135-1145.	11.4	67

#	Article	IF	CITATIONS
919	Effects of micropitted/nanotubular titania topographies on bone mesenchymal stem cell osteogenic differentiation. Biomaterials, 2012, 33, 2629-2641.	11.4	273
920	Magnetite-loaded fluorine-containing polymeric micelles for magnetic resonance imaging and drug delivery. Biomaterials, 2012, 33, 3013-3024.	11.4	136
921	Synergistic treatment of ovarian cancer by co-delivery of survivin shRNA and paclitaxel via supramolecular micellar assembly. Biomaterials, 2012, 33, 6580-6591.	11.4	114
922	Formation and electrochemical behavior of Al and O plasma-implanted biodegradable Mg-Y-RE alloy. Materials Chemistry and Physics, 2012, 132, 187-191.	4.0	41
923	Fabrication and dielectric properties of oriented polyvinylidene fluoride nanocomposites incorporated with graphene nanosheets. Materials Chemistry and Physics, 2012, 134, 867-874.	4.0	96
924	Ex situ and in situ evaluation of carbon ion-implanted stainless steel bipolar plates in polymer electrolyte membrane fuel cells. Journal of Power Sources, 2012, 199, 207-213.	7.8	23
925	First-principle study of energy band structure of armchair graphene nanoribbons. Solid State Communications, 2012, 152, 1089-1093.	1.9	35
926	Dual Ti and C ion-implanted stainless steel bipolar plates in polymer electrolyte membrane fuel cells. Surface and Coatings Technology, 2012, 206, 2914-2921.	4.8	16
927	Effects of surface alloying on electrochemical corrosion behavior of oxygen-plasma-modified biomedical magnesium alloy. Surface and Coatings Technology, 2012, 206, 3186-3195.	4.8	47
928	Oxidation behavior of Ti–B–C–N coatings deposited by reactive magnetron sputtering. Vacuum, 2012, 86, 1505-1512.	3.5	9
929	Surfaced-enhanced cellular fluorescence imaging. Progress in Surface Science, 2012, 87, 23-45.	8.3	26
930	Fluorine-containing thermo-sensitive core/shell microgel particles: Preparation, characterization, and their applications in controlled drug release. Journal of Fluorine Chemistry, 2012, 135, 75-82.	1.7	16
931	Cuprous oxide created on sepiolite: Preparation, characterization, and photocatalytic activity in treatment of red water from 2,4,6-trinitrotoluene manufacturing. Journal of Hazardous Materials, 2012, 217-218, 11-18.	12.4	53
932	Biological response of endothelial cells to diamondâ€like carbonâ€coated NiTi alloy. Journal of Biomedical Materials Research - Part A, 2012, 100A, 496-506.	4.0	24
933	Fluorine-containing pH-responsive core/shell microgel particles: preparation, characterization, and their applications in controlled drug release. Colloid and Polymer Science, 2012, 290, 349-357.	2.1	19
934	Amplification of localized surface plasmon resonance signals by a gold nanorod assembly and ultra-sensitive detection of mercury. Chemical Communications, 2011, 47, 6897.	4.1	52
935	Miniature supercapacitors composed of nickel/cobalt hydroxide on nickel-coated silicon microchannel plates. Journal of Materials Chemistry, 2011, 21, 19093.	6.7	35
936	Highly Conductive, Mechanically Robust, and Electrochemically Inactive TiC/C Nanofiber Scaffold for High-Performance Silicon Anode Batteries. ACS Nano, 2011, 5, 8346-8351.	14.6	122

#	Article	IF	CITATIONS
937	Tunable Silver Nanocap Superlattice Arrays for Surface-Enhanced Raman Scattering. Journal of Physical Chemistry C, 2011, 115, 24328-24333.	3.1	28
938	Synthesis, Growth Mechanism, and Electrochemical Properties of Hollow Mesoporous Carbon Spheres with Controlled Diameter. Journal of Physical Chemistry C, 2011, 115, 17717-17724.	3.1	125
939	Mn ²⁺ -Bonded Reduced Graphene Oxide with Strong Radiative Recombination in Broad Visible Range Caused by Resonant Energy Transfer. Nano Letters, 2011, 11, 3951-3956.	9.1	82
940	Charged Diphenylalanine Nanotubes and Controlled Hierarchical Self-Assembly. ACS Nano, 2011, 5, 4448-4454.	14.6	105
941	Novel plasma immersion ion implantation and deposition hardware and technique based on high power pulsed magnetron discharge. Review of Scientific Instruments, 2011, 82, 033511.	1.3	12
942	Microstructure and mechanical properties of CrN films fabricated by high power pulsed magnetron discharge plasma immersion ion implantation and deposition. Applied Surface Science, 2011, 258, 242-246.	6.1	21
943	Degradation behaviour of pure magnesium in simulated body fluids with different concentrations of. Corrosion Science, 2011, 53, 1522-1528.	6.6	133
944	Oxygen vacancy density-dependent transformation from infrared to Raman active vibration mode in SnO_2 nanostructures. Optics Letters, 2011, 36, 4296.	3.3	20
945	Microstructural evolution in NiTi alloy subjected to surface mechanical attrition treatment and mechanism. Intermetallics, 2011, 19, 1136-1145.	3.9	34
946	Plasma-Modified Biomaterials for Self-Antimicrobial Applications. ACS Applied Materials & Interfaces, 2011, 3, 2851-2860.	8.0	61
947	Recyclable and High-Sensitivity Electrochemical Biosensing Platform Composed of Carbon-Doped TiO ₂ Nanotube Arrays. Analytical Chemistry, 2011, 83, 8138-8144.	6.5	69
948	Plasma Immersion Ion Implantation Into Inner Surface of Cylindrical Bore Using Moving Auxiliary Electrode. IEEE Transactions on Plasma Science, 2011, 39, 3120-3124.	1.3	3
949	Recent Progress in Patterned Silicon Nanowire Arrays: Fabrication, Properties and Applications. Recent Patents on Nanotechnology, 2011, 5, 62-70.	1.3	5
950	Quasi-Aligned Ag-Nb2O5 Nanobelt Arrays with Enhanced Photocatalytic and Antibacterial Activities. Journal of the American Ceramic Society, 2011, 94, 2330-2338.	3.8	37
951	Green light stimulates terahertz emission from mesocrystal microspheres. Nature Nanotechnology, 2011, 6, 103-106.	31.5	131
952	Electrochemical stability of TiO2 nanotubes with different diameters in artificial saliva. Surface and Coatings Technology, 2011, 206, 63-67.	4.8	36
953	Uniformity enhancement of incident dose on concave surface in plasma immersion ion implantation assisted by beam-line ion source. Surface and Coatings Technology, 2011, 206, 2021-2024.	4.8	8
954	Extraction of organic materials from red water by metal-impregnated lignite activated carbon. Journal of Hazardous Materials, 2011, 197, 352-360.	12.4	18

#	Article	IF	CITATIONS
955	Analysis of hazardous organic residues from sodium hydrosulfite industry and utilization as raw materials in a novel solid lubricant production. Journal of Hazardous Materials, 2011, 198, 65-69.	12.4	7
956	Graded phase structure in the surface layer of NiTi alloy processed by surface severe plastic deformation. Scripta Materialia, 2011, 64, 1011-1014.	5.2	27
957	Corrosion behavior on orthopedic NiTi alloy with nanocrystalline/amorphous surface. Materials Chemistry and Physics, 2011, 126, 102-107.	4.0	52
958	Improved tribological properties of TiC with porous nanostructured TiO2 intermediate layer. Materials Chemistry and Physics, 2011, 131, 420-424.	4.0	4
959	Rapid degradation of biomedical magnesium induced by zinc ion implantation. Materials Letters, 2011, 65, 661-663.	2.6	47
960	Controllable degradation of biomedical magnesium by chromium and oxygen dual ion implantation. Materials Letters, 2011, 65, 2171-2173.	2.6	49
961	Corrosion behavior of SS316L in simulated and accelerated PEMFC environments. International Journal of Hydrogen Energy, 2011, 36, 13032-13042.	7.1	79
962	Preparation of Controllable Coreâ^'Shell Gold Nanoparticles and Its Application in Detection of Silver Ions. ACS Applied Materials & Interfaces, 2011, 3, 183-190.	8.0	35
963	Phase transformation and size tuning in controlled-growth of nanocrystals via self-seeded nucleation with preferential thermodynamic stability. Chemical Communications, 2011, 47, 12544.	4.1	16
964	Reversible phase transformation in graphene nano-ribbons: Lattice shearing based mechanism. Acta Materialia, 2011, 59, 6783-6789.	7.9	22
965	Arrays of nanofibers composed of a TiC core and a carbon coating for sensitive electrochemical detection of hydrazine. Mikrochimica Acta, 2011, 175, 137-143.	5.0	13
966	Si–Si optical phonon behavior in localized Si clusters ofÂSi x Ge1â^'x ÂalloyÂnanocrystals. Applied Physics A: Materials Science and Processing, 2011, 103, 361-365.	2.3	4
967	Surface carbon layer and visible-light photocatalytic activities of carbon-coated TiO 2 nanotubes synthesized in organic electrolytes. Applied Physics A: Materials Science and Processing, 2011, 105, 703-707.	2.3	7
968	Radiation tolerance of Cu/W multilayered nanocomposites. Journal of Nuclear Materials, 2011, 413, 11-15.	2.7	125
969	Preparation and characterization of Cu2O–ZnO immobilized on diatomite for photocatalytic treatment of red water produced from manufacturing of TNT. Chemical Engineering Journal, 2011, 171, 61-68.	12.7	69
970	A Localized Surface Plasmon Resonance Biosensor Based on Integrated Controllable Au2S/AuAgS-Coated Gold Nanorods Composite. Plasmonics, 2011, 6, 1-9.	3.4	12
971	Optimization of Optoelectronic Plasmonic Structures. Plasmonics, 2011, 6, 319-325.	3.4	10
972	Light-emitting diodes enhanced by localized surface plasmon resonance. Nanoscale Research Letters, 2011, 6, 199.	5.7	147

#	Article	IF	CITATIONS
973	Effects of Water Molecules on Photoluminescence from Hierarchical Peptide Nanotubes and Water Probing Capability. Small, 2011, 7, 2801-2807.	10.0	43
974	New Ultraviolet Photodetector Based on Individual Nb ₂ O ₅ Nanobelts. Advanced Functional Materials, 2011, 21, 3907-3915.	14.9	285
975	Suppressed primary osteoblast functions on nanoporous titania surface. Journal of Biomedical Materials Research - Part A, 2011, 96A, 100-107.	4.0	22
976	Immobilization of Ag nanoparticles/FGFâ€2 on a modified titanium implant surface and improved human gingival fibroblasts behavior. Journal of Biomedical Materials Research - Part A, 2011, 98A, 274-286.	4.0	51
977	Controllable Growth of Conical and Cylindrical TiO ₂ –Carbon Core–Shell Nanofiber Arrays and Morphologically Dependent Electrochemical Properties. Chemistry - A European Journal, 2011, 17, 14552-14558.	3.3	17
978	Nonenzymatic glucose sensor based on over-oxidized polypyrrole modified Pd/Si microchannel plate electrode. Biosensors and Bioelectronics, 2011, 26, 2579-2584.	10.1	24
979	High-sensitivity biosensors fabricated by tailoring the localized surface plasmon resonance property of core–shell gold nanorods. Analytica Chimica Acta, 2011, 683, 242-247.	5.4	21
980	Hydrogen release from titanium hydride in foaming of orthopedic NiTi scaffolds. Acta Biomaterialia, 2011, 7, 1387-1397.	8.3	31
981	Relationship between osseointegration and superelastic biomechanics in porous NiTi scaffolds. Biomaterials, 2011, 32, 330-338.	11.4	103
982	Hollow chitosan–silica nanospheres as pH-sensitive targeted delivery carriers in breast cancer therapy. Biomaterials, 2011, 32, 4976-4986.	11.4	245
983	Antibacterial nano-structured titania coating incorporated with silver nanoparticles. Biomaterials, 2011, 32, 5706-5716.	11.4	670
984	Pd/Ni/Si-microchannel-plate-based amperometric sensor for ethanol detection. Electrochimica Acta, 2011, 56, 4197-4202.	5.2	40
985	Biological actions of silver nanoparticles embedded in titanium controlled by micro-galvanic effects. Biomaterials, 2011, 32, 693-705.	11.4	307
986	Release of hydrogen during transformation from porous silicon to silicon oxide at normal temperature. International Journal of Hydrogen Energy, 2011, 36, 4513-4517.	7.1	38
987	Pump-power tunable white upconversion emission in lanthanide-doped hexagonal NaYF4 nanorods. Optical Materials, 2011, 33, 882-887.	3.6	39
988	An undercutting model of atomic oxygen for multilayer silica/alumina films fabricated by plasma immersion implantation and deposition on polyimide. Applied Surface Science, 2011, 257, 9158-9163.	6.1	18
989	Three-dimensional supercapacitors composed of Ba0.65Sr0.35TiO3 (BST)/NiSi2/silicon microchannel plates. Materials Science and Engineering B: Solid-State Materials for Advanced Technology, 2011, 176, 387-392.	3.5	14
990	Determination of surface oxygen vacancy position in SnO2 nanocrystals by Raman spectroscopy. Solid State Communications, 2011, 151, 811-814.	1.9	93

#	Article	IF	CITATIONS
991	Interaction Between Fluorinated Amphiphilic Copolymer P(HFMA)-g-P(SPEG) and BSA. Journal of Dispersion Science and Technology, 2011, 32, 1185-1190.	2.4	1
992	Diffusion behavior of dual capping layers in TiN/LaN/AlN/HfSiOx/Si stack. Applied Physics Letters, 2011, 99, 131914.	3.3	4
993	Influence of annular magnet on discharge characteristics in enhanced glow discharge plasma immersion ion implantation. Applied Physics Letters, 2011, 98, 021502.	3.3	2
994	Growth of tin oxide nanorods induced by nanocube-oriented coalescence mechanism. Applied Physics Letters, 2011, 98, 133102.	3.3	21
995	High voltage pulser with a fast fall-time for plasma immersion ion implantation. Review of Scientific Instruments, 2011, 82, 045102.	1.3	5
996	Morphology-dependent low-frequency Raman scattering in ultrathin spherical, cubic, and cuboid SnO2 nanocrystals. Applied Physics Letters, 2011, 99, 251902.	3.3	7
997	Modulation of surface-enhanced Raman spectra by depth selective excitation of embedded indium tin oxide nanoisland arrays. Journal Physics D: Applied Physics, 2011, 44, 215305.	2.8	5
998	Influence of Structure Parameters and Crystalline Phase on the Photocatalytic Activity of TiO ₂ Nanotube Arrays. Journal of Nanoscience and Nanotechnology, 2011, 11, 11200-11205.	0.9	20
999	Recent developments in optofluidic-surface-enhanced Raman scattering systems: Design, assembly, and advantages. Journal of Materials Research, 2011, 26, 170-185.	2.6	27
1000	Red mud/polypropylene composite with mechanical and thermal properties. Journal of Composite Materials, 2011, 45, 2811-2816.	2.4	35
1001	Coupling of Kelvin–Helmholtz instability and buoyancy instability in a thermally laminar plasma. Physics of Plasmas, 2011, 18, .	1.9	4
1002	Improved hydrogen ionization rate in enhanced glow discharge plasma immersion ion implantation by enlarging the interaction path using an insulating tube. Review of Scientific Instruments, 2011, 82, 023503.	1.3	6
1003	Osteoblast differentiation and disinfection induced by nitrogen plasma-treated surfaces. Bio-Medical Materials and Engineering, 2011, 21, 75-82.	0.6	9
1004	Electron field emission enhanced by geometric and quantum effects from nanostructured AlGaN/GaN quantum wells. Applied Physics Letters, 2011, 98, 152110.	3.3	14
1005	Anisotropic dissipative effects on the buoyancy instability with background heat flux. Physics of Plasmas, 2011, 18, 032106.	1.9	0
1006	Corrosion behavior of DLC-coated NiTi alloy in the presence of serum proteins. Diamond and Related Materials, 2010, 19, 1230-1234.	3.9	26
1007	Surface-enhanced Raman scattering from silver nanostructures with different morphologies. Applied Physics A: Materials Science and Processing, 2010, 100, 83-88.	2.3	18
1008	Microstructure, bioactivity and osteoblast behavior of monoclinic zirconia coating with nanostructured surface. Acta Biomaterialia, 2010, 6, 990-1000.	8.3	88

#	Article	IF	CITATIONS
1009	Osteoblast behavior on polytetrafluoroethylene modified by long pulse, high frequency oxygen plasma immersion ion implantation. Biomaterials, 2010, 31, 413-419.	11.4	68
1010	The role of sterilization in the cytocompatibility of titania nanotubes. Biomaterials, 2010, 31, 2055-2063.	11.4	112
1011	The influence of hierarchical hybrid micro/nano-textured titanium surface with titania nanotubes on osteoblast functions. Biomaterials, 2010, 31, 5072-5082.	11.4	401
1012	Mechanism of cell repellence on quasi-aligned nanowire arrays on Ti alloy. Biomaterials, 2010, 31, 8341-8349.	11.4	52
1013	Mechanical and biological characteristics of diamond-like carbon coated poly aryl-ether-ether-ketone. Biomaterials, 2010, 31, 8181-8187.	11.4	143
1014	Influence of Tris in simulated body fluid on degradation behavior of pure magnesium. Materials Chemistry and Physics, 2010, 124, 33-35.	4.0	33
1015	Surface Structures and Osteoblast Activity on Biomedical Polytetrafluoroethylene Treated by Longâ€Pulse, Highâ€Frequency Oxygen Plasma Immersion Ion Implantation. Advanced Engineering Materials, 2010, 12, B163.	3.5	10
1016	Capacitive humidity sensing behavior of ordered Ni/Si microchannel plate nanocomposites. Sensors and Actuators A: Physical, 2010, 160, 48-53.	4.1	13
1017	Preparation and characterization of fluorinated acrylate copolymer latexes by miniemulsion polymerization under microwave irradiation. Journal of Fluorine Chemistry, 2010, 131, 417-425.	1.7	62
1018	Surface nano-functionalization of biomaterials. Materials Science and Engineering Reports, 2010, 70, 275-302.	31.8	244
1019	Nano-networks have better adsorption capability than nano-rods. Nano Communication Networks, 2010, 1, 257-263.	2.9	14
1020	Preparation and characterization of novel nickel–palladium electrodes supported by silicon microchannel plates for direct methanol fuel cells. Journal of Power Sources, 2010, 195, 146-150.	7.8	46
1021	Nitrogen plasma-implanted titanium as bipolar plates in polymer electrolyte membrane fuel cells. Journal of Power Sources, 2010, 195, 6798-6804.	7.8	35
1022	Ni–Cr Co-implanted 316L stainless steel as bipolar plate in polymer electrolyte membrane fuel cells. International Journal of Hydrogen Energy, 2010, 35, 690-700.	7.1	62
1023	Ultra-sensitive detection of cysteine by gold nanorod assembly. Biosensors and Bioelectronics, 2010, 25, 2078-2083.	10.1	97
1024	Corrosion behavior of NiTi alloy in fetal bovine serum. Electrochimica Acta, 2010, 55, 5551-5560.	5.2	59
1025	Recent applications of plasma-based ion implantation and deposition to microelectronic, nano-structured, and biomedical materials. Surface and Coatings Technology, 2010, 204, 2853-2863.	4.8	28
1026	Hybrid plasma surface modification and ion implantation of biopolymers. Surface and Coatings Technology, 2010, 204, 2892-2897.	4.8	11

#	Article	IF	CITATIONS
1027	Microstructure, mechanical properties, and blood compatibility of zirconium nitride deposited on nickel–titanium shape memory alloy. Surface and Coatings Technology, 2010, 204, 2841-2845.	4.8	9
1028	DLC deposition inside tubes using hollow cathode discharge plasma immersion ion implantation and deposition. Surface and Coatings Technology, 2010, 204, 2909-2912.	4.8	15
1029	Corrosion behavior and electrical conductivity of niobium implanted 316L stainless steel used as bipolar plates in polymer electrolyte membrane fuel cells. Surface and Coatings Technology, 2010, 205, 85-91.	4.8	41
1030	Wear resistance of NiTi alloy after surface mechanical attrition treatment. Surface and Coatings Technology, 2010, 205, 506-510.	4.8	33
1031	Rat calvaria osteoblast behavior and antibacterial properties of O2 and N2 plasma-implanted biodegradable poly(butylene succinate). Acta Biomaterialia, 2010, 6, 154-159.	8.3	45
1032	Effect of titanium incorporation on the structural, mechanical and biocompatible properties of DLC thin films prepared by reactive-biased target ion beam deposition method. Applied Surface Science, 2010, 257, 143-150.	6.1	53
1033	A biodegradable polymer-based coating to control the performance of magnesium alloy orthopaedic implants. Biomaterials, 2010, 31, 2084-2096.	11.4	521
1034	Cationic fluorine-containing amphiphilic graft copolymers as DNA carriers. Biomaterials, 2010, 31, 2673-2685.	11.4	63
1035	Activation of mitogen-activated protein kinases cellular signal transduction pathway in mammalian cells induced by silicon carbide nanowires. Biomaterials, 2010, 31, 7856-7862.	11.4	14
1036	Synthesis and characterization of fluorescent copolymer containing rare earth metal complex and its interaction with DNA. Journal of Polymer Science Part A, 2010, 48, 5961-5967.	2.3	13
1037	Group IV Nanoparticles: Synthesis, Properties, and Biological Applications. Small, 2010, 6, 2080-2098.	10.0	264
1038	Synthesis and Photocatalytic Activity of Highly Ordered TiO ₂ and SrTiO ₃ /TiO ₂ Nanotube Arrays on Ti Substrates. Journal of the American Ceramic Society, 2010, 93, 2771-2778.	3.8	108
1039	Hot spots in silver nano-dendrites fabricated by self-selective electroless plating. , 2010, , .		1
1040	Enhanced retained dose uniformity in NiTi spinal correction rod treated by three-dimensional mesh-assisted nitrogen plasma immersion ion implantation. Journal of Vacuum Science and Technology A: Vacuum, Surfaces and Films, 2010, 28, 407-410.	2.1	3
1041	Ultralow-threshold field emission from oriented nanostructured GaN films on Si substrate. Applied Physics Letters, 2010, 96, 092101.	3.3	13
1042	Thermal convective and rotational instability in dissipative magnetohydrodynamics. Physics of Plasmas, 2010, 17, 052102.	1.9	5
1043	Twinning Ge0.54Si0.46 nanocrystal growth mechanism in amorphous SiO2 films. Applied Physics Letters, 2010, 96, .	3.3	13
1044	lon focusing in enhanced glow discharge plasma immersion ion implantation of hydrogen and nitrogen into silicon. Journal of Applied Physics, 2010, 108, 033304.	2.5	5

#	Article	IF	CITATIONS
1045	Origin of flat-band voltage sharp roll-off in metal gate/high-k/ultrathin- SiO2/Si p-channel metal-oxide-semiconductor stacks. Applied Physics Letters, 2010, 97, 132908.	3.3	9
1046	Fermi-Level Pinning at Metal/High-\$k\$ Interface Influenced by Electron State Density of Metal Gate. IEEE Electron Device Letters, 2010, 31, 1101-1103.	3.9	10
1047	Influence of Test Solutions on In Vitro Studies of Biomedical Magnesium Alloys. Journal of the Electrochemical Society, 2010, 157, C238.	2.9	110
1048	Trace detection of multiwalled carbon nanotubes using Raman-enhancing silver nanocap arrays. Journal Physics D: Applied Physics, 2010, 43, 455302.	2.8	4
1049	Direct growth of Nb <inf>2</inf> O <inf>5</inf> nanobelts on Nb foil. , 2010, , .		0
1050	The effect of the Hall term on Jeans instability in quantum magnetoplasma with resistive effects. Physics of Plasmas, 2010, 17, .	1.9	35
1051	Fabrication and Photocatalytic Activity of Nanoporous WO ₃ Film. Nanoscience and Nanotechnology Letters, 2010, 2, 51-57.	0.4	15
1052	Carbon coated stainless steel bipolar plates in polymer electrolyte membrane fuel cells. Diamond and Related Materials, 2010, 19, 1354-1361.	3.9	49
1053	Corrosion products and mechanism on NiTi shape memory alloy in physiological environment. Journal of Materials Research, 2010, 25, 350-358.	2.6	53
1054	High-Sensitivity and Stable Cellular Fluorescence Imaging by Patterned Silver Nanocap Arrays. ACS Applied Materials & Interfaces, 2010, 2, 2465-2470.	8.0	36
1055	Size-independent low-frequency Raman scattering in Ge-nanocrystal-embedded SiO_2 films. Optics Letters, 2010, 35, 1022.	3.3	9
1056	Longitudinal optical phonon–plasmon coupling in luminescent 3C–SiC nanocrystal films. Optics Letters, 2010, 35, 4024.	3.3	15
1057	A Specially Designed PLC-Based High-Voltage Pulse Modulator for Plasma Immersion Ion Implantation. IEEE Transactions on Plasma Science, 2010, 38, 3083-3088.	1.3	6
1058	Glycerol-Bonded 3C-SiC Nanocrystal Solid Films Exhibiting Broad and Stable Violet to Blue-Green Emission. Nano Letters, 2010, 10, 1466-1471.	9.1	58
1059	Plasma immersion ion implantation into cylindrical bore using internal inductively-coupled radio-frequency discharge. Surface and Coatings Technology, 2010, , .	4.8	0
1060	Hybrid particle-in-cell (PIC) ions and Boltzmann electron distribution simulation of direct-current plasma immersion ion implantation into three-dimensional objects. Journal Physics D: Applied Physics, 2010, 43, 095203.	2.8	7
1061	Photoluminescence from colloids containing aluminum hydroxide nanocrystals with uniform size. Applied Physics Letters, 2010, 97, 121901.	3.3	10
1062	Core–shell TiC/C quasi-aligned nanofiber arrays on biomedical Ti6Al4V for sensitive electrochemical biosensing. Chemical Communications, 2010, 46, 6828.	4.1	34

#	Article	IF	CITATIONS
1063	Identification of local silicon cluster nanostructures inside SixGe1â^'x alloy nanocrystals by Raman spectroscopy. Chemical Communications, 2010, 46, 5539.	4.1	13
1064	Magnetic and upconverted luminescent properties of multifunctional lanthanide doped cubic KGdF4 nanocrystals. Nanoscale, 2010, 2, 2805.	5.6	78
1065	Surface-Enhanced Raman Scattering Sensor Based on Silver Dendritic Nanostructures. Sensor Letters, 2010, 8, 395-398.	0.4	6
1066	Raman investigation of oxidation mechanism of silicon nanowires. Applied Physics Letters, 2009, 95, .	3.3	14
1067	Role of interface dipole in metal gate/high-k effective work function modulation by aluminum incorporation. Applied Physics Letters, 2009, 94, .	3.3	20
1068	Effects of long pulse width and high pulsing frequency on surface superhydrophobicity of polytetrafluoroethylene in quasi-direct-current plasma immersion ion implantation. Journal of Applied Physics, 2009, 105, 053302.	2.5	13
1069	Plasma sheath physics and dose uniformity in enhanced glow discharge plasma immersion ion implantation and deposition. Journal of Applied Physics, 2009, 106, 013313.	2.5	4
1070	Electrostatic drift modes in quantum dusty plasmas with Jeans terms. Physics of Plasmas, 2009, 16, .	1.9	41
1071	Magnetothermal instability of plasmas in a horizontal magnetic field. Physics of Plasmas, 2009, 16, 102109.	1.9	6
1072	Stress influence on band-edge luminescence properties of 4H-AlN. Applied Physics Letters, 2009, 95, 121902.	3.3	2
1073	Impact energy and retained dose uniformity in enhanced glow discharge plasma immersion ion implantation. Applied Physics Letters, 2009, 95, 061503.	3.3	10
1074	Damping of surface acoustic vibration induced by electrons trapped on SnO2 nanocrystal surface. Applied Physics Letters, 2009, 95, 211903.	3.3	6
1075	Asymmetrical reorientation of bimetallic core–shell nanowires. Nanotechnology, 2009, 20, 045601.	2.6	3
1076	Enhancement of ductility in Mg–3Al–1Zn alloy with tilted basal texture by electropulsing. Journal of Materials Research, 2009, 24, 3674-3679.	2.6	23
1077	Nano-Scale Surface Morphology, Wettability and Osteoblast Adhesion on Nitrogen Plasma-Implanted NiTi Shape Memory Alloy. Journal of Nanoscience and Nanotechnology, 2009, 9, 3449-3454.	0.9	15
1078	One-step, non-contact pattern transfer by direct-current plasma immersion ion implantation. Journal Physics D: Applied Physics, 2009, 42, 195201.	2.8	2
1079	Recent Progress in Fabrication of Anisotropic Nanostructures for Surface- Enhanced Raman Spectroscopy. Recent Patents on Nanotechnology, 2009, 3, 10-20.	1.3	16
1080	A unique technology to transform inorganic nanorods into nano-networks. Nanotechnology, 2009, 20, 20, 255302.	2.6	34

#	Article	IF	CITATIONS
1081	Synthesis and Field Emission Properties of Rutile TiO ₂ Nanowires Arrays Grown Directly on a Ti Metal Self-Source Substrate. Journal of Nanoscience and Nanotechnology, 2009, 9, 3341-3346.	0.9	59
1082	Electrochemical Stability of Orthopedic Porous NiTi Shape Memory Alloys Treated by Different Surface Modification Techniques. Journal of the Electrochemical Society, 2009, 156, C187.	2.9	12
1083	Corrosion behavior of ZnO nanosheets on brass substrate in NaCl solutions. Materials Chemistry and Physics, 2009, 115, 439-443.	4.0	17
1084	Comparison of oxidation resistance of copper treated by beam-line ion implantation and plasma immersion ion implantation. Materials Chemistry and Physics, 2009, 116, 519-522.	4.0	7
1085	3D ordered NiO/silicon MCP array electrode materials for electrochemical supercapacitors. Materials Research Bulletin, 2009, 44, 1920-1925.	5.2	22
1086	Three-Dimensional Quasi-Direct-Current Plasma Immersion Ion Implantation Into Biomedical Nickel–Titanium Shape Memory Alloy Rod. IEEE Transactions on Plasma Science, 2009, 37, 2245-2249.	1.3	3
1087	Corrosion resistance and cytocompatibility of biodegradable surgical magnesium alloy coated with hydrogenated amorphous silicon. Journal of Biomedical Materials Research - Part A, 2009, 89A, 717-726.	4.0	58
1088	Nickel release behavior and surface characteristics of porous NiTi shape memory alloy modified by different chemical processes. Journal of Biomedical Materials Research - Part A, 2009, 89A, 483-489.	4.0	14
1089	Antibacterial coatings on titanium implants. Journal of Biomedical Materials Research - Part B Applied Biomaterials, 2009, 91B, 470-480.	3.4	732
1090	Amperometric glucose sensor based on 3D ordered nickel–palladium nanomaterial supported by silicon MCP array. Sensors and Actuators B: Chemical, 2009, 141, 338-342.	7.8	53
1091	Biocompatibility of silver and copper plasma doped polyethylene. Surface and Coatings Technology, 2009, 203, 2550-2553.	4.8	17
1092	Corrosion behavior of ZrN/Zr coated biomedical AZ91 magnesium alloy. Surface and Coatings Technology, 2009, 203, 2554-2557.	4.8	112
1093	Applications of plasma-based technology to microelectronics and biomedical engineering. Surface and Coatings Technology, 2009, 203, 2793-2798.	4.8	28
1094	Optical and biological sensing capabilities of Au2S/AuAgS coated gold nanorods. Biomaterials, 2009, 30, 5622-5630.	11.4	43
1095	Bonding strength of fluorinated and hydrogenated surfactant to bovine serum albumin. Journal of Fluorine Chemistry, 2009, 130, 870-877.	1.7	11
1096	XPS and biocompatibility studies of titania film on anodized NiTi shape memory alloy. Journal of Materials Science: Materials in Medicine, 2009, 20, 223-228.	3.6	24
1097	A novel hydrothermal route to synthesize solid SnO2 nanospheres and their photoluminescence property. Applied Physics A: Materials Science and Processing, 2009, 97, 581-585.	2.3	23
1098	Controlled Assembly of Highly Ramanâ€Enhancing Silver Nanocap Arrays Templated by Porous Anodic Alumina Membranes. Small, 2009, 5, 2333-2337.	10.0	92

#	Article	IF	CITATIONS
1099	Synthesis and properties of fluorine ontaining amphiphilic graft copolymer P(HFMA)â€gâ€P(SPEG). Journal of Polymer Science Part A, 2009, 47, 4895-4907.	2.3	24
1100	Investigation of plasma potential and pulsed discharge characteristics in enhanced glow discharge plasma immersion ion implantation and deposition. Nuclear Instruments & Methods in Physics Research B, 2009, 267, 1696-1700.	1.4	7
1101	Conductive amorphous carbon-coated 316L stainless steel as bipolar plates in polymer electrolyte membrane fuel cells. International Journal of Hydrogen Energy, 2009, 34, 6771-6777.	7.1	105
1102	Optical properties of plastic scintillators coated with copper, aluminum and silver by magnetron sputtering. Thin Solid Films, 2009, 517, 4443-4447.	1.8	3
1103	Mechanical properties of Al2O3/Al bi-layer coated AZ91 magnesium alloy. Thin Solid Films, 2009, 517, 5357-5360.	1.8	25
1104	Mechanical properties of tungsten doped amorphous hydrogenated carbon films prepared by tungsten plasma immersion ion implantation. Surface and Coatings Technology, 2009, 203, 2612-2616.	4.8	5
1105	High-voltage glow discharge plasma immersion ion implantation assisted by magnetic field. Surface and Coatings Technology, 2009, 203, 2751-2754.	4.8	2
1106	Aligned silver nanorod arrays for surface-enhanced Raman spectroscopy. Physica B: Condensed Matter, 2009, 404, 1523-1526.	2.7	16
1107	Intracellular chromosome breaks on silicon surface. Biomaterials, 2009, 30, 2661-2665.	11.4	10
1108	Biocompatibility and bioactivity of plasma-treated biodegradable poly(butylene succinate). Acta Biomaterialia, 2009, 5, 279-287.	8.3	104
1109	Microstructure, nickel suppression and mechanical characteristics of electropolished and photoelectrocatalytically oxidized biomedical nickel titanium shape memory alloy. Acta Biomaterialia, 2009, 5, 2238-2245.	8.3	32
1110	Structure and gas-barrier properties of amorphous hydrogenated carbon films deposited on inner walls of cylindrical polyethylene terephthalate by plasma-enhanced chemical vapor deposition. Applied Surface Science, 2009, 255, 3983-3988.	6.1	10
1111	Fabrication and optical properties of C/β-SiC/Si hybrid rolled-up microtubes. Journal of Applied Physics, 2009, 105, 016103.	2.5	13
1112	Tailoring light emission properties of organic emitter by coupling to resonance-tuned silver nanoantenna arrays. Applied Physics Letters, 2009, 95, .	3.3	26
1113	Structural Regulation and Optical Properties of One-Dimensional ZnO Nanomaterials in Situ Grown from and on Brass Substrates. Journal of Physical Chemistry C, 2009, 113, 170-173.	3.1	32
1114	Surface mechanical attrition treatment induced phase transformation behavior in NiTi shape memory alloy. Journal of Alloys and Compounds, 2009, 482, 298-301.	5.5	15
1115	Texture evolution in cold-rolled AZ31 magnesium alloy during electropulsing treatment. Journal of Alloys and Compounds, 2009, 487, 309-313.	5.5	72
1116	Surface-polarization-induced formation of amorphous foliaceous SiO2 helical nanobelts. Applied Physics Letters, 2009, 94, 253110.	3.3	5

#	Article	IF	CITATIONS
1117	Optical and vibrational properties of 2H-, 4H-, and 6H-AlN: First-principle calculations. Journal of Applied Physics, 2009, 105, 083511.	2.5	11
1118	Influence of GeSi interfacial layer on Ge–Ge optical phonon mode in SiO2 films embedded with Ge nanocrystals. Applied Physics Letters, 2009, 95, .	3.3	11
1119	Corrosion products on biomedical magnesium alloy soaked in simulated body fluids. Journal of Materials Research, 2009, 24, 2711-2719.	2.6	57
1120	Bioactive SrTiO ₃ Nanotube Arrays: Strontium Delivery Platform on Ti-Based Osteoporotic Bone Implants. ACS Nano, 2009, 3, 3228-3234.	14.6	198
1121	Surface Properties of AZ31B Magnesium Alloy by Oxygen Plasma Immersion Ion Implantation. Plasma Science and Technology, 2009, 11, 33-37.	1.5	3
1122	Hot spots in highly Raman-enhancing silver nano-dendrites. Journal Physics D: Applied Physics, 2009, 42, 175403.	2.8	53
1123	Effects of aluminum and nitrogen plasma immersion ion implantation on mechanical properties and oxidation resistance of copper. , 2009, , .		0
1124	Label-free optical biosensor based on localized surface plasmon resonance of immobilized gold nanorods. Colloids and Surfaces B: Biointerfaces, 2009, 71, 96-101.	5.0	49
1125	Theoretical investigation of plasma immersion ion implantation of cylindrical bore using hollow cathode plasma discharge. Surface and Coatings Technology, 2009, 203, 2727-2730.	4.8	7
1126	Identification of Surface Structures on 3C-SiC Nanocrystals with Hydrogen and Hydroxyl Bonding by Photoluminescence. Nano Letters, 2009, 9, 4053-4060.	9.1	105
1127	Raman scattering study of zinc blende and wurtzite ZnS. Journal of Applied Physics, 2009, 106, .	2.5	235
1128	Magnetorotational instability in dissipative dusty plasmas. Physics of Plasmas, 2009, 16, 122107.	1.9	9
1129	Tin Oxide Nanoribbons with Vacancy Structures in Luminescence-Sensitive Oxygen Sensing. Nano Letters, 2009, 9, 1926-1931.	9.1	89
1130	Fabrication and Surface Modification of Porous Nano-Structured NiTi Orthopedic Scaffolds for Bone Implants. Materials Research Society Symposia Proceedings, 2009, 1181, 7.	0.1	1
1131	Improved detection resolution in single particle microbeam system. Nuclear Instruments and Methods in Physics Research, Section A: Accelerators, Spectrometers, Detectors and Associated Equipment, 2008, 595, 312-316.	1.6	2
1132	UV-irradiation-induced bioactivity on TiO2 coatings with nanostructural surface. Acta Biomaterialia, 2008, 4, 544-552.	8.3	88
1133	Ag and Ag/N2 plasma modification of polyethylene for the enhancement of antibacterial properties and cell growth/proliferation. Acta Biomaterialia, 2008, 4, 2028-2036.	8.3	79
1134	In vitro corrosion behavior of TiN layer produced on orthopedic nickel–titanium shape memory alloy by nitrogen plasma immersion ion implantation using different frequencies. Surface and Coatings Technology, 2008, 202, 2463-2466.	4.8	15

#	Article	IF	CITATIONS
1135	3C–SiC Nanocrystals as Fluorescent Biological Labels. Small, 2008, 4, 1058-1062.	10.0	165
1136	Plasma ion implantation to thin polymer foils. Physica Status Solidi (A) Applications and Materials Science, 2008, 205, 953-956.	1.8	0
1137	Versatile Approach for Integrative and Functionalized Tubes by Strain Engineering of Nanomembranes on Polymers. Advanced Materials, 2008, 20, 4085-4090.	21.0	608
1138	Experimental investigation of discharge characteristics in enhanced glow discharge plasma immersion ion implantation. Physics Letters, Section A: General, Atomic and Solid State Physics, 2008, 372, 6183-6186.	2.1	7
1139	Thermal stability of titania films prepared on titanium by micro-arc oxidation. Materials Science & Engineering A: Structural Materials: Properties, Microstructure and Processing, 2008, 476, 78-82.	5.6	69
1140	Self-selective electroless plating: An approach for fabrication of functional 1D nanomaterials. Materials Science and Engineering Reports, 2008, 61, 59-77.	31.8	85
1141	Silver fractal networks for surface-enhanced Raman scattering substrates. Applied Surface Science, 2008, 254, 5399-5402.	6.1	26
1142	Self-organized formation of silver nanowires, nanocubes and bipyramids via a solvothermal method. Acta Materialia, 2008, 56, 2508-2513.	7.9	66
1143	Influence of aggressive ions on the degradation behavior of biomedical magnesium alloy in physiological environment. Acta Biomaterialia, 2008, 4, 2008-2015.	8.3	341
1144	Origin of the 745 nm photoluminescence from small diameter silicon nanowires. Solid State Communications, 2008, 148, 182-185.	1.9	3
1145	In vitro bioactivity and osteoblast response on chemically modified biomedical porous NiTi synthesized by capsule-free hot isostatic pressing. Surface and Coatings Technology, 2008, 202, 2458-2462.	4.8	12
1146	Enhancement of antibacterial properties and biocompatibility of polyethylene by silver and copper plasma immersion ion implantation. Surface and Coatings Technology, 2008, 203, 909-912.	4.8	38
1147	Tunable emission from composite polymer nanoparticles based on resonance energy transfer. Thin Solid Films, 2008, 516, 6287-6292.	1.8	22
1148	Catalysis of dispersed silver particles on directional etching of silicon. Applied Surface Science, 2008, 254, 3061-3066.	6.1	17
1149	Silicon-induced DNA damage pathway and its modulation by titanium plasma immersion ion implantation. Biomaterials, 2008, 29, 544-550.	11.4	18
1150	New plasma surface-treated memory alloys: Towards a new generation of "smart―orthopaedic materials. Materials Science and Engineering C, 2008, 28, 454-459.	7.3	13
1151	Surface structure and biomedical properties of chemically polished and electropolished NiTi shape memory alloys. Materials Science and Engineering C, 2008, 28, 1430-1434.	7.3	45
1152	Mechanism of apatite formation on silicon suboxide film prepared by pulsed metal vacuum arc deposition. Materials Chemistry and Physics, 2008, 109, 342-346.	4.0	5

#	Article	IF	CITATIONS
1153	Synthesis, growth mechanism, and light-emission properties of twisted SiO2 nanobelts and nanosprings. Journal of Chemical Physics, 2008, 129, 164702.	3.0	13
1154	A Biomimetic Hierarchical Scaffold: Natural Growth of Nanotitanates on Three-Dimensional Microporous Ti-Based Metals. Nano Letters, 2008, 8, 3803-3808.	9.1	124
1155	Electrostatic drift waves in nonuniform quantum magnetized plasmas. Physics of Plasmas, 2008, 15, 082103.	1.9	18
1156	Effects of tungsten pre-implanted layer on corrosion and electrochemical characteristics of amorphous carbon films on stainless steel. Diamond and Related Materials, 2008, 17, 1738-1742.	3.9	14
1157	Tribological properties of graded diamond-like carbon films on Ti ion-implanted aluminum substrate. Diamond and Related Materials, 2008, 17, 1844-1849.	3.9	22
1158	Formation mechanism and photoluminescence of AlN nanowhiskers. Journal Physics D: Applied Physics, 2008, 41, 025101.	2.8	38
1159	Uniformity of Plasma Density and Film Thickness of Coatings Deposited Inside a Cylindrical Tube by Radio Frequency Sputtering. Plasma Science and Technology, 2008, 10, 560-564.	1.5	0
1160	BIOMIMETIC DEPOSITION OF APATITE ON SURFACE CHEMICALLY MODIFIED POROUS NITI SHAPEMEMORY ALLOY. Surface Review and Letters, 2008, 15, 97-104.	1.1	4
1161	Corrosion resistance of ZrO ₂ –Zr-coated biodegradable surgical magnesium alloy. Journal of Materials Research, 2008, 23, 312-319.	2.6	30
1162	Fabrication of graded TiN coatings on nitinol occluders and effects on in vivo nickel release. Bio-Medical Materials and Engineering, 2008, 18, 387-393.	0.6	8
1163	Electrochemical Behavior Al[sub 2]O[sub 3]â^•Al Coated Surgical AZ91 Magnesium Alloy in Simulated Body Fluids. Journal of the Electrochemical Society, 2008, 155, C178.	2.9	65
1164	Electromagnetic drift waves in nonuniform quantum magnetized electron–positron–ion plasmas. Journal of Physics A: Mathematical and Theoretical, 2008, 41, 115501.	2.1	21
1165	Nanocrystal-induced line narrowing of surface acoustic phonons in the Raman spectra of embedded <mml:math <br="" xmlns:mml="http://www.w3.org/1998/Math/MathML">display="inline"><mml:mrow><mml:msub><mml:mrow><mml:mtext>Ge</mml:mtext></mml:mrow><mml:mi>x- nanocrystals. Physical Review B. 2008, 78, .</mml:mi></mml:msub></mml:mrow></mml:math>	د/mml:mi>	
1166	Direct coupling of pulsed radio frequency and pulsed high power in novel pulsed power system for plasma immersion ion implantation. Review of Scientific Instruments, 2008, 79, 043501.	1.3	2
1167	Investigation of plasma distribution in electron-focused electric field enhanced glow discharge plasma immersion ion implantation. Journal of Applied Physics, 2008, 104, 043303.	2.5	11
1168	Role of fluorine in plasma nitridated ZrO2 thin films under irradiation. Applied Physics Letters, 2008, 93, 122907.	3.3	2
1169	One-step growth and field emission properties of quasialigned TiO2 nanowire/carbon nanocone core-shell nanostructure arrays on Ti substrates. Applied Physics Letters, 2008, 93, .	3.3	60
1170	In situ growth of aligned CdS nanowire arrays on Cd foil and their optical and electron field emission properties. Journal of Applied Physics, 2008, 104, 014312.	2.5	19

#	Article	IF	CITATIONS
1171	Theoretical investigation of sheath expansion and implant fluence uniformity in enhanced glow discharge plasma immersion ion implantation. Applied Physics Letters, 2008, 93, 091501.	3.3	8
1172	Investigation of plasma immersion ion implantation of nickel-titanium rod by multiple-grid particle-in-cell simulation. Journal of Applied Physics, 2008, 103, 053308.	2.5	7
1173	Fabrication of silicon-on-insulator (SOI) and high-k materials using plasma technology. , 2008, , .		1
1174	Temperature dependent photoluminescence from ZnO nanowires and nanosheets on brass substrate. Applied Physics Letters, 2008, 93, .	3.3	32
1175	Fabrication for multilayered composite thin films by dual-channel vacuum arc deposition. Review of Scientific Instruments, 2008, 79, 065104.	1.3	1
1176	lon trajectories in plasma ion implantation of slender cylindrical bores using a small inner end source. Applied Physics Letters, 2008, 93, 191501.	3.3	3
1177	Interface-induced pseudoelastic behavior in Bi-metal multilayer nanowires. Applied Physics Letters, 2008, 92, 123103.	3.3	9
1178	Response to "Comment on `Effects of magnetic field gradient on ion beam current in cylindrical Hall ion source' '' [J. Appl. Phys. 104, 066102 (2008)]. Journal of Applied Physics, 2008, 104, 066103.	2.5	0
1179	Degradation susceptibility of surgical magnesium alloy in artificial biological fluid containing albumin. Journal of Materials Research, 2007, 22, 1806-1814.	2.6	130
1180	Influence of acetylene to argon flow rate ratios on structure and properties of hydrogenated amorphous carbon films produced on steel substrates by plasma immersion ion implantation and deposition. Journal of Materials Research, 2007, 22, 982-988.	2.6	1
1181	Activation volume and incipient plastic deformation of uniaxially-loaded gold nanowires at very high strain rates. Nanotechnology, 2007, 18, 455702.	2.6	10
1182	Energy anisotropy of bimetal core–shell nanorods and its effects on morphology. Nanotechnology, 2007, 18, 445101.	2.6	3
1183	Experimental and theoretical investigation of the effects of sample size on copper plasma immersion ion implantation into polyethylene. Journal of Applied Physics, 2007, 101, 113302.	2.5	2
1184	A ground-based radio frequency inductively coupled plasma apparatus for atomic oxygen simulation in low Earth orbit. Review of Scientific Instruments, 2007, 78, 103301.	1.3	6
1185	Interfacial compound suppression and dielectric properties enhancement of F–N codoped ZrO2 thin films. Applied Physics Letters, 2007, 90, 082906.	3.3	8
1186	Spontaneous reorientation of bimetal multilayer nanowires. Applied Physics Letters, 2007, 91, 253114.	3.3	14
1187	Effects of magnetic field gradient on ion beam current in cylindrical Hall ion source. Journal of Applied Physics, 2007, 102, 123305.	2.5	12
1188	Mechanism of enhanced adhesion between hydrogenated amorphous carbon films and tungsten preimplanted steel substrates. Journal of Applied Physics, 2007, 101, 053520.	2.5	3

#	Article	IF	CITATIONS
1189	Corrosion resistance of titanium ion implanted AZ91 magnesium alloy. Journal of Vacuum Science and Technology A: Vacuum, Surfaces and Films, 2007, 25, 334-339.	2.1	68
1190	Effects of plasma immersion ion nitridation on dielectric properties of HfO2. Applied Physics Letters, 2007, 90, 122901.	3.3	21
1191	Dependence of ion sheath collapse on secondary electron emission in plasma immersion ion implantation. Applied Physics Letters, 2007, 90, 131503.	3.3	7
1192	Behaviors of Platelets Adherent on Si-N(H) Surface Prepared from Ammonia Plasma-Implanted Silicon. Key Engineering Materials, 2007, 330-332, 889-892.	0.4	2
1193	Nano-film and Coating for Biomedical Application Prepared by Plasma-based Technologies. Materials Research Society Symposia Proceedings, 2007, 1020, 1.	0.1	0
1194	Effects of Ti/TiN multilayer on corrosion resistance of nickel–titanium orthodontic brackets in artificial saliva. Corrosion Science, 2007, 49, 3783-3796.	6.6	93
1195	Plasma-Treated Biomaterials. IEEE Transactions on Plasma Science, 2007, 35, 181-187.	1.3	72
1196	Microwave enhanced ion-cut silicon layer transfer. Journal of Applied Physics, 2007, 101, 114915.	2.5	2
1197	Comparative study of mechanical properties of a-C:H films produced on tungsten pre-implanted stainless steel substrate by plasma immersion ion implantation and deposition. Diamond and Related Materials, 2007, 16, 1304-1311.	3.9	5
1198	A flexible curvilinear electromagnetic filter for direct current cathodic arc source. Review of Scientific Instruments, 2007, 78, 095103.	1.3	2
1199	Mechanical and tribological properties of TiC/amorphous hydrogenated carbon composite coatings fabricated by DC magnetron sputtering with and without sample bias. Diamond and Related Materials, 2007, 16, 181-186.	3.9	78
1200	Structure and properties of zirconia (ZrO2) films fabricated by plasma-assisted cathodic arc deposition. Journal Physics D: Applied Physics, 2007, 40, 2293-2299.	2.8	48
1201	Hemocompatibility and anti-bacterial properties of silver doped diamond-like carbon prepared by pulsed filtered cathodic vacuum arc deposition. Diamond and Related Materials, 2007, 16, 1353-1360.	3.9	100
1202	Quantum-confined and tunable optical emission from sub-10-nm silicon oxide nanowires in aqueous suspension. Applied Physics Letters, 2007, 91, 193111.	3.3	3
1203	Evolution mechanism of nanocrystalline tungsten-carbon and effects on tungsten implanted amorphous hydrogenated carbon. Journal of Applied Physics, 2007, 102, 113517.	2.5	5
1204	Corrosion behavior of biomedical AZ91 magnesium alloy in simulated body fluids. Journal of Materials Research, 2007, 22, 2004-2011.	2.6	189
1205	Structure and topographies of diamond-like carbon films produced on tungsten pre-implanted stainless steel substrate by plasma immersion ion implantation and deposition. Diamond and Related Materials, 2007, 16, 1490-1499.	3.9	7
1206	Direct and Large-Area Growth of One-Dimensional ZnO Nanostructures from and on a Brass Substrate. Journal of Physical Chemistry C, 2007, 111, 5876-5881.	3.1	70

#	Article	IF	CITATIONS
1207	Dispersion of linear waves in quantum plasmas. Physics of Plasmas, 2007, 14, 062102.	1.9	83
1208	Polarized Raman scattering of Ge nanocrystals embedded in a-SiO2. Applied Physics Letters, 2007, 90, 081909.	3.3	12
1209	Behavior of human umbilical vein endothelial cells on micro-patterned amorphous hydrogenated carbon films produced by plasma immersion ion implantation & deposition and plasma etching. Diamond and Related Materials, 2007, 16, 550-557.	3.9	12
1210	Nickel release behavior, cytocompatibility, and superelasticity of oxidized porous single-phase NiTi. Journal of Biomedical Materials Research - Part A, 2007, 81A, 948-955.	4.0	41
1211	Surface characteristics, biocompatibility, and mechanical properties of nickel-titanium plasma-implanted with nitrogen at different implantation voltages. Journal of Biomedical Materials Research - Part A, 2007, 82A, 469-478.	4.0	34
1212	Antimicrobial polyethylene with controlled copper release. Journal of Biomedical Materials Research - Part A, 2007, 83A, 838-844.	4.0	53
1213	Enhancement of surface properties of biomaterials using plasma-based technologies. Surface and Coatings Technology, 2007, 201, 8076-8082.	4.8	67
1214	Plasma processing of AISI 304 stainless steel using radio frequency hollow cathode discharge. Surface and Coatings Technology, 2007, 201, 8650-8653.	4.8	7
1215	Effects of pulsing frequency on shape recovery and investigation of nickel out-diffusion after mechanical bending of nitrogen plasma implanted NiTi shape memory alloys. Surface and Coatings Technology, 2007, 201, 8286-8290.	4.8	10
1216	Plasma surface treatment of artificial orthopedic and cardiovascular biomaterials. Surface and Coatings Technology, 2007, 201, 5601-5606.	4.8	61
1217	Nitrogen plasma-implanted nickel titanium alloys for orthopedic use. Surface and Coatings Technology, 2007, 201, 5607-5612.	4.8	27
1218	Particle-in-cell numerical simulation of non-uniform plasma immersion ion implantation. Surface and Coatings Technology, 2007, 201, 5458-5462.	4.8	6
1219	Enhancement of corrosion resistance of AISI 420 stainless steels by nitrogen and silicon plasma immersion ion implantation. Surface and Coatings Technology, 2007, 201, 4879-4883.	4.8	23
1220	Microstructure and visible-photoluminescence of titanium dioxide thin films fabricated by dual cathodic arc and nitrogen plasma deposition. Surface and Coatings Technology, 2007, 201, 4897-4900.	4.8	11
1221	Fabrication and characteristics of novel microelectronic structures fabricated by plasma-based techniques. Surface and Coatings Technology, 2007, 201, 6745-6751.	4.8	1
1222	Effects of plasma treatment on bioactivity of TiO2 coatings. Surface and Coatings Technology, 2007, 201, 6878-6881.	4.8	12
1223	Effects of pulse parameters on macro-particle production in pulsed cathodic vacuum arc deposition. Surface and Coatings Technology, 2007, 201, 6542-6544.	4.8	5
1224	Plasma distribution in the slender bore excited by coaxial rf electrode. Surface and Coatings Technology, 2007, 201, 6651-6654.	4.8	4

#	Article	IF	CITATIONS
1225	Behavior of endothelial cells on micro-patterned titanium oxide fabricated by plasma immersion ion implantation and deposition and plasma etching. Surface and Coatings Technology, 2007, 201, 6874-6877.	4.8	17
1226	Effects of electron-focusing electric field upon enhanced glow discharge plasma ion implantation. Surface and Coatings Technology, 2007, 201, 6516-6519.	4.8	8
1227	Antibacterial copper-containing titanium nitride films produced by dual magnetron sputtering. Surface and Coatings Technology, 2007, 201, 8606-8609.	4.8	79
1228	Improvement of interfacial and microstructure properties of high-k ZrO2 thin films fabricated by filtered cathodic arc deposition using nitrogen incorporation. Surface and Coatings Technology, 2007, 201, 8282-8285.	4.8	14
1229	Fabrication of highly (1000) oriented textured zinc oxide films by metal cathodic arc and oxygen dual plasma deposition and their optical properties. Surface and Coatings Technology, 2007, 201, 8348-8351.	4.8	7
1230	Corrosion behavior of AZ91 magnesium alloy treated by plasma immersion ion implantation and deposition in artificial physiological fluids. Thin Solid Films, 2007, 516, 422-427.	1.8	111
1231	Comparative studies on influence of acetylene to argon flow rate ratios on nano-scratch behavior of a-C:H films produced on steel substrates by plasma immersion ion implantation and deposition. Thin Solid Films, 2007, 516, 252-256.	1.8	6
1232	Optical and mechanical properties of alumina films fabricated on Kapton polymer by plasma immersion ion implantation and deposition using different biases. Applied Surface Science, 2007, 253, 9483-9488.	6.1	16
1233	Pore formation mechanism and characterization of porous NiTi shape memory alloys synthesized by capsule-free hot isostatic pressing. Acta Materialia, 2007, 55, 3437-3451.	7.9	86
1234	Synthesis and characterization of super hard, self-lubricating Ti–Si–C–N nanocomposite coatings. Acta Materialia, 2007, 55, 6350-6355.	7.9	99
1235	Hydrogen plasma surface activation of silicon for biomedical applications. New Biotechnology, 2007, 24, 113-117.	2.7	15
1236	Platelet activation behavior on nitrogen plasma-implanted silicon. Materials Science and Engineering C, 2007, 27, 928-932.	7.3	17
1237	Oxygen and sodium plasma-implanted nickel–titanium shape memory alloy: A novel method to promote hydroxyapatite formation and suppress nickel leaching. Nuclear Instruments & Methods in Physics Research B, 2007, 257, 687-691.	1.4	4
1238	Characteristics of end Hall ion source with magnetron hollow cathode discharge. Nuclear Instruments & Methods in Physics Research B, 2007, 257, 796-800.	1.4	11
1239	Structure and wear properties of NiTi modified by nitrogen plasma immersion ion implantation. Materials Science & Engineering A: Structural Materials: Properties, Microstructure and Processing, 2007, 444, 192-197.	5.6	21
1240	Influence of heat treatment on degradation behavior of bio-degradable die-cast AZ63 magnesium alloy in simulated body fluid. Materials Science & Engineering A: Structural Materials: Properties, Microstructure and Processing, 2007, 456, 350-357.	5.6	160
1241	Effective passivation on Si nanocrystal surface by peroxide. Journal of Crystal Growth, 2007, 304, 86-89.	1.5	3
1242	Luminescence properties of ultrasmall amorphous Si nanoparticles with sizes smaller than 2nm. Journal of Crystal Growth, 2007, 304, 476-480.	1.5	7

#	Article	IF	CITATIONS
1243	Plasmaâ€Treated Polyethylene Surfaces for Improved Binding of Active Protein. Plasma Processes and Polymers, 2007, 4, 583-590.	3.0	42
1244	Chemical and Physical Properties of Copper and Nitrogen Plasma-Implanted Polyethylene. Plasma Processes and Polymers, 2007, 4, 158-164.	3.0	6
1245	Formation of apatite on hydrogenated amorphous silicon (a-Si:H) film deposited by plasma-enhanced chemical vapor deposition. Materials Chemistry and Physics, 2007, 101, 124-128.	4.0	20
1246	Luminescent small-diameter 3C-SiC nanocrystals fabricated via a simple chemical etching method. Nanotechnology, 2007, 18, 365603.	2.6	87
1247	Surface structure and properties of biomedical NiTi shape memory alloy after Fenton's oxidation. Acta Biomaterialia, 2007, 3, 795-806.	8.3	71
1248	Effects of water plasma immersion ion implantation on surface electrochemical behavior of NiTi shape memory alloys in simulated body fluids. Applied Surface Science, 2007, 253, 3154-3159.	6.1	22
1249	Effects of NH3, O2, and N2 co-implantation on Cu out-diffusion and antimicrobial properties of copper plasma-implanted polyethylene. Applied Surface Science, 2007, 253, 8981-8985.	6.1	28
1250	Mechanical properties, bioactivity and corrosion resistance of oxygen and sodium plasma treated nickel titanium shape memory alloy. Surface and Coatings Technology, 2007, 202, 1308-1312.	4.8	9
1251	In vitro and in vivo characterization of novel plasma treated nickel titanium shape memory alloy for orthopedic implantation. Surface and Coatings Technology, 2007, 202, 1247-1251.	4.8	37
1252	Origin of low-temperature photoluminescence from SnO2 nanowires fabricated by thermal evaporation and annealed in different ambients. Applied Physics Letters, 2006, 88, 183112.	3.3	128
1253	Synthesis and low-temperature photoluminescence properties of SnO2nanowires and nanobelts. Nanotechnology, 2006, 17, 1695-1699.	2.6	228
1254	Effects of pulsing parameters on production and distribution of macroparticles in cathodic vacuum arc deposition. Journal of Vacuum Science and Technology A: Vacuum, Surfaces and Films, 2006, 24, 957-961.	2.1	2
1255	Local vibration at the surface of a Ge nanocrystal embedded in a silicon oxide matrix. Journal of Applied Physics, 2006, 99, 014301.	2.5	11
1256	Silver nanocrystal superlattice coating for molecular sensing by surface-enhanced Raman spectroscopy. Applied Physics Letters, 2006, 89, 131914.	3.3	39
1257	The effect of N+-implanted aluminum substrate on the mechanical properties of TiN films. Surface and Coatings Technology, 2006, 200, 2672-2678.	4.8	11
1258	Nucleation and growth of amorphous carbon film on tungsten-implanted stainless steel substrates. Diamond and Related Materials, 2006, 15, 1580-1584.	3.9	9
1259	Biocompatibility of calcium and phosphorus doped diamond-like carbon thin films synthesized by plasma immersion ion implantation and deposition. Diamond and Related Materials, 2006, 15, 893-897.	3.9	52
1260	Surface-enhanced Raman characteristics of Ag cap aggregates on silicon nanowire arrays. Nanotechnology, 2006, 17, 5769-5772.	2.6	58

#	Article	IF	CITATIONS
1261	Characteristics and surface energy of silicon-doped diamond-like carbon films fabricated by plasma immersion ion implantation and deposition. Diamond and Related Materials, 2006, 15, 1276-1281.	3.9	46
1262	Improvement of adhesion strength of amorphous carbon films on tungsten ion implanted 321 stainless steel substrate. Diamond and Related Materials, 2006, 15, 952-957.	3.9	17
1263	Luminescence from colloidal 3C-SiC nanocrystals in different solvents. Applied Physics Letters, 2006, 88, 041909.	3.3	76
1264	Current transport studies of ZnOâ^•p-Si heterostructures grown by plasma immersion ion implantation and deposition. Applied Physics Letters, 2006, 88, 132104.	3.3	76
1265	Nitrogen binding behavior in ZnO films with time-resolved cathodoluminescence. Applied Surface Science, 2006, 252, 8131-8134.	6.1	12
1266	Improvement of surface porosity and properties of alumina films by incorporation of Fe micrograins in micro-arc oxidation. Applied Surface Science, 2006, 253, 863-868.	6.1	66
1267	Effects of nitrogen ion implantation and implantation energy on surface properties and adhesion strength of TiN films deposited on aluminum by magnetron sputtering. Materials Science & Engineering A: Structural Materials: Properties, Microstructure and Processing, 2006, 415, 140-144.	5.6	14
1268	Mechanism of mechanical property enhancement in nitrogen and titanium implanted 321 stainless steel. Materials Science & Engineering A: Structural Materials: Properties, Microstructure and Processing, 2006, 425, 1-6.	5.6	17
1269	Ion implantation of organisms. Materials Science and Engineering Reports, 2006, 54, 49-120.	31.8	75
1270	Bioactivity of plasma implanted biomaterials. Nuclear Instruments & Methods in Physics Research B, 2006, 242, 1-7.	1.4	23
1271	Ignition and dynamics of high-voltage glow discharge plasma implantation. Nuclear Instruments & Methods in Physics Research B, 2006, 242, 275-278.	1.4	8
1272	Water plasma implantation/oxidation of magnesium alloys for corrosion resistance. Nuclear Instruments & Methods in Physics Research B, 2006, 242, 300-302.	1.4	26
1273	Improvement on corrosion resistance of NiTi orthopedic materials by carbon plasma immersion ion implantation. Nuclear Instruments & Methods in Physics Research B, 2006, 242, 270-274.	1.4	13
1274	Effects of O2 and H2O plasma immersion ion implantation on surface chemical composition and surface energy of poly vinyl chloride. Applied Surface Science, 2006, 252, 7884-7889.	6.1	15
1275	Stability of luminescent 3C-SiC nanocrystallites in aqueous solution. Physics Letters, Section A: General, Atomic and Solid State Physics, 2006, 360, 336-338.	2.1	31
1276	Antimicrobial properties of copper plasma-modified polyethylene. Polymer, 2006, 47, 7441-7445.	3.8	91
1277	Structure and mechanical properties of magnesium alloy treated by micro-arc discharge oxidation using direct current and high-frequency bipolar pulsing modes. Materials Science & Engineering A: Structural Materials: Properties, Microstructure and Processing, 2006, 435-436, 123-126.	5.6	78
1278	On the origin of light emission from porous anodic alumina formed in sulfuric acid. Solid State Communications, 2006, 137, 621-624.	1.9	52

#	Article	IF	CITATIONS
1279	In vitro bioactivity of plasma-sprayed TiO2 coating after sodium hydroxide treatment. Surface and Coatings Technology, 2006, 200, 5487-5492.	4.8	39
1280	Structure and microwave-absorbing properties of Fe-particle containing alumina prepared by micro-arc discharge oxidation. Surface and Coatings Technology, 2006, 201, 292-295.	4.8	47
1281	Anti-corrosion characteristics of nitride-coated AISI 316L stainless steel coronary stents. Surface and Coatings Technology, 2006, 201, 2802-2806.	4.8	43
1282	Surface modification of W9Cr4V2Mo high-temperature bearing steel by rare earth ion implantation. Surface and Coatings Technology, 2006, 201, 4357-4360.	4.8	8
1283	Nucleation and growth of calcium–phosphate on Ca-implanted titanium surface. Surface Science, 2006, 600, 651-656.	1.9	29
1284	Low-dimensional SiC nanostructures: Fabrication, luminescence, and electrical properties. Progress in Materials Science, 2006, 51, 983-1031.	32.8	312
1285	Antibacterial properties of plasma-modified and triclosan or bronopol coated polyethylene. Polymer, 2006, 47, 931-936.	3.8	75
1286	Hemocompatibility of lanthanum oxide films fabricated by dual plasma deposition. Thin Solid Films, 2006, 515, 1219-1222.	1.8	30
1287	Plasma surface modification of poly vinyl chloride for improvement of antibacterial properties. Biomaterials, 2006, 27, 44-51.	11.4	130
1288	Bioactivity and cytocompatibility of zirconia (ZrO2) films fabricated by cathodic arc deposition. Biomaterials, 2006, 27, 3904-3911.	11.4	106
1289	Intergrowth mechanism of silicon nanowires and silver dendrites. Journal of Electronic Materials, 2006, 35, 1879-1884.	2.2	60
1290	Characterization of amorphous and nanocrystalline carbon films. Materials Chemistry and Physics, 2006, 96, 253-277.	4.0	967
1291	Surface antibacterial characteristics of plasma-modified polyethylene. Biopolymers, 2006, 83, 62-68.	2.4	25
1292	Surface characteristics, mechanical properties, and cytocompatibility of oxygen plasma-implanted porous nickel titanium shape memory alloy. Journal of Biomedical Materials Research - Part A, 2006, 79A, 139-146.	4.0	38
1293	Plasma-nitrided high-k polycrystalline nano-array induced by electron irradiation. Nanotechnology, 2006, 17, 4379-4383.	2.6	4
1294	Si nanowires sheathed with thin diamondlike carbon films. Journal of Vacuum Science & Technology B, 2006, 24, 1702.	1.3	1
1295	Resonant electron transfer and luminescent enhancement in a toluene suspension of Si nanocrystals. Journal of Chemical Physics, 2006, 125, 054713.	3.0	9
1296	Fabrication of silicon-on-SiO2/diamondlike-carbon dual insulator using ion cutting and mitigation of self-heating effects. Applied Physics Letters, 2006, 88, 142108.	3.3	13

#	Article	IF	CITATIONS
1297	In situ fabrication of alumina nanotube array and photoluminescence. Applied Physics Letters, 2006, 89, 073114.	3.3	16
1298	Energy band mixing in core-shell-structured Siâ^•FeSi2 nanocomposites. Applied Physics Letters, 2006, 89, 053114.	3.3	1
1299	Optical emission from C60-coupled Î ² -FeSi2 nanocomposites. Applied Physics Letters, 2006, 89, 233114.	3.3	2
1300	Corrosion resistance and antithrombogenic behavior of La and Nd ion implanted stainless steels. Journal of Vacuum Science and Technology A: Vacuum, Surfaces and Films, 2006, 24, 1790-1794.	2.1	8
1301	Light-induced bioactive TiO2 surface. Applied Physics Letters, 2006, 88, 013905.	3.3	32
1302	Optical emission from the aggregated state in poly [2-methoxy-5-(2â€2-ethyl-hexyloxy)-p-phenylene vinylene]. Journal of Vacuum Science and Technology A: Vacuum, Surfaces and Films, 2006, 24, 202-205.	2.1	11
1303	Control of interfacial silicate between HfO2 and Si by high concentration ozone. Applied Physics Letters, 2006, 88, 072903.	3.3	30
1304	Fabrication of novel silicon-on-insulator substrates using plasma-based technology. , 2006, , .		0
1305	Experimental and numerical evaluations of adhesion strength and stress in TiN films deposited on ti-implanted aluminum. Journal of Vacuum Science and Technology A: Vacuum, Surfaces and Films, 2006, 24, 212-217.	2.1	3
1306	Enhanced electron field emission from oriented columnar AlN and mechanism. Applied Physics Letters, 2006, 88, 251103.	3.3	10
1307	Silver nanocrystal superlattices: Self-assembly and optical emission. Applied Physics Letters, 2006, 88, 143111.	3.3	12
1308	Vacuum electron field emission from SnO2 nanowhiskers annealed in N2 and O2 atmospheres. Applied Physics Letters, 2006, 88, 013109.	3.3	29
1309	Synthesis and magnetic properties of Zn1â^'xCoxO nanorods. Journal of Applied Physics, 2006, 99, 074303.	2.5	69
1310	Photoluminescence from C60-coupled porous structures formed on Fe+-implanted silicon. Journal of Chemical Physics, 2006, 125, 014706.	3.0	2
1311	Fabrication and field emission property of a Si nanotip array. Nanotechnology, 2006, 17, 5573-5576.	2.6	22
1312	Fabrication of rutile TiO2 thin films by low-temperature, bias-assisted cathodic arc deposition and their dielectric properties. Journal of Materials Research, 2006, 21, 844-850.	2.6	7
1313	Interfacial characteristics of fully depleted SiGe-on-insulator (SGOI) substrate fabricated by modified Ge condensation. Semiconductor Science and Technology, 2005, 20, L31-L35.	2.0	2
1314	Formation of silicon on plasma synthesized SiOxNy and reaction mechanism. Applied Surface Science, 2005, 243, 89-95.	6.1	3

#	Article	IF	CITATIONS
1315	Plasma nitridation and microstructure of high-k ZrO2 thin films fabricated by cathodic arc deposition. Journal of Crystal Growth, 2005, 277, 422-427.	1.5	19
1316	From Si nanotubes to nanowires: Synthesis, characterization, and self-assembly. Journal of Crystal Growth, 2005, 277, 143-148.	1.5	66
1317	Catalytic growth of α-FeSi2 and silicon nanowires. Journal of Crystal Growth, 2005, 280, 286-291.	1.5	6
1318	Strain relaxation mechanism in SiGe-on-insulator fabricated by Ge condensation. Journal of Crystal Growth, 2005, 281, 275-280.	1.5	10
1319	Mo-containing diamond-like carbon films with blue emission. Journal of Crystal Growth, 2005, 281, 538-542.	1.5	4
1320	Self-organized synthesis of micrometer scale silver disks by electroless metal deposition on Si-incorporated diamond-like carbon films. Journal of Crystal Growth, 2005, 284, 470-476.	1.5	5
1321	Polycrystalline tubular nanostructures of germanium. Journal of Crystal Growth, 2005, 285, 59-65.	1.5	6
1322	Light emission from as-prepared and oxidized Si nanowires with diameters of 5–15nm. Journal of Crystal Growth, 2005, 285, 620-626.	1.5	13
1323	Solvent effect on light-emitting property of Si nanocrystals. Physics Letters, Section A: General, Atomic and Solid State Physics, 2005, 334, 447-452.	2.1	23
1324	Anti-corrosion performance of oxidized and oxygen plasma-implanted NiTi alloys. Materials Science & Engineering A: Structural Materials: Properties, Microstructure and Processing, 2005, 390, 444-451.	5.6	47
1325	Relaxed SiGe-on-insulator fabricated by dry oxidation of sandwiched Si/SiGe/Si structure. Materials Science and Engineering B: Solid-State Materials for Advanced Technology, 2005, 124-125, 153-157.	3.5	10
1326	Bioconductivity and mechanical properties of plasma-sprayed dicalcium silicate/zirconia composite coating. Materials Science and Engineering C, 2005, 25, 509-515.	7.3	25
1327	Determination of nitrogen-related defects in N-implanted ZnO films by dynamic cathodoluminescence. Nuclear Instruments & Methods in Physics Research B, 2005, 237, 307-311.	1.4	12
1328	Surface modification of polymeric materials by plasma immersion ion implantation. Nuclear Instruments & Methods in Physics Research B, 2005, 237, 417-421.	1.4	49
1329	Improvements of anti-corrosion and mechanical properties of NiTi orthopedic materials by acetylene, nitrogen and oxygen plasma immersion ion implantation. Nuclear Instruments & Methods in Physics Research B, 2005, 237, 411-416.	1.4	46
1330	Formation of titanium nitride barrier layer in nickel–titanium shape memory alloys by nitrogen plasma immersion ion implantation for better corrosion resistance. Thin Solid Films, 2005, 488, 20-25.	1.8	50
1331	Effects of pretreatment by ion implantation and interlayer on adhesion between aluminum substrate and TiN film. Thin Solid Films, 2005, 493, 152-159.	1.8	30
1332	Structure and properties of Ca-plasma-implanted titanium. Surface and Coatings Technology, 2005, 191, 43-48.	4.8	36

#	Article	IF	CITATIONS
1333	Electrical properties of AlN thin films prepared by ion beam enhanced deposition. Surface and Coatings Technology, 2005, 196, 130-134.	4.8	27
1334	Influence of ion energies on the surface morphology of carbon films. Surface and Coatings Technology, 2005, 196, 241-245.	4.8	15
1335	Corrosion resistance improvement of magnesium alloy using nitrogen plasma ion implantation. Surface and Coatings Technology, 2005, 198, 454-458.	4.8	75
1336	Improvement of surface bioactivity on titanium by water and hydrogen plasma immersion ion implantation. Biomaterials, 2005, 26, 6129-6135.	11.4	102
1337	Plasma-treated nanostructured TiO2 surface supporting biomimetic growth of apatite. Biomaterials, 2005, 26, 6143-6150.	11.4	110
1338	Experimental investigation of hybrid-evaporation-glow discharge plasma immersion ion implantation. Journal of Applied Physics, 2005, 97, 113301.	2.5	19
1339	Formation of silicon-on-aluminum nitride using ion-cut and theoretical investigation of self-heating effects. Materials Letters, 2005, 59, 510-513.	2.6	2
1340	Early apatite deposition and osteoblast growth on plasma-sprayed dicalcium silicate coating. Journal of Biomedical Materials Research - Part A, 2005, 74A, 356-365.	4.0	28
1341	Bioactivity of titanium following sodium plasma immersion ion implantation and deposition. Biomaterials, 2005, 26, 5465-5473.	11.4	65
1342	Controlled Growth of ZnO films on Si Substrate and N-doping Behavior. Materials Research Society Symposia Proceedings, 2005, 864, 7111.	0.1	1
1343	Self-assembled growth and blue emission of a SiOx-capped (x= 0.5–0.8) silicon nanowire array. Nanotechnology, 2005, 16, 2222-2226.	2.6	5
1344	Improvement of interfacial and dielectric properties of sputtered Ta2O5 thin films by substrate biasing and the underlying mechanism. Journal of Applied Physics, 2005, 97, 114106.	2.5	24
1345	Visible cathodoluminescence of 4 Ã single-walled carbon nanotubes. Applied Physics Letters, 2005, 87, 213114.	3.3	17
1346	Microwave-cut silicon layer transfer. Applied Physics Letters, 2005, 87, 224103.	3.3	12
1347	Thermal stability of diamondlike carbon buried layer fabricated by plasma immersion ion implantation and deposition in silicon on insulator. Journal of Applied Physics, 2005, 98, 053502.	2.5	22
1348	Improvement of nitrogen retained dose using ammonia as a precursor in nitrogen plasma immersion ion implantation of silicon. Journal of Vacuum Science and Technology A: Vacuum, Surfaces and Films, 2005, 23, 1346-1349.	2.1	7
1349	Germanium movement mechanism in SiGe-on-insulator fabricated by modified Ge condensation. Journal of Applied Physics, 2005, 97, 064504.	2.5	31
1350	Silicon layer transfer using plasma hydrogenation. Applied Physics Letters, 2005, 87, 111910.	3.3	12

#	Article	IF	CITATIONS
1351	Low-frequency Raman scattering of Ge and Si nanocrystals in silica matrix. Journal of Applied Physics, 2005, 98, 064303.	2.5	20
1352	Investigation of plasma hydrogenation and trapping mechanism for layer transfer. Applied Physics Letters, 2005, 86, 031904.	3.3	27
1353	Anti-Corrosion Properties of Nitrogen and Oxygen Plasma-Implanted Nickel-Titanium Shape Memory Alloy. Solid State Phenomena, 2005, 107, 111-114.	0.3	3
1354	Cr/CrN Compound Films Prepared by Ion Beam Assisted Deposition for Improving the Performance of Bearing Steel. Plasma Science and Technology, 2005, 7, 2959-2961.	1.5	3
1355	Self-assembled growth and green emission of gold nanowhiskers. Applied Physics Letters, 2005, 87, 223115.	3.3	21
1356	Plasma hydrogenation of strained Siâ^•SiGeâ^•Si heterostructure for layer transfer without ion implantation. Applied Physics Letters, 2005, 87, 091902.	3.3	40
1357	Experimental Evidence for the Quantum Confinement Effect in 3C-SiC Nanocrystallites. Physical Review Letters, 2005, 94, 026102.	7.8	288
1358	Linear ion source with magnetron hollow cathode discharge. Review of Scientific Instruments, 2005, 76, 113502.	1.3	11
1359	Self-assembled growth and enhanced blue emission of SiOxNy-capped silicon nanowire arrays. Applied Physics Letters, 2005, 86, 193111.	3.3	23
1360	Surface energy, wettability, and blood compatibility phosphorus doped diamond-like carbon films. Diamond and Related Materials, 2005, 14, 78-85.	3.9	230
1361	Thermal stability of metal-doped diamond-like carbon fabricated by dual plasma deposition. Diamond and Related Materials, 2005, 14, 1489-1493.	3.9	46
1362	Synthesis and optical properties of germanium nanorod array fabricated on porous anodic alumina and Si-based templates. Applied Physics Letters, 2005, 86, 021111.	3.3	30
1363	Implantation dynamics of plasma implantation into insulating strips. Journal Physics D: Applied Physics, 2004, 37, 50-54.	2.8	11
1364	Formation of silicon on plasma synthesized aluminum nitride structure by ion cutting. Journal of Vacuum Science & Technology an Official Journal of the American Vacuum Society B, Microelectronics Processing and Phenomena, 2004, 22, 2748.	1.6	2
1365	Influence of thickness and dielectric properties on implantation efficacy in plasma immersion ion implantation of insulators. Journal of Applied Physics, 2004, 95, 3319-3323.	2.5	14
1366	Low-temperature photoluminescence of hydrogen Ion and plasma implanted silicon and porous silicon. Journal of Applied Physics, 2004, 96, 248-251.	2.5	5
1367	Formation of silicon-on-diamond by direct bonding of plasma-synthesized diamond-like carbon to silicon. Applied Physics Letters, 2004, 85, 2532-2534.	3.3	16
1368	Optical emission from silicon-based SiO2 islands fabricated by anodic alumina templates. Journal of Applied Physics, 2004, 96, 1443-1446.	2.5	4

#	Article	IF	CITATIONS
1369	Synthesis of aluminum nitride films by plasma immersion ion implantation–deposition using hybrid gas–metal cathodic arc gun. Review of Scientific Instruments, 2004, 75, 719-724.	1.3	9
1370	Plasma hydrogenation of strain-relaxed SiGeâ^•Si heterostructure for layer transfer. Applied Physics Letters, 2004, 85, 4944-4946.	3.3	5
1371	Mechanism of apatite formation on hydrogen plasma-implanted single-crystal silicon. Applied Physics Letters, 2004, 85, 3623-3625.	3.3	13
1372	Effects of mesh-assisted carbon plasma immersion ion implantation on the surface properties of insulating silicon carbide ceramics. Journal of Vacuum Science and Technology A: Vacuum, Surfaces and Films, 2004, 22, 356-360.	2.1	13
1373	Recent developments and applications of plasma immersion ion implantation. Journal of Vacuum Science & Technology an Official Journal of the American Vacuum Society B, Microelectronics Processing and Phenomena, 2004, 22, 289.	1.6	106
1374	Fabrication of silicon carbide thin films by plasma immersion ion implantation with self-ignited glow discharge. Thin Solid Films, 2004, 447-448, 153-157.	1.8	6
1375	Mechanism of apatite formation on wollastonite coatings in simulated body fluids. Biomaterials, 2004, 25, 1755-1761.	11.4	315
1376	Surface composition and surface energy of Teflon treated by metal plasma immersion ion implantation. Surface Science, 2004, 573, 426-432.	1.9	45
1377	Oxygen segregation and Ge diffusion in annealed oxygen ion-implanted relaxed SiGe/Si heterostructures. Journal of Electronic Materials, 2004, 33, 207-212.	2.2	1
1378	Hemocompatibility of nitrogen-doped, hydrogen-free diamond-like carbon prepared by nitrogen plasma immersion ion implantation-deposition. Journal of Biomedical Materials Research Part B, 2004, 70A, 107-114.	3.1	45
1379	Microstructure investigation of BaxSr1â^'xTiO3 thin film grown on porous silicon substrate. Materials Science in Semiconductor Processing, 2004, 7, 253-258.	4.0	9
1380	Biomimetic growth of apatite on hydrogen-implanted silicon. Biomaterials, 2004, 25, 5575-5581.	11.4	41
1381	Plasma surface modification of titanium for hard tissue replacements. Surface and Coatings Technology, 2004, 186, 227-233.	4.8	54
1382	Plasma immersion ion implantation of industrial gears. Surface and Coatings Technology, 2004, 186, 260-264.	4.8	10
1383	Two-dimensional numerical simulation of non-uniform plasma immersion ion implantation. Surface and Coatings Technology, 2004, 186, 47-52.	4.8	11
1384	Molybdenum–carbon film fabricated using metal cathodic arc and acetylene dual plasma deposition. Surface and Coatings Technology, 2004, 186, 112-117.	4.8	28
1385	Growth and visible photoluminescence of highly oriented (100) zinc oxide film synthesized on silicon by plasma immersion ion implantation. Materials Science in Semiconductor Processing, 2004, 7, 459-462.	4.0	9
1386	Cu oxide nanowire array grown on Si-based SiO2 nanoscale islands via nanochannels. Acta Materialia, 2004, 52, 5051-5055.	7.9	16

#	Article	IF	CITATIONS
1387	Formation of Si-based nano-island array on porous anodic alumina. Acta Materialia, 2004, 52, 5633-5637.	7.9	13
1388	Interactions between plasma and ionization gauge in plasma immersion ion implantation. Surface and Coatings Technology, 2003, 169-170, 36-40.	4.8	4
1389	Room-temperature electroluminescence from H-plasma-implanted silicon. Semiconductor Science and Technology, 2003, 18, L55-L58.	2.0	4
1390	Oxygen profile engineering in silicon by germanium addition and high-temperature annealing. Applied Physics Letters, 2003, 83, 305-307.	3.3	5
1391	Flexible system for multiple plasma immersion ion implantation-deposition processes. Review of Scientific Instruments, 2003, 74, 5137-5140.	1.3	9
1392	Current control for magnetized plasma in direct-current plasma-immersion ion implantation. Applied Physics Letters, 2003, 82, 2014-2016.	3.3	11
1393	Effects of assistant anode on planar inductively coupled magnetized argon plasma in plasma in masma in plasma immersion ion implantation. Journal of Applied Physics, 2003, 93, 5883-5887.	2.5	15
1394	Enhancement of implantation energy using a conducting grid in plasma immersion ion implantation of dielectric/polymeric materials. Review of Scientific Instruments, 2003, 74, 3697-3700.	1.3	29
1395	Anode double layer in magnetized radio frequency inductively coupled hydrogen plasma. Journal of Applied Physics, 2003, 94, 1390-1395.	2.5	11
1396	Relaxed silicon–germanium-on-insulator substrates by oxygen implantation into pseudomorphic silicon germanium/silicon heterostructure. Applied Physics Letters, 2003, 82, 2452-2454.	3.3	14
1397	Characteristics and polarization-enhanced model of wurtzite aluminum nitride thin films synthesized on Si(100) substrates by pulsed laser deposition. Journal of Applied Physics, 2003, 94, 1934-1940.	2.5	10
1398	Semiconductor applications of plasma immersion ion implantation. Plasma Physics and Controlled Fusion, 2003, 45, 555-570.	2.1	25
1399	Silicon carbide formation by methane plasma immersion ion implantation into silicon. Journal of Vacuum Science & Technology an Official Journal of the American Vacuum Society B, Microelectronics Processing and Phenomena, 2003, 21, 1375.	1.6	17
1400	Automatically reigniting dc vacuum arc plasma source. Review of Scientific Instruments, 2002, 73, 2971-2973.	1.3	3
1401	Effects of bias voltage on the corrosion resistance of titanium nitride thin films fabricated by dynamic plasma immersion ion implantation-deposition. Journal of Vacuum Science and Technology A: Vacuum, Surfaces and Films, 2002, 20, 160-164.	2.1	14
1402	Enhancement of implantation efficiency by grid biasing in radio-frequency inductively coupled plasma direct-current plasma immersion ion implantation. Journal of Vacuum Science & Technology an Official Journal of the American Vacuum Society B, Microelectronics Processing and Phenomena, 2002, 20, 1452.	1.6	5
1403	Plasma transport in magnetic duct filter. Journal Physics D: Applied Physics, 2002, 35, 3176-3180.	2.8	11
1404	Effects of cathode materials and arc current on optimal bias of a cathodic arc through a magnetic duct. Applied Physics Letters, 2002, 80, 3700-3702.	3.3	18

#	Article	IF	CITATIONS
1405	Effects of magnetic field on pulse wave forms in plasma immersion ion implantation in a radio-frequency, inductively coupled plasma. Journal of Applied Physics, 2002, 92, 2284-2289.	2.5	6
1406	Multiple ion-focusing effects in plasma immersion ion implantation. Applied Physics Letters, 2002, 81, 3744-3746.	3.3	15
1407	Charging of dielectric substrate materials during plasma immersion ion implantation. Nuclear Instruments & Methods in Physics Research B, 2002, 187, 485-491.	1.4	30
1408	Bias voltage influence on surface morphology of titanium nitride synthesized by dynamic nitrogen and titanium plasma immersion ion implantation and deposition. Materials Science & Engineering A: Structural Materials: Properties, Microstructure and Processing, 2002, 337, 236-240.	5.6	6
1409	Structural analysis of arc deposited diamond-like carbon films by Raman and X-ray photoelectron spectroscopy. Materials Science and Engineering B: Solid-State Materials for Advanced Technology, 2002, 94, 95-101.	3.5	40
1410	Fabrication of SOI structure with AlN film as buried insulator by Ion-Cut process. Applied Surface Science, 2002, 199, 287-292.	6.1	18
1411	Nitrogen depth profiles in plasma implanted stainless steel. Physics Letters, Section A: General, Atomic and Solid State Physics, 2002, 299, 577-580.	2.1	12
1412	Contamination issues in hydrogen plasma immersion ion implantation of silicon—a brief review. Surface and Coatings Technology, 2002, 156, 244-252.	4.8	17
1413	Experimental investigation of the electrical characteristics and initiation dynamics of pulsed high-voltage glow discharge. Journal Physics D: Applied Physics, 2001, 34, 354-359.	2.8	27
1414	Hydrogen-induced surface blistering of sample chuck materials in hydrogen plasma immersion ion implantation. Journal of Vacuum Science and Technology A: Vacuum, Surfaces and Films, 2001, 19, 2301-2306.	2.1	7
1415	Preparation of gallium nitride (GaN) and related compounds by plasma immersion ion implantation and rapid thermal annealing. Surface and Coatings Technology, 2001, 136, 142-145.	4.8	8
1416	Energy distribution and depth profile in BF3 plasma doping. Surface and Coatings Technology, 2001, 136, 146-150.	4.8	13
1417	Applications of plasma immersion ion implantation in microelectronics — a brief review. Surface and Coatings Technology, 2001, 136, 151-156.	4.8	28
1418	Dynamic nitrogen and titanium plasma ion implantation/deposition at different bias voltages. Thin Solid Films, 2001, 390, 139-144.	1.8	11
1419	Steady-state direct-current plasma immersion ion implantation using an electron cyclotron resonance plasma source. Thin Solid Films, 2001, 390, 145-148.	1.8	9
1420	Oxygen-induced nickel segregation in nitrogen plasma implanted AISI 304 stainless steel. Materials Science & Engineering A: Structural Materials: Properties, Microstructure and Processing, 2001, 316, 200-204.	5.6	42
1421	Target temperature simulation during fast-pulsing plasma immersion ion implantation. Journal Physics D: Applied Physics, 2001, 34, 1639-1645.	2.8	11
1422	Silicon-on-Insulator Structure Fabricated by Electron Beam Evaporation of Si on Porous Si and Epitaxial Layer Transfer. Chinese Physics Letters, 2001, 18, 662-664.	3.3	4

#	Article	IF	CITATIONS
1423	Damage in hydrogen plasma implanted silicon. Journal of Applied Physics, 2001, 90, 1735-1739.	2.5	23
1424	Quasi-direct current plasma immersion ion implantation. Applied Physics Letters, 2001, 79, 3044-3046.	3.3	10
1425	Investigation of low-pressure elevated-temperature plasma immersion ion implantation of AISI 304 stainless steel. Journal of Vacuum Science and Technology A: Vacuum, Surfaces and Films, 2001, 19, 1008-1012.	2.1	14
1426	Steady-state direct-current plasma immersion ion implantation using a multipolar magnetic field electron cyclotron resonance plasma source. Journal of Vacuum Science and Technology A: Vacuum, Surfaces and Films, 2001, 19, 2889.	2.1	4
1427	Intense blue-light emission from carbon-plasma-implanted porous silicon. Applied Physics Letters, 2001, 78, 37-39.	3.3	35
1428	Metallic contamination in hydrogen plasma immersion ion implantation of silicon. Journal of Applied Physics, 2001, 90, 3743-3749.	2.5	10
1429	Modeling of the relationship between implantation parameters and implantation dose during plasma immersion ion implantation. Physics Letters, Section A: General, Atomic and Solid State Physics, 2000, 277, 42-46.	2.1	21
1430	Electrochemical corrosion properties of AISI304 steel treated by low-temperature plasma immersion ion implantation. Scripta Materialia, 2000, 43, 417-422.	5.2	19
1431	Efficacy of high-frequency, low-voltage plasma immersion ion implantation of a bar-shaped target. Journal of Applied Physics, 2000, 88, 2221-2225.	2.5	13
1432	Modeling of incident particle energy distribution in plasma immersion ion implantation. Journal of Applied Physics, 2000, 88, 4961-4966.	2.5	22
1433	Direct temperature monitoring for semiconductors in plasma immersion ion implantation. Review of Scientific Instruments, 2000, 71, 2839-2842.	1.3	23
1434	Profile control in BF3 plasma doping. Journal of Applied Physics, 2000, 88, 3198-3201.	2.5	13
1435	The effect of high-dose nitrogen plasma immersion ion implantation on silicone surfaces. Journal Physics D: Applied Physics, 2000, 33, 2869-2874.	2.8	31
1436	Direct current plasma implantation using a grounded conducting grid. Journal of Applied Physics, 2000, 87, 4094-4097.	2.5	29
1437	Special modulator for high frequency, low-voltage plasma immersion ion implantation. Review of Scientific Instruments, 1999, 70, 1824-1828.	1.3	36
1438	Accurate determination of pulsed current waveform in plasma immersion ion implantation processes. Journal of Applied Physics, 1999, 86, 3567-3570.	2.5	24
1439	Particle-in-cell and Monte Carlo simulation of the hydrogen plasma immersion ion implantation process. Journal of Applied Physics, 1999, 86, 1817-1821.	2.5	35
1440	In situ sample temperature measurement in plasma immersion ion implantation. Review of Scientific Instruments, 1999, 70, 2818-2821.	1.3	17

#	Article	IF	CITATIONS
1441	Surface metal contamination on silicon wafers after hydrogen plasma immersion ion implantation. Nuclear Instruments & Methods in Physics Research B, 1999, 155, 75-78.	1.4	16
1442	Inner surface ion implantation using deflecting electric field. Nuclear Instruments & Methods in Physics Research B, 1998, 143, 306-310.	1.4	10
1443	Microcavity engineering by plasma immersion ion implantation. Materials Chemistry and Physics, 1998, 57, 1-16.	4.0	24
1444	Plasma immersion ion implantation for SOI synthesis: SIMOX and ion-cut. Journal of Electronic Materials, 1998, 27, 1059-1066.	2.2	13
1445	Floating low-temperature radio-frequency plasma oxidation of polycrystalline silicon-germanium. Applied Physics Letters, 1998, 73, 360-362.	3.3	10
1446	Sample stage induced dose and energy nonuniformity in plasma immersion ion implantation of silicon. Applied Physics Letters, 1998, 73, 202-204.	3.3	24
1447	Low-Dielectric Constant SiO(F,C) Films for ULSI Interconnections Prepared by CF4 Plasma Ion Implantation. Materials Research Society Symposia Proceedings, 1998, 511, 63.	0.1	0
1448	Ion-cut silicon-on-insulator fabrication with plasma immersion ion implantation. Applied Physics Letters, 1997, 71, 2767-2769.	3.3	42
1449	Hydrogen induced silicon surface layer cleavage. Applied Physics Letters, 1997, 71, 1804-1806.	3.3	72
1450	Separation of plasma implantation of oxygen to form silicon on insulator. Applied Physics Letters, 1997, 70, 1748-1750.	3.3	30
1451	Combined impurity gettering effects of helium-induced cavities and oxygen precipitates created by plasma immersion ion implantation. Thin Solid Films, 1997, 300, 64-67.	1.8	11
1452	Synthesis of Soi Materials Using Plasma Immersion Ion Implantation. Materials Research Society Symposia Proceedings, 1996, 438, 333.	0.1	6
1453	Formation of Buried Porous Silicon Structure by Hydrogen Plasma Immersion Ion Implantation. Materials Research Society Symposia Proceedings, 1996, 452, 427.	0.1	3
1454	Plasma immersion ion implantation—a fledgling technique for semiconductor processing. Materials Science and Engineering Reports, 1996, 17, 207-280.	31.8	335
1455	Improving the plasma immersion ion implantation impact energy inside a cylindrical bore by using an auxiliary electrode. Applied Physics Letters, 1996, 69, 3815-3817.	3.3	42
1456	SIMS and microelectronics. Materials Chemistry and Physics, 1994, 38, 203-223.	4.0	11
1457	Determination of oxygen concentration in heavily doped silicon. Journal of Vacuum Science & Technology an Official Journal of the American Vacuum Society B, Microelectronics Processing and Phenomena, 1993, 11, 92.	1.6	6
1458	Quantitative determination of boron and phosphorus in borophosphosilicate glass by secondary ion mass spectrometry. Analytical Chemistry, 1985, 57, 1071-1074.	6.5	17

#	Article	IF	CITATIONS
1459	SIMS studies on anomalous behavior of phosphorus and other implants in silicon. Radiation Effects, 1982, 61, 201-205.	0.4	2
1460	Secondary ion mass spectrometric image depth profile analysis of thin layers. Analytical Chemistry, 1982, 54, 2208-2210.	6.5	12
1461	<i>In Vitro</i> Degradation and Biocompatibility of WE43, ZK60, and AZ91 Biodegradable Magnesium Alloys. Advanced Materials Research, 0, 287-290, 2008-2014.	0.3	7
1462	Topochemical Synthesis of Copper Phosphide Nanoribbons for Flexible Optoelectronic Memristors. Advanced Functional Materials, 0, , 2110900.	14.9	11